Order Number 9417447

Measurement of normal stress and the shape and extent of the void formed by a horizontal jet in a fluidized bed

Chen, Libin, Ph.D.

City University of New York, 1994

U·M·I
300 N. Zeeb Rd.
Ann Arbor, MI 48106

MEASUREMENT OF NORMAL STRESS AND THE SHAPE AND EXTENT OF THE VOID FORMED BY A HORIZONTAL JET IN A FLUIDIZED BED

by

Libin Chen

A dissertation submitted to the Graduate faculty in Engineering in partial fulfillment of the requirements for the degree of Doctor of philosophy, The City University of New York

1994

This manuscript has been read and accepted for the Graduate Faculty in Engineering in satisfaction of the dissertation requirement for the degree of Doctor of Philosophy

January 11, 1994
Date

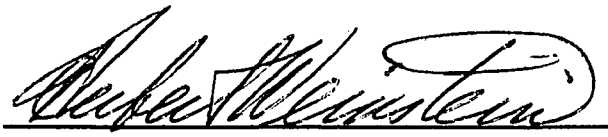
Chair of Examining Committee

1/11/94
Date

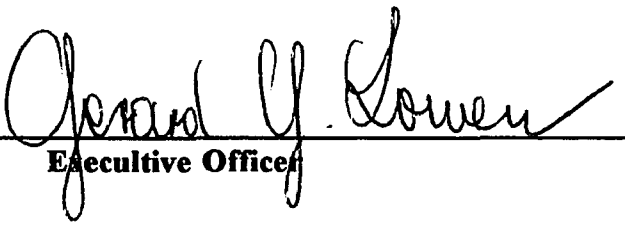
Executive Officer

Prof. H. Weinstein

Prof. R.A. Graff

Prof. G. Tardos

Prof. R. Mauri

Dr. J.M. Matsen

Supervisory Committee

The City University of New York

ABSTRACT

MEASUREMENT OF NORMAL STRESS AND THE SHAPE AND EXTENT OF THE VOID FORMED BY A HORIZONTAL JET IN A FLUIDIZED BED

by

Libin Chen

Advisor: Professor Herbert Weinstein

This work consists of three separate investigations of fluidized bed behavior as follows:

Part I	Measurement of Normal Stress and Hindrance Factor in a Collapsing Fluidized Bed
Part II	Shape and Extent of the Void Formed by a Horizontal Jet in a Fluidized Bed
Part III	Axial and Radial Pressure Measurements in a Transported Fluidized Bed

Abstract to Part I

An experimental apparatus and approach were developed to measure the instantaneous changes in pressure gradient and solid volume fraction with time along a collapsing fluidized bed. Measurements were made for a single fluid cracking catalyst. The Pressure transducer and X-ray data were in excellent agreement. These data along with straightforward one-dimensional descriptions of both gas and solid phases were used to obtain the solid normal stress modulus and the drag coefficient for the catalyst powder in the solid fraction range between minimum fluidization and loose packing.

Abstract to Part II

The introduction of reactant gas into a fluidized bed chemical reactor as a jet is a common design practice. However, the shape and extent of the void formed by a jet into a fluidized bed and the manner in which the void breaks up into bubbles have still not been described well.

An experimental study of a horizontal jet into a 15 cm by 38 cm cross-section

bubbling fluidized bed was carried out using an X-ray system. Instantaneous solid fraction averaged along 15 cm chords across the bed were measured. The mean value and the fluctuating component of solid fraction were determined for two initial jet diameters, 0.64 and 1.27 cm, and three initial jet velocities, 23, 46 and 69 m/s. Maps of the mean solid fraction and of statistical properties of the fluctuating component show that there are three discernable regions in the jet-influenced area of the bed. These are a coherent void, bubble trains and a surrounding compaction zone.

Abstract to Part III

The evaluation of solid fraction or holdup in a riser fluidized bed is made most often with an axial differential pressure measurement at the bed wall. Since the solid fraction is a critical characteristic of bed operation, the effect of pressure tap spacing on this measurement was investigated. A second experimental study was also carried out to determine whether or not a mean radial pressure gradient exists in a circulating fluidized bed riser. The existence of such a gradient could help in understanding and modeling the mixing of solids and gas.

It was found that for high velocity beds in the 0.152 m D column,

measurements with tap spacings of less than a column diameter yielded smaller solid fraction values than equivalent measurements with tap spacings of greater than one column diameter. It was also shown that the normalized standard deviation (NSD) of the fluctuations increases with decreasing tap spacing over the whole regime spectrum. However, the characteristic shape of the NSD curve over the velocity range (regime spectrum) was essentially independent of tap spacing.

The experimental data also showed that a strong radial pressure gradient exists in high velocity fluidized beds. Its value is the same order of magnitude as that of the axial pressure gradient.

ACKNOWLEDGEMENTS

There are no words to express my sincere gratitude to my mentor, Professor Herbert Weinstein, for his support, advice and guidance throughout this intense and rewarding period of research. His patience and encouragement during my hard times are much appreciated.

I would like to thank the members of my thesis committee, Professor R.A. Graff, Professor G. Tardos, Professor R. Mauri and Dr. J.M. Masten for their interest in this work and helpful suggestions.

I am grateful to the technical staff of the Chemical Engineering Department at the City College for their support and assistance, especially technician Xu, Zhen Rong who designed and built some experimental parts.

I have had much help in this effort, not the least of which has come from my wife, Ping Zhang, whose efforts have kept our home life on track.

Financial support for this work was given by Exxon Research and Engineering Co. under Grant # 776263, by Advanced Fuel Research, Inc. under Grant #776396, and by National Science Foundation under Grant #440800.

To My Wife

TABLE OF CONTENTS

LIST OF TABLE

TABLES TO PART I

TABLES TO PART II

LIST OF FIGURES

FIGURES TO PART I

FIGURES TO PART II

FIGURES TO PART III

GENERAL INTRODUCTION

Objectives

Fluidized bed reactors have been used on an industrial scale for over sixty years. Today, the use of fluidization is wide-spread in industrial applications. In the development of these fluidized bed processes, both design successes and failures have been recorded along with their preceeding research efforts so that an enormous amount of work has been carried out in all aspects of the fluidization field. Unfortunately, there is still much confusion and contradiction in the reported literature. In addition, as new applications of the technology and improvements of existing processes are continually being made, many challenging research areas have emerged.

Today, industrial designers of successful fluidization processes need a robust hydrodynamic description for a model. The two interpenetrating phases model currently in vogue appears to have great potential to provide this type of model. These have received considerable attention in recent years. They require a solid stress term to prevent the solid phase from exhibiting a compressible behavior as loose packing is approached. To our knowledge, an experimentally determined correlation for particle-to-particle and particle-to-fluid interaction forces which make up the solid stress term in the solid fraction region between minimum fluidization and loose packing has not been advanced.

A second issue, of great concern to the fluidized bed reactor designer, is understanding the dynamics of gas and solid motion resulting from the introduction of a horizontal jet into a fluidized bed. The study of jets in fluidized bed reactors is relevant to the design of reactant gas injection systems and to the development of certain processes involving fast chemical reactions which require good initial contact between gas and solids. Such processes are frequently controlled by the jet phenomena. However, the shape and extent of the void formed by a jet into a fluidized bed and the manner in which the void breaks up into bubbles have still not been described well.

A third topic of importance is the measurement of axial and radial pressure gradients and their interpretation in a riser fluidized bed. The measurement of axial pressure is the most common measurement made in a fluidized bed in the study of gas-solid fluidized bed hydrodynamics. For example, the evaluation of solid fraction or hold up in a fluidized bed is made most often with an axial differential pressure measurement at the bed wall. Since the solid fraction is a critical characteristic of bed operation, the axial pressure measurement at the bed wall must be made carefully to avoid introducing error. Numerous papers have appeared reporting the measurements of axial pressure and its fluctuations, but none of them focused on the effect of the tap spacing on the such pressure measurements.

Another issue in risers is whether or not a radial pressure gradient exists. The

existence of a radial gradient of particle concentration in the vertical transport of a solid powder by a gas has been known for over thirty years. However, the existence of a radial pressure gradient has usually been ignored by fluidized bed researchers and designers because models have been typically one-dimensional. The existence of such a gradient could help elucidate the mechanism which maintains the strong radial solid concentration profiles which occur in these flows and which must be described in two-dimensional interpenetrating phase models. Because so little attention has been paid to both of these problems, this work aims at providing an improved understanding of the measurement and interpretation of both the axial and radial pressure gradients in order to help describe the dynamics of the flow field in a riser fluidized bed .

In addressing the three topics discussed above, several experimental projects have been carried out in both bubbling and circulating fluidized beds. This thesis consists of descriptions of these experimental studies and the results. The measurement of normal stress and hindrance factor are described in part I, while the shape and extent of the void formed by a horizontal jet are discussed in part II. Finally, part III deals with the measurements of axial and radial pressure gradients and their interpretations.

Organization

This thesis consists of three parallel investigations of both bubbling and circulating fluidized bed behavior. The topics of this research are listed as follow:

Part I	Measurement of Normal Stress and Hindrance Factor in a Fluidized Bed;
Part II	The Shape and Extent of the Void Formed by a Horizontal Jet in a Fluidized Bed;
Part III	Axial and Radial Measurements in a Transported Fluidized Bed.

The three parts can be read independently, according to the reader's interest in the subjects, respectively. However, for convenient reference, the sections of the thesis are numbered consecutively throughout all of the three parts.

PART I. MEASUREMENT OF NORMAL STRESS AND HINDRANCE FACTOR IN A COLLAPSING FLUIDIZED BED

INTRODUCTION

When the air supply to a fluidized bed is switched off, the bed starts to collapse and eventually reaches a nonfluidized state known as loose packing. Measurements of bed height as a function of time during bed collapse have been used to characterize the fluidization properties of the bed powder. The phenomena associated with bed collapse are closely related to those of sedimentation, which has received much consideration in the literature. However, the hydrodynamic behavior of a fine, aeratable powder in a gas fluidized bed between loose packing and approximately minimum fluidization has not been described well. A full description of a collapsing bed is therefore useful. It would provide the normal stress relation in the solid phase and the drag coefficient (hindrance factor) in this solid fraction range, as well as a measure of the powder fluidization properties.

Mutsers and Rietema (1977) as well as Abrahamsen and Geldart (1980) all asserted that interparticle forces play an important role in the nonbubbling expansion of beds of fine particles above minimum fluidization solid fraction. Jean et al. (1992) reviewed the interparticle attraction literature in this solid fraction range and characterized fluidization quality with bubble flow rate using bed collapse measurements with polymer particles. Tsinontides and Jackson (1991) report measurements of bed expansion and pressure drop during fluidization-defluidization cycles from which they determined yield stresses in the particulate fluidization range.

A number of equations have been developed to predict the particle-to-particle interaction coefficient as a normal stress modulus. These should predict values through the minimum fluidization to loose packing range. Gidaspow and coworkers (Gidaspow et al., 1983; Ettehadieh et al., 1984; Shih et al., 1987; Gidaspow et al., 1989, Bouillard et al., 1989, Aldis, et al., 1989) have reported several. However all but one of their equations were synthesized to stabilize calculations numerically with dynamic flow models and had no empirical foundation. One equation used in Shih et al., (1987), was obtained from very low solid fraction sedimentation data in a solid-liquid system reported in Shih et al, (1986). Massoudi and his coworkers (1992) recently addressed the fact that the values given by these competing equations are orders of magnitude apart. To our

knowledge, an experimental correlation for normal stress modulus or particle-to-particle interaction force based on direct measurement has not been reported for the range of solid fraction between minimum fluidization and loose packing.

An experimentally determined correlation for particle-to-particle and particle-to-fluid interaction forces in the solid fraction region between minimum fluidization and loose packing appears to have great potential for the two interpenetrating phases models currently in vogue. These have received considerable attention in recent years. They require a solid stress term to prevent the solid phase from exhibiting a compressible behavior as loose packing is approached.

In this study, an experimental apparatus and approach were developed to measure the change in pressure gradient as well as solid fraction along the bed with time. Thus, the gas and solid velocities could be followed during the bed collapse. A one dimensional description of continuity and momentum transfer provide the equations for the direct evaluation of the desired quantities. A set of experimental data for a single solid powder, a fluid cracking catalyst, is analyzed to demonstrate the method.

EXPERIMENTAL

Equipment

The arrangement of equipment is indicated schematically in Fig.I1. The bed was contained in a rectangular vessel of Plexiglas, with dimensions of 0.406 m X 0.381 m X 1.219 m. The vessel was filled with solid particles to a height of 0.720 m. The solids, initially resting on a sintered metal gas distributor plate, were fluidized by the gas flow. The solid powder was HFZ-33 FCC cracking catalyst, with an average particle size of 56 μm and particle density of 1.45 g/cm^3, supplied by the Englehard Corp. The gas used for the experiment was air at ambient conditions. Rotameters fitted into the line metered the air flow rate. The initial velocity was 0.150 m/s for the experiment. X-ray flow visualization during steady-state operation showed the fluidized bed to be uniform in both transverse directions.

A solenoid actuated valve was installed into the line upstream of all the rotameters. The valve was a two-way, direct acting, instant on-off valve. Upon de-energizing the valve, the valve closed and the supply, both of the fluidizing air and the purge air, was shut off immediately, shunting the upstream airflow to a vent. The valve permitted no air flow into the bed while the bed collapsed.

As is indicated in Fig.I1, five pressure taps were installed at several different heights mounted along the side of the bed. Pressure-time signals at several levels along the vessel were measured by means of five piezo-resistive pressure transducers. Two pressure taps, mounted 0.013 m above and below the distributor, were connected to pressure transducer A. Another four pressure taps were installed vertically along the bed, each pair was connected sequentially across transducers B, C and D, with distances of 0.292, 0.212 and 0.170 m respectively between them. In order to prevent blockage at each tap, purge gas was passed continuously through the taps during fluidization. Air was used as purge gas and was controlled using needle valves.

An X-ray absorption system was used to obtain the instantaneous solid fraction signals. The X-ray source was designed for continuous output and high-intensity operation. The X-ray image of the bed was projected onto a 23 cm image intensifier screen. The image intensifier converted the X-ray into visible light and projected it onto a 8 cm output screen. A mirror with an angle of 45^0 to the screen projected 90% of the light through a lens and onto a curved 15 cm screen. This screen was equipped with 48 phototransistors all at equal distance from the image intensifier screen. These were arranged such that three rows of 16 transistors scanned the projected image of the bed across three elevations at 1 cm intervals. The entire X-ray system was mounted on a platform that could be moved up and

down along the vessel at 1 cm intervals.

The output voltages of pressure and solid fraction signals were sent to a real-time data acquisition. The signals were sampled at the rate of 50 Hz by a Dell 386/20 mhz computer with a Metra-byte Das-20 analog to digital converter board. The X-ray and data acquisition systems, including calibration procedures, are described in detail in Feindt (1990).

Procedure

A run was made by obtaining pressure-time and solid fraction-time signals for a bubbling bed whose air supply was abruptly shut off at the fifth second of recording time. The data collection time of each run was more than 60 s. This gave a record for the whole process of the bed collapse.

During each experiment, the X-ray assembly was stationed along the bed at 3 cm elevation increments from the distributor to the top of the bed. The bed collapse and data sampling was repeated with the X-ray at each elevation under the same experimental conditions.

ANALYTICAL

A one-dimensional, unsteady analytical model of a collapsing bed is readily derived from the following separate phase continuity and momentum equations.

The continuity equation for solid phase:

$$\rho_s \frac{\partial \alpha}{\partial t} + \rho_s \frac{\partial}{\partial x}(\alpha u_s) = 0 \qquad (1)$$

The continuity equation for fluid phase:

$$\frac{\partial}{\partial t}[\rho(1-\alpha)] + \frac{\partial}{\partial x}[\rho u_g(1-\alpha)] = 0 \qquad (2)$$

The momentum equation for the solid phase:

$$\frac{\partial}{\partial t}(\rho_s u_s \alpha) + \frac{\partial}{\partial x}(\rho_s \alpha u_s^2) + \frac{\partial \sigma}{\partial x} + \alpha \frac{\partial p}{\partial x} + \rho_s \alpha g - K(u_g - u_s) = 0 \qquad (3)$$

The momentum equation for the fluid phase:

$$\frac{\partial}{\partial t}[\rho u_g(1-\alpha)] + \frac{\partial}{\partial x}[\rho u_g^2(1-\alpha)] + (1-\alpha)\left[\frac{\partial P}{\partial x} + \rho g\right] + K(u_g - u_s) = 0 \qquad (4)$$

Because the sedimentation process is slow, the creeping-flow approximation may be employed in the momentum equations leading respectively,to

$$\frac{\partial \sigma}{\partial x} + \alpha \frac{\partial p}{\partial x} + \rho_s \alpha g - K(u_g - u_s) = 0 \qquad (5)$$

$$(1-\alpha)\left(\frac{\partial p}{\partial x} + \rho g\right) + K(u_g - u_s) = 0 \qquad (6)$$

The total momentum balance is obtained by combining eqs (5) and (6)

$$\frac{\partial}{\partial x}(p+\sigma) + [\rho_s \alpha + \rho(1-\alpha)]\, g = 0 \qquad (7)$$

Neglecting the gas density in comparison to that of the solid we obtain

$$\frac{\partial}{\partial x}(p+\sigma) + \rho_s \alpha g = 0 \qquad (8)$$

By rearranging eq.(8) and applying the chain rule, it becomes

$$\frac{\partial p}{\partial x} + \frac{\partial \sigma}{\partial \alpha}\frac{\partial \alpha}{\partial x} + \rho_s \alpha g = 0 \qquad (9)$$

The modulus $\partial\sigma/\partial\alpha$, which is only a function of α, can be calculated from this

equation and the experimental data.

Assuming incompressible gas behavior, eq.(2) can be slightly simplified to

$$\frac{\partial}{\partial t}(1-\alpha)+\frac{\partial}{\partial x}[u_g(1-\alpha)]=0 \qquad (10)$$

The total continuity equation is obtained from combining eqs (1) and (10)

$$\frac{\partial}{\partial x}[\alpha u_s+(1-\alpha)u_g]=0 \qquad (11)$$

Equation (11) may be integrated, and with the boundary condition $u_s=u_g=0$ at the distributor, yield

$$\alpha u_s+(1-\alpha)u_g=0 \qquad (12)$$

From this equation and one of the species continuity equations, along with the experimental data, the gas and solid velocity can be calculated.

RESULTS AND DISCUSSION

Experimental results

A set of experimental measurements were taken using the equipment and procedure described in the preceding section.

For the distributor, Darcy's law can be applied:

$$u_0 = -\frac{k}{\mu}\Delta p \qquad (13)$$

The change in pressure drop across the distributor with time was measured by means of pressure transducer A. Thus, the change of gas velocity passing through the distributor with time can be calculated, as indicated in Fig.I2. It shows that once the air supply to the fluidized bed was shut off, the velocity was reduced to zero within 3 s and the bed started to collapse immediately.

The primary pressure data were a set of pressure drops against time at several locations above the distributor plate. The pressure drop per unit length decreases as a function of time at these locations as indicated in Fig.I3. The figures show that the whole process of bed collapse consists of several stages.

At first, upon shutting off the air supply, the large bubbles are discharged from the bed in a short time, about 2 or 3 s. The bed then comes into a state approaching minimum fluidization. Immediately following the discharge of the bubbles, the particles begin to settle out of the minimum fluidization state starting at the distributor plate. The air displaced by the settling particles moves upward keeping the particles above at or near minimum fluidization conditions. The particle settling moves up the bed as a sedimentation wave which is "seen" as a sudden fall off in the local pressure gradient or increase in solid fraction. Following the passage of the sedimentation wave, the particles continue to compact slightly from the weight of the settled particles above and the pressure gradient approaches zero.

This morphology of bed collapse is shown clearly in Fig.I3. The pressure drop per unit length across three adjacent bed sections, lower, middle and upper, are plotted against time. The earliest record with large fluctuations is the period of bubble discharge. Following it is a period during which the sedimentation wave passes through the lower section where the average pressure gradient falls while the two higher sections remain at minimum fluidization. The next period shows the wave in the middle section while the lower section compacts and the upper section remains at minimum fluidization. Finally, the wave enters the upper section while the lower two sections continue to compact.

As schematically displayed in Fig.I4, the bed can, at any instant of time during its collapse, be described in terms of three zones. Zone 1 is the approximately minimum fluidization condition zone which stretches from the top of the bed down to the upper face of the sedimentation wave. This zone has a uniform solid fraction, α_{mf}. It is assumed that the normal stress is zero at this solid fraction. The sedimentation wave, which has a finite thickness, is zone 2. The solid fraction changes from that of minimum fluidization to that of loose packing continuously from the top to the bottom of this zone. The bottom zone, 3, is a packed bed undergoing a slight compaction. Its solid fraction is essentially uniform, changes being so slight that they are not measurable with the x-ray system. During the period of bed collapse, zone 1 shrinks in length from that of the expanded bed height to zero, while zone 3 grows in length from zero to that of the loose packed bed height.

The sedimentation wave speed can be determined from Fig.3 by dividing the height of each pressure tap by the time at which the pressure gradient at that tap begins to change. Table I1 shows that the wave speed is constant through out the bed collapse.

The X-ray data which describes the sedimentation wave as it passes a point (a few mm in diameter) in the bed are shown in Fig I5(a). The thickness of the line

is due to a 10 Hz oscillation in the X-ray intensity as described by the power spectrum of the intensity, Fig.I5(b). A deconvolution of the oscillation gives a clearer description of the wave passage, Fig.I5(c).

Figure I6 is a plot of the solid fraction as a function of time as measured by the X-ray at a set of points at different elevations. It shows a constant sedimentation wave speed of 0.027 m/s, in excellent agreement with the wave speed obtained from the pressure measurement. Furthermore, it shows that the shape of the wave does not change significantly with elevation in the bed.

A plot of the position of the lower surface of the wave with time, Fig.I7, demonstrates the constancy of wave speed with bed elevation at 0.027 m/s. Extrapolating the line down to the distributor plate gives a sedimentation wave inception time of 3.08 s after the solenoid valve cut the air supply. Thus, as described above, all flow through the distributor ceased before the sedimentation wave left the distributor. With the wave speed, wave shape and wave inception time, the solid fraction in both time and space (elevation) can be described.

Computed results

Calculation of the normal stress modulus

By means of eq. (9), the normal stress modulus can be expressed as

$$\frac{\partial \sigma}{\partial \alpha} = -\frac{\frac{\partial p}{\partial x} + \rho_s \alpha g}{\frac{\partial \alpha}{\partial x}} \qquad (14)$$

The normal stress modulus in the above relation is a function of pressure gradient, solid fraction gradient and solid fraction. This relationship is readily evaluated from the measurements.

Using the chain rule in the X direction, we obtain

$$\frac{\partial p}{\partial x} = \frac{\partial p}{\partial t}\frac{\partial t}{\partial x} \qquad (15)$$

As already described, $\partial x/\partial t$, which is wave speed v_w, remains constant with time. A plot of pressure above freeboard pressure at different elevations along the bed vs collapsing time is given in Fig.I8. It shows that the pressure falls slowly when the wave is below the pressure tap and then rapidly as the wave passes the pressure tap. The slow fall period is due to the decreasing bed height while the

wave is still below the pressure tap. Thus, in order to collapse the corresponding curves of this pressure vs collapsing time into a function of a single variable, two adjustments must be made. An adjustment in time is made by defining an effective time, t^*, during the time the wave passes through an elevation X. Herein t^* is defined by

$$t^* = t - \frac{X - X_0}{v_w} \tag{16}$$

The second adjustment is to correct for the falling bed height by extrapolating the slowly falling pressure period through the rapidly falling pressure period and obtaining the difference between the two curves.

It can be seen from Fig.I9 that the corrected $\partial p/\partial t^*$ is clearly only a function of the time, t^*, during the wave passage. The data requires only a linear equation to provide an excellent fit during the wave passage for the three taps as

$$\frac{\partial p}{\partial t^*} = -195.1 + 4.571 t^* \tag{17}$$

Substituting eq.(17) into eq.(15), and with $\partial p/\partial t = \partial p/\partial t^*$, we have

$$\frac{\partial p}{\partial x} = -7226 + 169.3\, t^* \qquad (18)$$

Similarly, it may be seen from Fig.I6 that solid fraction within the sedimentation wave at any elevation changes from its initial value to its final value as a function only of the time, t^*. A linear equation is used here also to represent the data.

$$\alpha = \alpha_{mf} + 6.667 \times 10^{-3}\, t^* \qquad (19)$$

Since both p and α are only functions of t^* during the wave passage, we can substitute eq.(19) into eq.(18) to obtain

$$\frac{\partial p}{\partial x} = -2.018 \times 10^4 + 2.539 \times 10^4 \alpha \qquad (20)$$

The expression of solid fraction gradient can be found from eq.(19) and the wave speed

$$-\frac{\partial \alpha}{\partial x} = \frac{\dfrac{\partial \alpha}{\partial t^*}}{\dfrac{\partial x}{\partial t^*}} = 0.248 \qquad (21)$$

From these experimental data, the expression for normal stress modulus, eq.(14), can be evaluated

$$\frac{\partial \sigma}{\partial \alpha} = 1.597X10^{5}\alpha - 8.137X10^{4} \qquad (22)$$

It should be noted that an equation for solid normal stress modulus in which $\partial\sigma/\partial\alpha$ varies linearly with solid fraction, is an approximation for α near the values for minimum fluidization and loose packing. The data near the endpoints of the range are not accurate enough to include in the data fitting program.

Gidaspow and coworkers have defined $G(\varepsilon)=\partial\sigma/\partial\varepsilon$ as a particle-to-particle interaction coefficient(or modulus of elasticity). They have given various equations for $G(\varepsilon)$ which can readily be converted to $G(\alpha)$ by substituting $\varepsilon=1-\alpha$. Table I2 shows a comparison of our model with various equations obtained by Gidaspow and coworkers, as well as the correlations proposed by Massoudi et al. The equations of Shih et al. and Massoudi et al. give values of reasonable magnitude in the middle and at the loose packing end of the range. These give unreasonably high values near minimum fluidization conditions for our FCC powder.

It is expected that the stress increases exponentially in the range from loose packing to dense packing and our equation does not indicate this. Also, the normal stress modulus at the near minimum fluidization condition for our powder is essentially zero, which is a condition of our model that implies $dp/dx=\alpha\rho_s g$ at minimum fluidization.

Calculation of gas and solid velocities

As already shown in Fig.I5, the solid fraction distribution along the bed at any instant may be expressed as a function of the bed height as follows

$$\alpha = \alpha_{lp} \qquad X < X_w$$

$$\alpha = \alpha_{lp} - 0.248\,(X - X_w) \qquad X_w < X < X_w + \delta_w$$

$$\alpha = \alpha_{mf} \qquad X > X_w + \delta_w$$

where

α_{mf} - solid fraction at minimum fluidization

α_{lp} - solid fraction at loose packing

X_w - axial position of wave lower surface

δ_w - thickness of sedimentation wave

As the wave begins to pass a specified position X, an integration of solid fraction over the bed height to X yields

$$\int_0^X \alpha\, dX = \int_0^{X_w} \alpha_{lp}\, dX + \int_{X_w}^X [\alpha_{lp} - 0.248\,(X - X_w)]\, dX = \alpha_{lp} X - \frac{0.248}{2}\,(X - X_w)^2 \quad (23)$$

Differentiation and substitution gives

$$\frac{\partial}{\partial t}\int_0^X \alpha dX = 0.027\,(\alpha_{lp}-\alpha) \qquad (24)$$

This is the rate at which gas leaves the bed below the elevation X. From eq.(12), one of the species continuity equations and the above equation, both gas and solid velocities can be obtained as follows:

$$u_g = 0.027\,\frac{\alpha_{lp}-\alpha}{1-\alpha} \qquad (25)$$

$$u_s = \frac{-0.027}{\alpha}\,(\alpha_{lp}-\alpha) \qquad (26)$$

Calculation of hindrance factor or drag coefficient

The drag force coefficient K, representing the drag force exerted by the fluid on the particles in eq.(3), can be estimated by substituting eqs (25) and (26) into eq.(6) and neglecting changes in the gas density

$$K = \frac{\alpha(1-\alpha)^2}{0.027\,(\alpha_{lp}-\alpha)}\left(-\frac{\partial p}{\partial x}\right) \qquad (27)$$

Substituting in the $\partial p/\partial X$ data, the following drag force coefficient K can be

derived

$$K=\frac{\alpha(1-\alpha)^2}{0.027(\alpha_{lp}-\alpha)}(2.018\times10^4-2.539\times10^4\alpha) \qquad (28)$$

A comparison between this and other correlations is given in Table I3. It may be seen that the value of drag coefficient calculated by eq.(28) is close to the values obtained by the other two correlations except for α close to α_{lp}. As α approaches to α_{lp} , the drag coefficient from eq.(27) becomes undefined.

Considering Stokes settling of particles, we define the sum of the drag coefficient for all particles as

$$K_0=\frac{18\alpha\mu}{d_p^2} \qquad (29)$$

The particle settling hindrance factor caused by the presence of other particles in the suspension is defined as

$$f=\frac{K_0}{K} \qquad (30)$$

which can be expressed as a function of solid fraction from eqs (28) and (29)

$$f=\frac{0.486\mu}{d_p^2}\frac{\alpha_{lp}-\alpha}{(1-\alpha)^2(2.018\times10^4-2.539\times10^4\alpha)} \qquad (31)$$

CONCLUSIONS

Measurements of instantaneous pressure drop and local solid fraction at several elevations along a collapsing fluidized bed show very good agreement on the passage of the sedimentation wave. The wave velocity for the fluid cracking catalyst used in this experiment is 0.027 m/s.

The measurements along with a one-dimensional hydrodynamic model provide a linear equation for solid normal stress modulus between minimum fluidization and loose packing solid fraction for this powder. The drag coefficient in the gas phase momentum equation is evaluated directly from the measurements and is also evaluated as a hindrance factor. The drag coefficient agrees well with the Richardson-Zaki and Kozeny-Carman correlations.

ACKNOWLEDGMENT

This work was supported in part by the EXXON Research and Engineering

Company, Florham Park, NJ. Professor Chaim Gutfinger of the Department of Mechanical Engineering, Technion, Israel, provided the equations of the analytical section.

NOTATIONS

A	pressure transducer
B	pressure transducer
C	pressure transducer
d	diameter of particle
D	pressure transducer
f	hindrance factor
g	magnitude of the acceleration due to gravity, m/s^2
k	permeability, m^2
K	drag force coefficient, $N\text{-}s/m^4$
K_0	drag force coefficient defined by eq.(28), $N\text{-}s/m^4$
n	index of Richardson and Zaki's equation
p	pressure above freeboard pressure, N/m^2
t	collapsing time, s
t^*	effective time, defined by eq.(16), s
u_g	gas fluidizing velocity, m/s
u_0	average superficial gas velocity, m/s
u_s	particle velocity, m/s
v_w	speed of sedimentation wave, m/s
v_t	terminal velocity, m/s

X	axial coordinate, direction from the bottom toward top of the bed
X_w	axial position of wave upper surface, m
X_0	wave passes a specify point, m

GREEK LETTERS

α	solid fraction
α_{mf}	solid fraction of minimum fluidization
α_{lp}	solid fraction of loose packing
$G(\alpha)$	modulus of normal stress, N/m^2
δ_w	thickness of sedimentation wave, m
Δp	pressure drop, N/m^2
ε	void fraction
$G(\varepsilon)$	particle-to-particle interaction coefficient(modulus of elasticity)
μ	viscosity, kg/ms
ρ	density of fluidizing gas, kg/m^3
ρ_s	density of solid particle, kg/m^3
σ	solid normal stress, N/m^2

REFERENCES

Abrahamsen, A. R. and Geldart, D., 1980, Behaviour of gas-fluidized beds of fine powders. Part I. Homogeneous expansion. Powder Technol. **26**, 35-46.

Aldis, D. F. and Gidaspow, D., 1989, Combustion of a polydispersed solid using a

particle population balance. Powder Tech. **57**, 281-294.

Bouillard, J. X., Lyczkowski, R. W., Folga, S., Gidaspow, D., and Berry, G. F., 1977, Hydrodynamics of erosion of heat exchanger tubes in fluidized bed combustor. Can. J. Chem. Engng. **67**, 218-229

Ettehadieh, B., Gidaspow, D., and Lyczkowski, R. W., 1984, Hydrodynamics of fluidization in a semicircular bed with a jet. A.I.Ch.E. J. **30**, 529-536

Feindt, H. J., 1990, Radial and axial density fluctuations in a high velocity fluidized bed. Ph.D Thesis, The City University of New York, New York

Gidaspow, D., and Ettehdieh, B., 1983, Fluidization in two-dimensional beds with a jet: 2. Hydrodynamic modeling. I & EC Fundam. **22**, 193-201

Gidaspow, D., Shih, Y. T., Bouillard, J. X., and Wasan, D., 1989, Hydrodynamics of a lamella electrosettler. A.I.Ch.E. J. **35** 714-724

Jean R.-H., Rhonda J.Eubanks, Jiang Peijun and Liang-Shih, 1992, Fluidization behavior of polymeric particles in gas-solid fluidized beds. Chem. Engng. Sci. **47**, 325-335

Massoudi M., Rajagopal, K. R., Ekmann, J. M., and Mathur, M. P., 1977, Remarks on the modeling of fluidized systems. A.I.Ch.E. J. **38**, 471-472

Mutsers S. M. P. and Rietema, K., 1977, The effect of interparticle forces on the expansion of homogeneous gas fluidized beds. Powder Technol. **18**, 239

Richardson, J. F. and Zaki, W. N., 1954, Sedimentation and fluidization. Trans. Instn. Chem.Engr. **32**, 35-53

Shih, Y. T., Gidaspow, D., and Wasan, D. T., 1986, Sedimentation of fine particles in nonaqueous media. Colloids and Surf. **21**, 393-429

Shih, Y. T., Gidaspow, D., and Wasan, D. T., 1987, Hydrodynamics of sedimentation of multisized particles. Powder Tech. **50**, 201-215

Tsinontides, S.C.and Jackson, Roy , 1991, Yield stresses in uniformly fluidized suspensions. DOE/NSF workshop on flow of particles and fluids.

Table I1. Speed of sedimentation wave

Bed Section	Differential time [s]	Differential Spacing [m]	Velocity of wave [m/s]
Lower	11.0	0.292	0.027
Middle	8.0	0.212	0.027
Upper	6.4	0.170	0.027

Table.I2 Comparison with various correlations for $G(\alpha)$

Authors	Normal Stress modulus $[G(\alpha)]$	α=0.51 $[N/m^2]$	α=0.53 $[N/m^2]$	α=0.55 $[N/m^2]$
Present	Eq.(22)	~ 0	$3.271X10^3$	$6.465X10^3$
Gidaspow & Ettehadieh(1983)*	$G(\alpha)=10^{8.76\alpha-3.33}$	13.728	20.549	30.761
Shih et al. (1987)**	$G(\alpha)=10^{8.76\alpha-0.96}$	$3.218X10^3$	$4.817X10^3$	$7.211X10^3$
Ettehadieh et al. (1984)*	$G(\alpha)=10^{10.46\alpha-3.883}$	28.288	45.793	74.131
Gidaspow et al. (1989)*	$G(\alpha)=10^{10.5\alpha-1.5}$	$0.716X10^4$	$1.161X10^4$	$1.884X10^4$
Bouillard et al. (1989)*	$G(\alpha)=10^5e^{-600(-\alpha+0.624)}$	$1.969X10^{-25}$	$3.205X10^{-20}$	$5.216X10^{-15}$
Massoudi et al. (1992) [1]	$G(\alpha)=10^{23.39\alpha-7.33}$	$0.397X10^5$	$1.166X10^5$	$3.424X10^5$
Massoudi et al. (1992) [2]	$G(\alpha)=10^{13.11\alpha-3.21}$	$2.993X10^3$	$5.473X10^3$	$10.0X10^3$

* Synthesized

** From sedimentation data

Table I3. Comparison with various correlations for $K(\alpha)$

Authors	Drag coefficient $[K(\alpha)]$	$\alpha=0.51$ $[N\text{-}s/m^4]$	$\alpha=0.53$ $[N\text{-}s/m^4]$	$\alpha=0.55$ $[N\text{-}s/m^4]$
Present	Eq.(28)	$0.826X10^6$	$1.375X10^6$	-
Richardson & Zaki	$K=[\alpha\ {}_s g]/[v_t(1-\alpha)^n]$ n=4	$0.998X10^6$	$1.225X10^6$	$1.513X10^6$
Kozeny-Carman	$K=[180\alpha^2\mu]/d^2(1-\alpha)^2$	$1.107X10^6$	$1.299X10^6$	$1.526X10^6$

Fig.I1 Experimental Setup

1.Compressor;2.Reducer;3.Pressure gage;4.Solenoid valve;5.Needle valve;6.Rotometer;7.Fluidizing air supply;8.Purge air supply;9,10,11,12.Pressure transducer A,B,C,D;13.Fluidized bed;14.Plenum

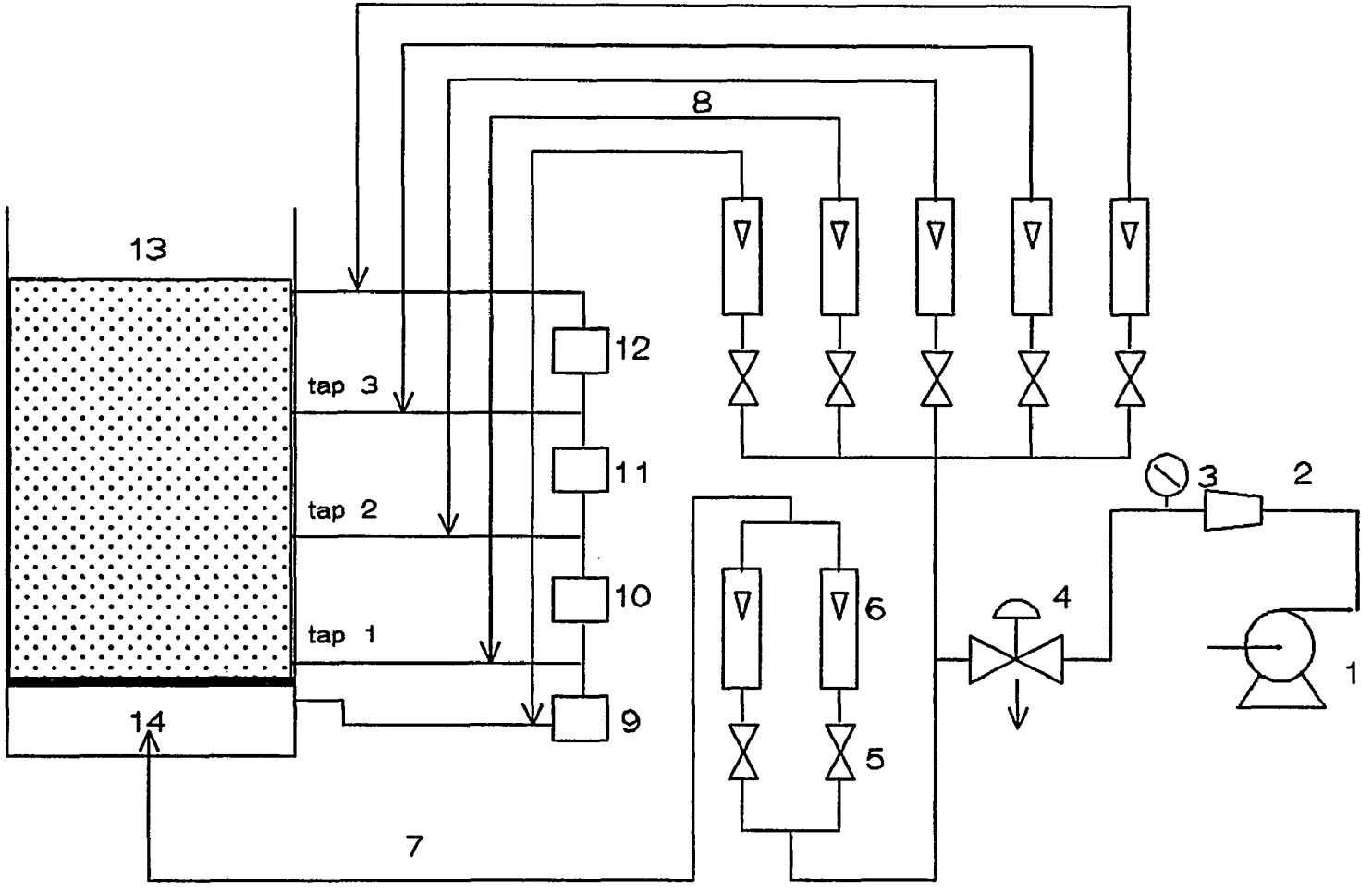

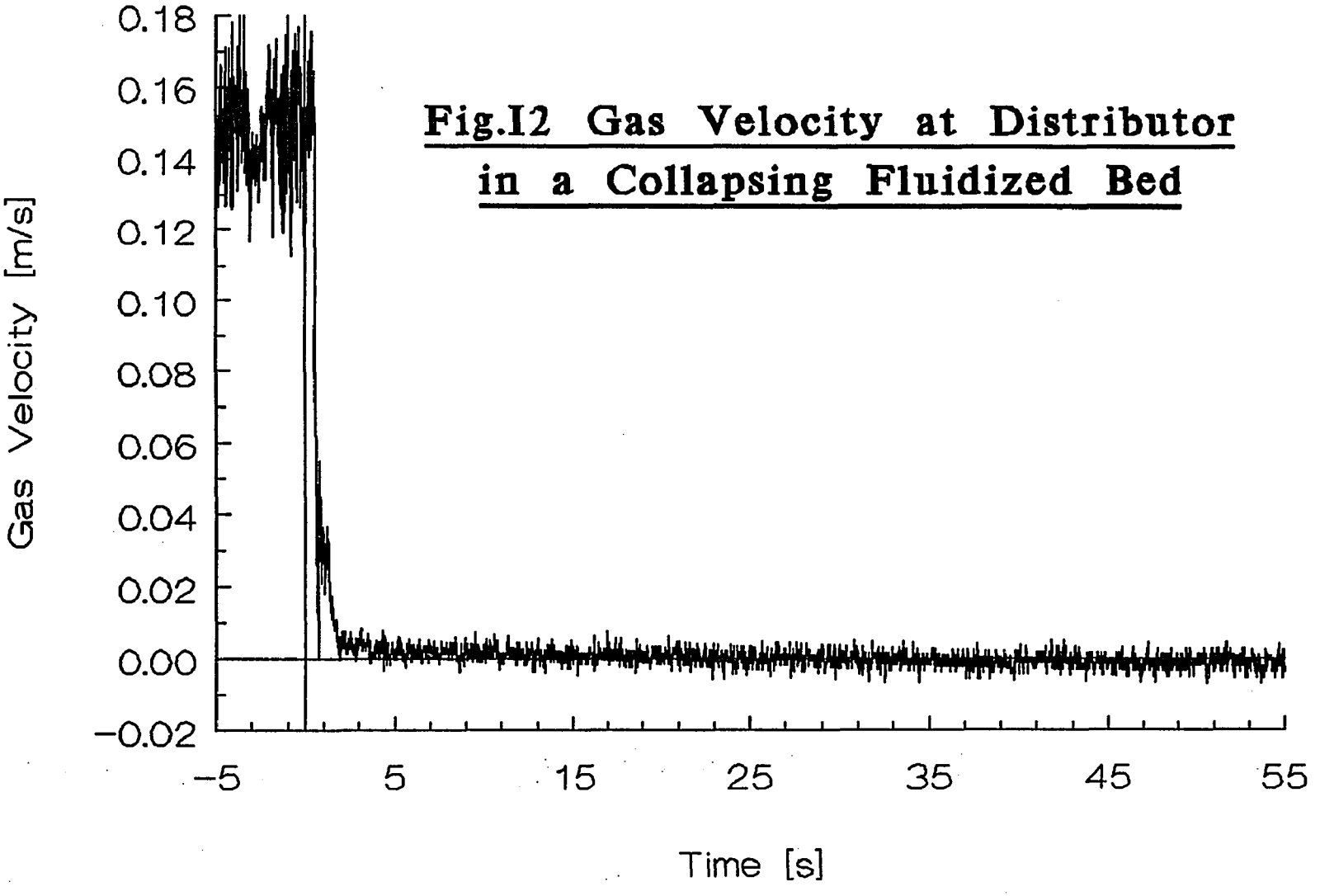

Fig.I2 Gas Velocity at Distributor in a Collapsing Fluidized Bed

Fig.I3 Pressure Drop Per Unit Length against Time for a Collapsing Fluidized Bed

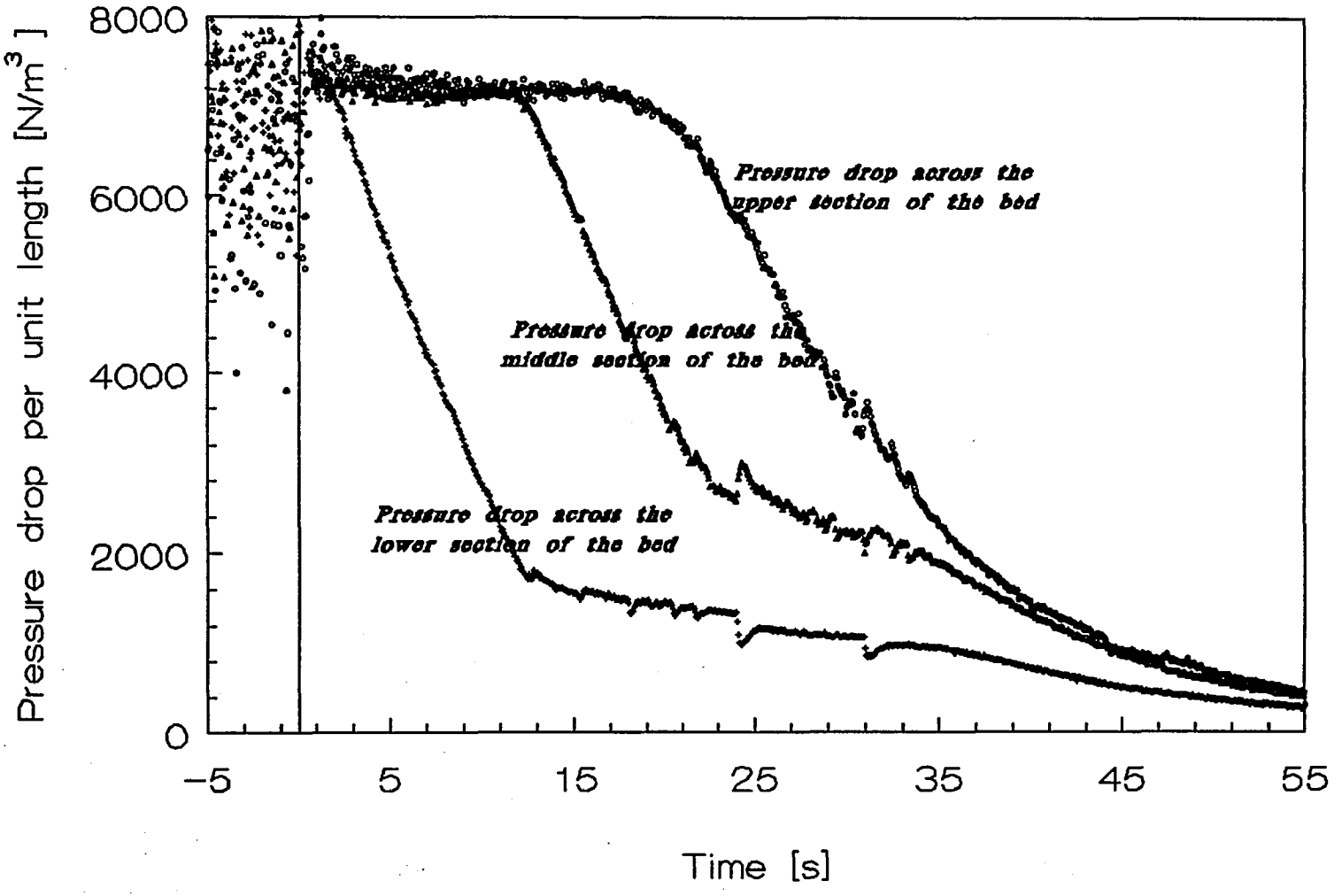

Fig.I4 Solid Fraction Zones in a Collapsing Fluidized Bed

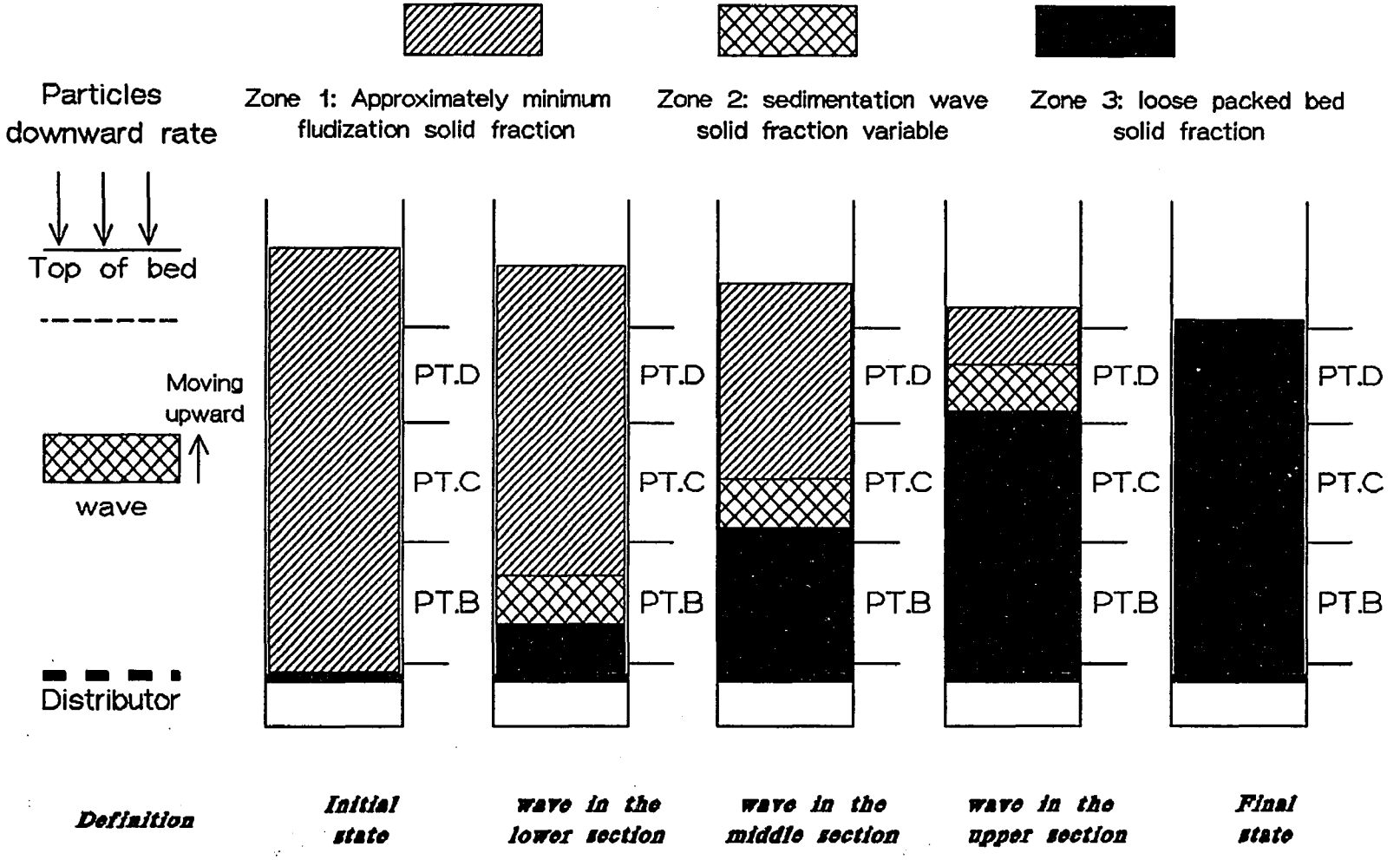

Fig.I5 X-ray Measured Solid Fraction as a Function of Time

Fig.5a The Solid Fraction as a Function of Time at different elevations

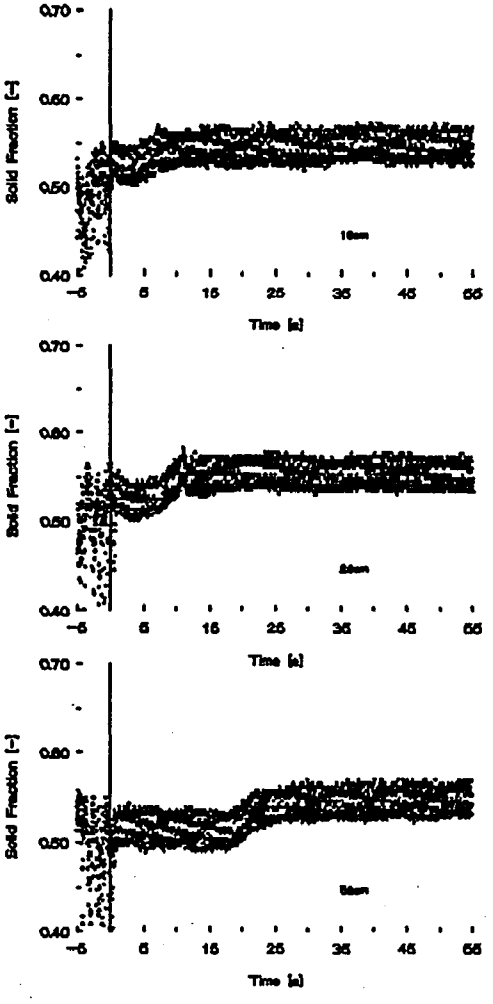

Fig.5b Power Spectrum of The Incident X-ray Intensity

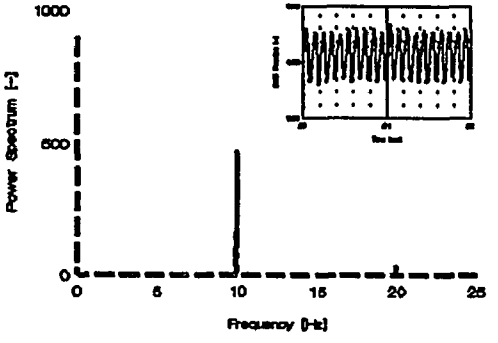

Fig.5c X-ray Solid Fraction Following Deconvolution

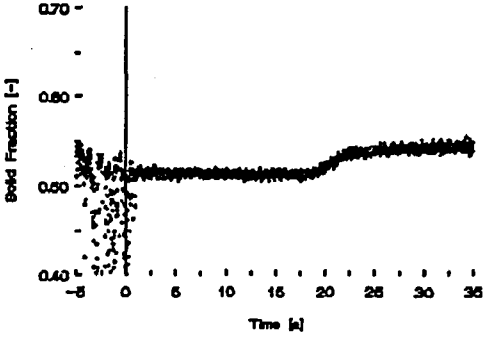

Fig.I6 Solid Fraction Distribution along the Bed as a Function of Time and Elevation

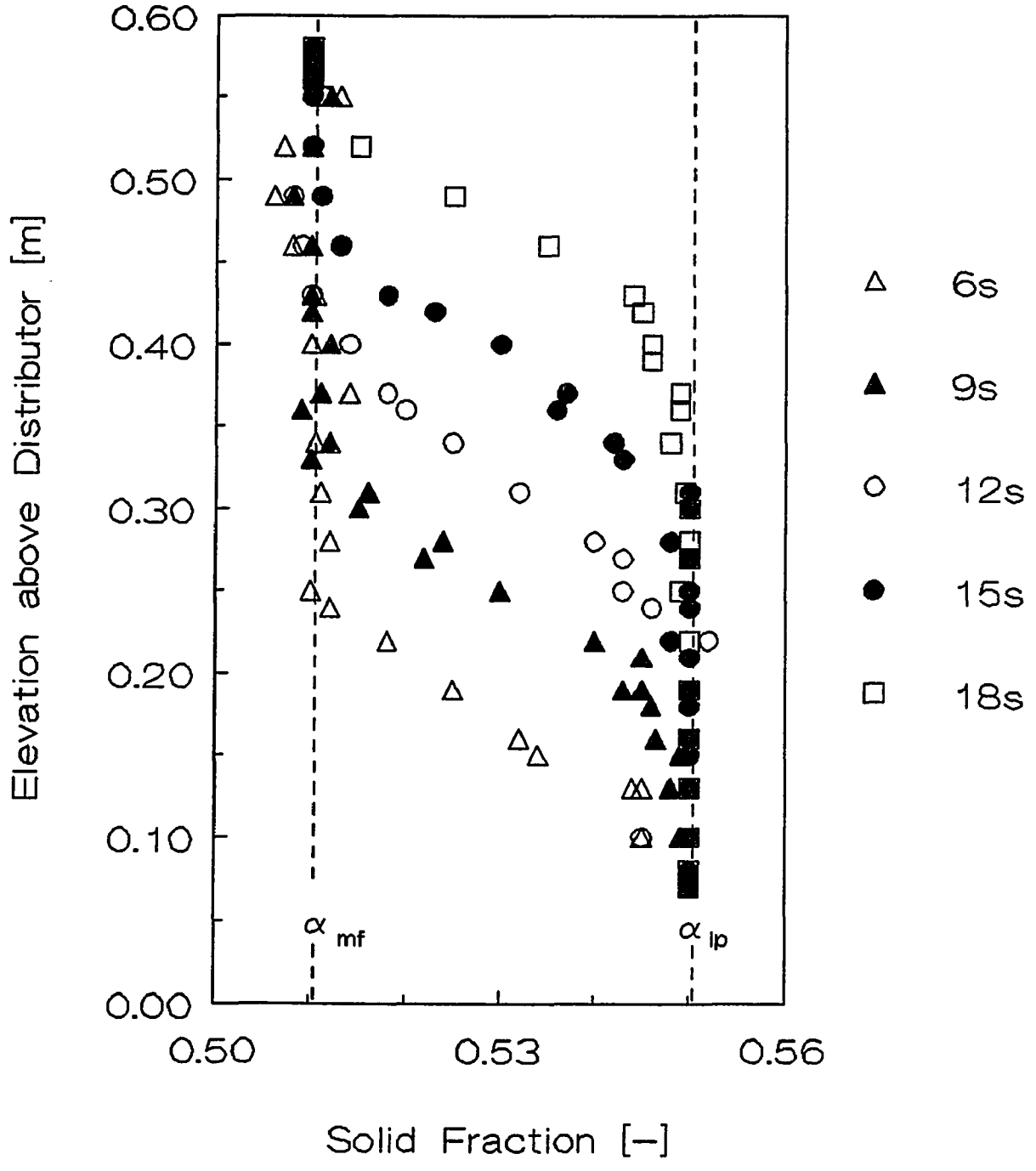

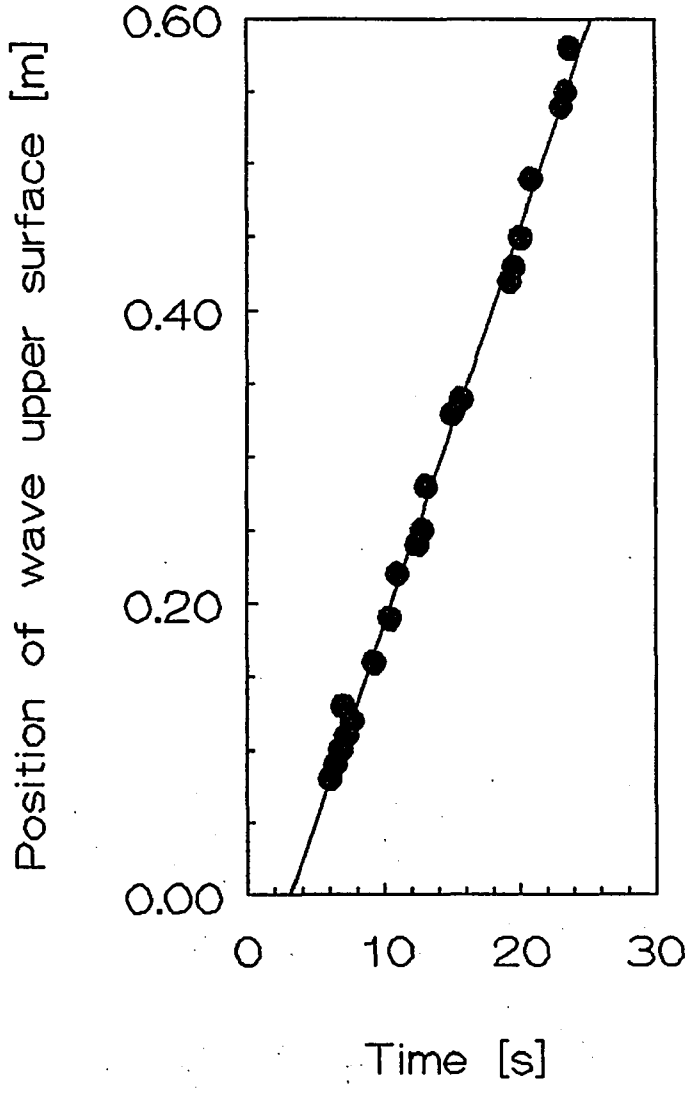

Fig.I7 Location of Wave lower Surface as a Function of Time

Speed of sedimentation wave
0.027 m/s

*** X-ray Data**

Fig.I8 Pressure above Freeboard Pressure at Different Elevations against Time

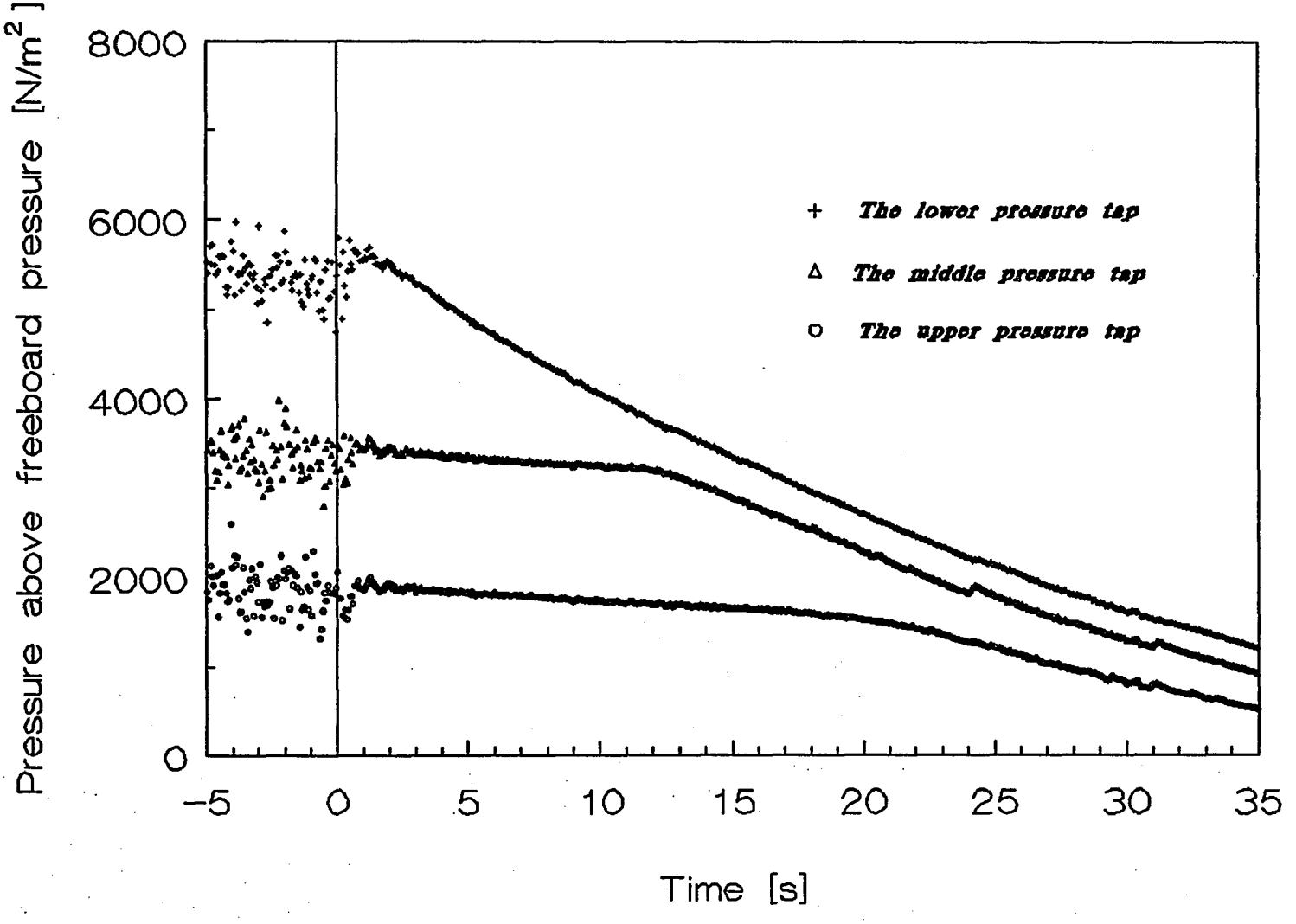

Fig.I9 The Pressure Gradient as a Function of Time at Different Elevations

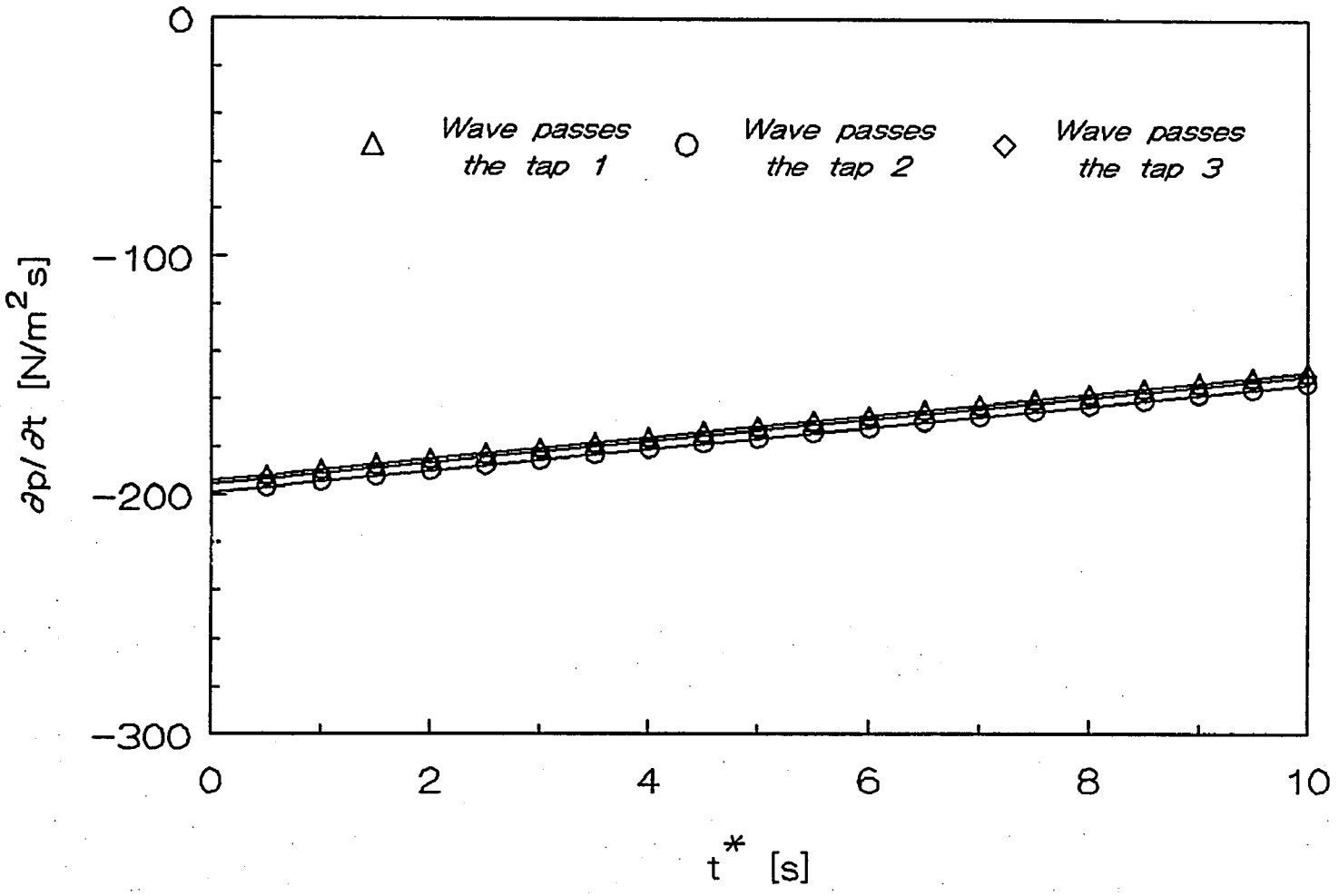

PART II. THE SHAPE AND EXTENT OF THE VOID FORMED BY A HORIZONTAL JET IN A FLUIDIZED BED

INTRODUCTION

In industrial fluidized bed reactors, reactant gas is often introduced into a reactor as a horizontally directed jet. Research seeking to understand the dynamics of gas and solid motion in such reactors resulting from the introduction of the jet has considerable significance for improving reactor design.

The literature to date reveals little of the dynamic behavior of gas and solid arising from a horizontal jet. Lummi and Baskakov (1967) injected a CO_2 tracer with an air jet and measured subsequent CO_2 concentrations in the bed to obtain mixing rates. Zenz (1968) presented a curve to predict horizontal jet penetration depth. Shakhova (1968) derived an expression for horizontal jet penetration depth. Kozin and Baskakov (1967) proposed a penetration correlation referred to a specific design of cap-type air distributor. Merry (1971) measured the penetration depths of horizontal air jets injected into fluidized beds of sand, kale seed and steel shot and derived a simple model for jet penetration depth. These workers were

mainly concerned with the expression for jet penetration depth. The dynamics of a jet discharged into a fluidized bed was reported on by Shakhova and Minakev (1971), using the ratio of the length of the gas plume to the height of the fluid bed above the nozzle to describe two characteristic modes of jet behavior, bubble flow and coherent flow. Two recent papers by Xuerub et al (1991a, 1991b) described the behavior of thin, two-dimensional, horizontal and inclined jets. They showed several important jet characteristics such as the proclivity of bubble tracks to hug the wall through which the jet is introduced. Further, they discussed the existence of a dragging zone of particles from the dense phase into the jet near the injection zone. However, the behavior of a two-dimensional system is expected to be quite different from that of a three-dimensional system because, in the latter case, these is a path for gas and solid to move around the sides of the jet. This prevents the jet ceiling from becoming a stagnant zone as it does in the two-dimensional geometry where the jet and the bubble track isolate the ceiling from the rest of the bed. Thus, the extent of the void formed by the three-dimensional horizontal jet and its coherence or integrity , as well as the distortion of the fluidized bed by the jet flow is still not understood well. Furthermore, a general technique for identifying the gas jet flow region and the bubble track region based on measurement is still lacking.

The aim of this work is to investigate the hydrodynamic behavior of a three-

dimensional fluidized bed with a horizontal gas jet. The technique employed is to use an X-ray system to obtain maps of the mean and fluctuating solid fraction. With these maps the extent of the void formed by the horizontal jet and the region compacted by the entrained gas can be obtained. Furthermore the regions of coherent jet flow and bubbling bed flow can be determined from the autocorrelation and power spectrum of the fluctuating signal. Finally, jet penetration correlations from the literature are compared the unique X-ray data obtained in this work.

EXPERIMENTAL

Apparatus

A schematic diagram of the apparatus used is shown in Fig.II1. The bed was contained in a rectangular vessel of Plexiglas, with dimensions 0.15 m X 0.38 m X 1.22 m high. A cyclone was located at the gas outlet of the vessel and exhaust from the cyclone passed through a bag filter. The solid disengaged in the cyclone was returned to the bed through a dipleg. The fluidized height was maintained at about 0.85 m. The solid powder was an Englelhard HFZ-33 FCC cracking catalyst, and its properties are given in Table II1. The fluidizing gas used for the experiment

was air at ambient conditions. Rotameters were fitted into the line to meter the air flow rate. The superficial fluidizing velocity was held at 0.04 m/s for the experiment. A circular jet nozzle module, either 0.64 or 1.27 cm in diameter, was located 0.31 m above the gas distributor. The jet was injected horizontally into the fluidized bed using a second metered compressed air supply.

An x-ray absorption system was used to obtain the solid fraction mean and fluctuation data. The system is described in detail in Feindt (1990). The x-ray source was designed for continuous output and high intensity operation. The x-ray image of the bed was projected onto an 23 cm image intensifier screen. It converted the x-ray into visible light and projected it onto a 8 cm output screen. A mirror with an angle of 45^0 to the screen projected 90% of the light onto a curved 15 cm screen through a lens. The screen was equipped with 48 phototransistors, all at equal distance from the image intensifier screen. Of these, 13 phototransistors arranged in a row scanning the projected image of the bed across a horizontal plane were used, as shown in Fig.II2. The entire x-ray system was mounted on a platform that could be moved up and down along the vessel.

Data analysis

The measurement principle is based on the Lambert-Beer law

$$dI = - \mu I \, ds \qquad (1)$$

where

dI = change of the intensity of the beam passing through the adsorbing medium

s = length of beam passing through absorbing medium

μ = attenuation coefficient

Introducing k for the mass attenuation coefficient and ρ for the medium density

$$\mu = k \cdot \rho \qquad (2)$$

In the system, the equation 1 can be expressed as:

$$\ln \frac{I_{[w+s]}}{I_0} - \ln \frac{I_w}{I_0} = - \int_s k \rho \xi (x, y) \, ds \qquad (3)$$

where

s = chord length

ξ = local solid fraction

Therefore, the instantaneous solid fraction at any desired elevation and horizontal position can be obtained by averaging on a chord through the 0.15 m thickness of the bed used, assuming that the attenuation coefficient of the air is negligible.

The voltage-time signals corresponding to the changes of intensity were sampled at the rate of 50 Hz by a Dell 386/20 mhz computer with an Metra-byte Das-20 analog to digital converter board. By means of Eq.3, the signals were converted to instantaneous solid fraction signals. The data acquired in this way was used to calculate the mean values, the auto-correlation functions, the power spectrum and the normalized standard deviations of the solid fraction values.

The mean solid fraction through the bed was computed as

$$1-\bar{\epsilon}=\frac{1}{T}\int_0^T (1-\epsilon)\,dt \qquad (4)$$

The difference between the time-mean solid fraction of the bubbling bed without the jet and with the jet was interpreted as a void or "hole" resulting from the jet

gas in the bed. i.e.

$$\overline{\epsilon_J}-\overline{\epsilon_B}=(1-\overline{\epsilon})_B-(1-\overline{\epsilon})_J \tag{5}$$

This term is called herein the solid fraction decrement. In order to use this data to calculate the statistical properties of the solid fraction, we define a fluctuating component (ε') as

$$1-\epsilon=(1-\overline{\epsilon})-(1-\epsilon)' \tag{6}$$

and

$$-(1-\epsilon)'=\epsilon' \tag{7}$$

Since a fluctuation in solid fraction is the negative of a fluctuation in void fraction.

The standard deviation (rms) of the apparent solid fraction fluctuation, σ, normalized by the x-ray mean value of the solid fraction (NSD) can be expressed as

$$NSD=\frac{\sigma}{1-\overline{\epsilon}} \tag{8}$$

The auto-correlation function and the auto-correlation coefficient can also be

expressed, respectively, as

$$R_{\epsilon'}(\tau)=\lim_{T\to\infty}\frac{1}{T}\int_0^T \epsilon'(t)\epsilon'(t+\tau)dt \tag{9}$$

$$\rho_{\epsilon'}(\tau)=\frac{R_{\epsilon'}(\tau)}{\sigma^2} \tag{10}$$

The power spectral density function can also be calculated by Fast Fourier Transform (FFT)

$$S_{\epsilon'}(f)=\int_{-\infty}^{\infty} R_{\epsilon'}(\tau)e^{-j2\pi f\tau}d\tau \tag{11}$$

and then, multiplying the complex spectrum by its complex conjugate, $S_{\epsilon'}^*$, yielding

$$PSDF=\overline{S_{\epsilon'}\cdot S_{\epsilon'}^*}=\overline{S_{\epsilon'}^2} \tag{12}$$

For each run, the instantaneous solid fraction with the jet turned on and with the jet turned off at 78 different vertical and horizontal positions were obtained by

moving the x-ray imaging system up and down along the bed. At each selected location, a set of 9216 data points were obtained for every experimental run. This set corresponds to about a three minutes record length, which was found experimentally to be sufficient to give a true steady state value.

RESULTS AND DISCUSSION

Four experimental series were carried out with the two jet nozzles, comprising two different jet velocities for each jet diameter: for the 0.64 cm nozzle, 23 and 69 m/s; for the 1.27 cm nozzle, 23 and 46 m/s.

The extent of the void formed by the horizontal jet

Mean solid fraction decrements as a function of horizontal position with vertical position as parameter are plotted in Figures II3A through II3D. These figures indicate the locations at which the void fractions are increased and decreased by the presence of the jet. The origin, (0,0), corresponds to the center of the nozzle position. As seen from these maps, the horizontal jet void discharges one or more

bubble trains from its upper surface. The bubble trains do not all leave from the far end of the void. One chain of bubbles is stabilized along the nozzle wall of the vessel. In addition, other bubble trains emerge from the void over its length. It is also seen from these figures that the length of the void or hole increases with increasing jet momentum and the bubble trains move further from the nozzle. Furthermore, the solid fraction decrements in the void region increase with the increasing mass flowrate of the gas jet. This indicates that the dimension of the hole parallel to the X-ray beam path also increases.

Two other observations of some importance can be made from these figures. The first is that the jet void curves upward away from the nozzle, as would be expected. The second is that the jet entrains gas from the bed underneath and to the right of the jet void causing a wake-like compaction (negative solid fraction decrement) of the solid. This latter point will be discussed in a later section.

The data shown in Figure II3 are replotted in Figs.II4 A, B, C and D by marking horizontal and vertical position with solid circles where the solid fraction decrements are larger than 0.01. Also plotted as open circles are the locations at which the decrement is negative. The dashed lines represent the bubble track paths. Examination of these figures leads to the conclusion that jet gas entering the bed produces a void region along the top of which bubble trains are discharged. For the

nozzle diameter of 0.64 cm, in the case of the lower jet velocity, two trains of bubbles are formed. Both of them are located close to the vessel wall. In the case of the higher velocity, one of the two bubble trains moves farther out, about 4 cm away from the wall, as indicated by an arrow in Fig.II4B, widening the high voidage area. For the nozzle diameter of 1.27 cm, both jet velocities have higher mass flowrates than the two cases with the 0.64 m nozzle diameter, establishing more bubble paths with higher voidage, as shown in Fig.II4C and Fig.II4D. In these figures, it is also seen that one train of bubbles still stayed close to the end wall, while the others moved farther out along the jet axis.

A statistical analysis of the solid fraction fluctuation signals yields further confirmation of these results. The normalized standard deviations of the fluctuation as a function of vertical position with horizontal position are plotted in Figs.II5A, B, C and D, respectively. In Fig.II5A, the smallest air flowrate in the experimental range, the solid fraction fluctuation signals recorded at both 2.96 and 5.1 cm away from the wall did not change along the bed height. This means that the jet did not discharge bubbles to these regions. However, the signals at the position near the wall showed large fluctuations, especially at 1.34 cm away from the wall. As mentioned above, this was the path of bubble train. In Fig.II5D, the largest flow rate in the experimental range, signals received from every position all showed extremely large fluctuations which indicated that bubble trains passed through all

measured positions and covered a large region. The picture of the bubble region discharged from the jet derived from Fig.II5A to II5D is similar to that derived from Fig.II4A to II4D. Thus, there is agreement between the bubble track paths obtained from the mean void fraction with these obtained from the standard deviation of the fluctuation.

Penetration length

In order to define a jet penetration length, it was assumed that the jet did not penetrate beyond the horizontal position at which all solid fraction decrements measured at different vertical positions were within ±0.015. This value was chosen empirically because it appeared to always separate the void-bubble train zone on the right from the compaction zone. Using this definition of penetration length, the experimental penetration length was compared with the values predicted by various correlations as plotted in Fig.II6. The figure shows that the experimental data agreed well with the data predicted by the correlations of Merry (1971), Zene (1968) as well as Shakhova (1968). The experimental data also confirmed Merry's conclusions that the penetration depth increases with nozzle diameter and jet nozzle velocity. The data of Xuereb et al. (1991a) also agreed reasonably well with the correlations of Merry and Shakhova.

The compacted region formed by the horizontal jet

Another characteristic region of the jet field, the compacted solid or wake region, is also illustrated by the figures discussed above. From Figs.II3A, B, C, and D or II4A, B, C, and D, it can be seen that the compacted region, which is shown by negative solid fraction decrements is extensive. This region forms because the pressure in the lower part of the void formed by the jet is lower than that in the surrounding two-phase region. The gas from the bed is entrained into the void and bubble trains. This compacted bed region below the void appears to be similar in nature to the wake below a bubble in a fluidized bed. Furthermore, as the bubble trains rise, the upper part solid carried up by the bubbles moves back down to the right of the train, compacting this region of the bed. The compaction appears to particularly strong in the regions below and just beyond jet void penetration. It appears that this compacted region coincides with the dragging zone of particles described by Xuereb et al. (1991a).

Differentiation between void, bubbles and compaction regions

The presence of a periodic component in the solid fraction fluctuations at a

location in the bed is indicative of the presence of a bubble train. Thus, by comparing the auto-correlation functions of signals at the different positions, the locations of jet void and bubble train can be differentiated. The upper graphs in Fig.II7 and Fig.II8 show the signals from the fluidized bed without a jet, while the middle and lower graphs show signals with different velocity jets. Fig.II7 shows that a periodic oscillation of the signal is present at (1 cm, 1.34 cm) with the 23 m/s jet but is not present without the jet or with the 69 m/s jet. Similar to Fig.II7, Fig.II8 shows periodicity only with the 69 m/s at (3 cm, 5.1 cm). As can be seen in Fig II3a, the 23 m/s jet has a strong solid fraction decrement at the point (1 cm, 1.34 cm). Coupling the two pieces of information supports the conclusion that a bubble train has already formed at this point. For the 69 m/s case, the solid fraction decrement is also large but the apparent lack of periodicity as shown by the autocorrelation leads to the conclusion that the coherent void occupies this space. Further away from the nozzle, the point at (3 cm, 5.1 cm), Fig.II8 shows an autocorrelation function consistent with the compaction zone shown in Fig II3a for the 23 m/s jet. However, for the high velocity jet, the autocorrelation function shows a bubble train consistent with the large solid fraction decrement shown at this point in Fig.II3b.

Another characteristic feature for identifying a coherent void, bubble track or compacted region is the power spectrum of the fluctuations of solid fraction.

Figure II9 shows the power spectrum calculated from the same signals as that of Fig.II8. There is a single major frequency peak in the power spectrum with the 69 m/s jet, which represents the characteristic frequency of the periodic component of the fluctuations in the bubble track. Due to the random component in the compacted region, such as solid entrained by the jet, no clear frequency peak is observed in the power spectrum of the signals with the 23 m/s jet. The power spectrum for a coherent void, which is not shown, also does not exhibit any characteristic peak region. This analysis is in agreement with the results of the auto-correlation functions. Consequently, for identification of the various regions in the fluidized bed formed by the horizontal jet, this method is proposed which utilizes the distinctive features of the mean solid fraction decrement, the auto-correlation functions and the power spectrum functions of fluctuating signals.

Based on this methodology, a description of the individual regions can be constructed. A typical flow region map obtained by analyzing the auto-correlation functions is shown in Fig.II10. As schematically displayed in this figure, three regions can be located in the X-ray field. Region 1 is the coherent void region, which does not show the periodicity typical of bubble trains. The bubble track region is region 2. The jet gas leaves the coherent void region as bubbles and the autocorrelation functions in the tracks show a clear periodic shape. The compacted region, 3, results from the wakelike behavor under and to the right of the void and

the downflow of solids to the right of the bubble tracks. As shown in Fig.II8, the autocorrelation function in this region also does not exhibit a clear periodic pattern.

CONCLUSIONS

The following conclusions can be drawn from the analysis of the experimental results presented herein:

This experimental technique clearly shows that the horizontal jet forms three regions in the fluidized bed - a coherent void, bubble trains and a surrounding compaction zone.

Wake jets turn upward close the inlet wall and form bubble trains along the wall. Strong jets penetrate deeper into the bed and form multiple bubble trains which leave from across the upper surface of the void.

The jet penetration lengths measured agreed with the correlations of Merry (1971), Zene (1968) and Shakhova (1968).

NOTATIONS

d_p	mean particle diameter, m
d_0	nozzle diameter, m
dI	change of the intensity of the beam passing through the adsorbing medium
g	acceleration of gravity, m/s2
I	intensity of x-ray beam
I_0	intensity of the reference x-ray beam
I_w	intensity of x-ray beam passing through the wall of the bed
I_s	Intensity of x-ray beam passing through the solid
k	mass attenuation coefficient
L	penetration length, m
NSD	normalized standard deviation
PSDF	power spectrum density function
$R_{\varepsilon'}$	auto correlation function
s	chord length
$S_{\varepsilon'}$	Fourier transform of the autocorrelation of ε'
u	superficial gas fluidizing velocity, m/s
u_j	jet velocity, m/s
u_{mf}	minimum fluidization velocity, m/s
x	length of beam passing through absorbing medium
X	co-ordinate, horizontal direction
Y	co-ordinate, vertical direction

GREEK LETTERS

ε	void fraction
ε_{mf}	void fraction at minimum fluidization
ε_J	void fraction with the jet
ε_b	void fraction without the jet
μ	attenuation coefficient
ξ	local solid fraction
ρ	density of solid particle [kg/m^3]
$\rho_{\varepsilon'}$	autocorrelation coefficient
σ	standard deviation
ϕ	sphericity of the solid particle

ACKNOWLEDGEMENTS

This work was supported by The EXXON Research and Engineering Company, Florham Park, NJ.

REFERENCES

Feindt, H.J. "Radial and Axial Density Fluctuations in A High Velocity Fluidized Bed" Ph.D. Thesis, The City Univ.of New York (1990)

Kozin, B.E. and Baskakov, A.P. Khim. Tekhnol.Topl.Masel 3, 4(1967)

Lummi, A.P. and Baskakov, A.P., Khim. Prom., 43,7,522 (1967)

Merry, J.M.D "Penetration of A Horizontal Gas Jet into A Fluidized Bed" Trans. Instn. Chem. Engrs.49, 189(1971)

Shakhova, N.A. Inzh. Fiz. Zh. 14, No. 1, 61,(1968)

Shakhova N.A. and G.A. Minayev "Aerodynamics of Jets Discharged into Fluidized Beds" Heat Transfer-Soviet Research, 4(1) 133 (1972)

Xuereb, C., C.Laguerie and et T.Baron "Etude du comportement de jets continus horizontaux ou inclines introduits dans un lit fluidise pan un gaz, deuxieme partie: profils de vitesse du vitesse du gaz dans les jets horizontaux" Powder Technol.,64, 271 (1991)

Xuereb, C., C.Laguerie and et T.Baron "Etude du comportement de jets continus horizontaux ou inclines introduits dans un lit fluidise pan un gaz, I:Morphologie des jets" Powder Technol.,67, 43 (1991)

Zenz, F.A. Inst. Chem. Eng. Symp. ser. 30, 136 (1968)

Table II1 The Solid Properties for Engelhard FCC Catalyst, HFZ-33

Mean Particle Size d_p [μm]	59
Particle Size Range [μm]	20~120
Sphericity [ϕ]	1
Particle Density [kg/m^3]	1450
Minimum Fluidization Velocity u_{mf}[cm/s]	0.9*
Minimum Void Fraction [-]	0.48

* Measured value

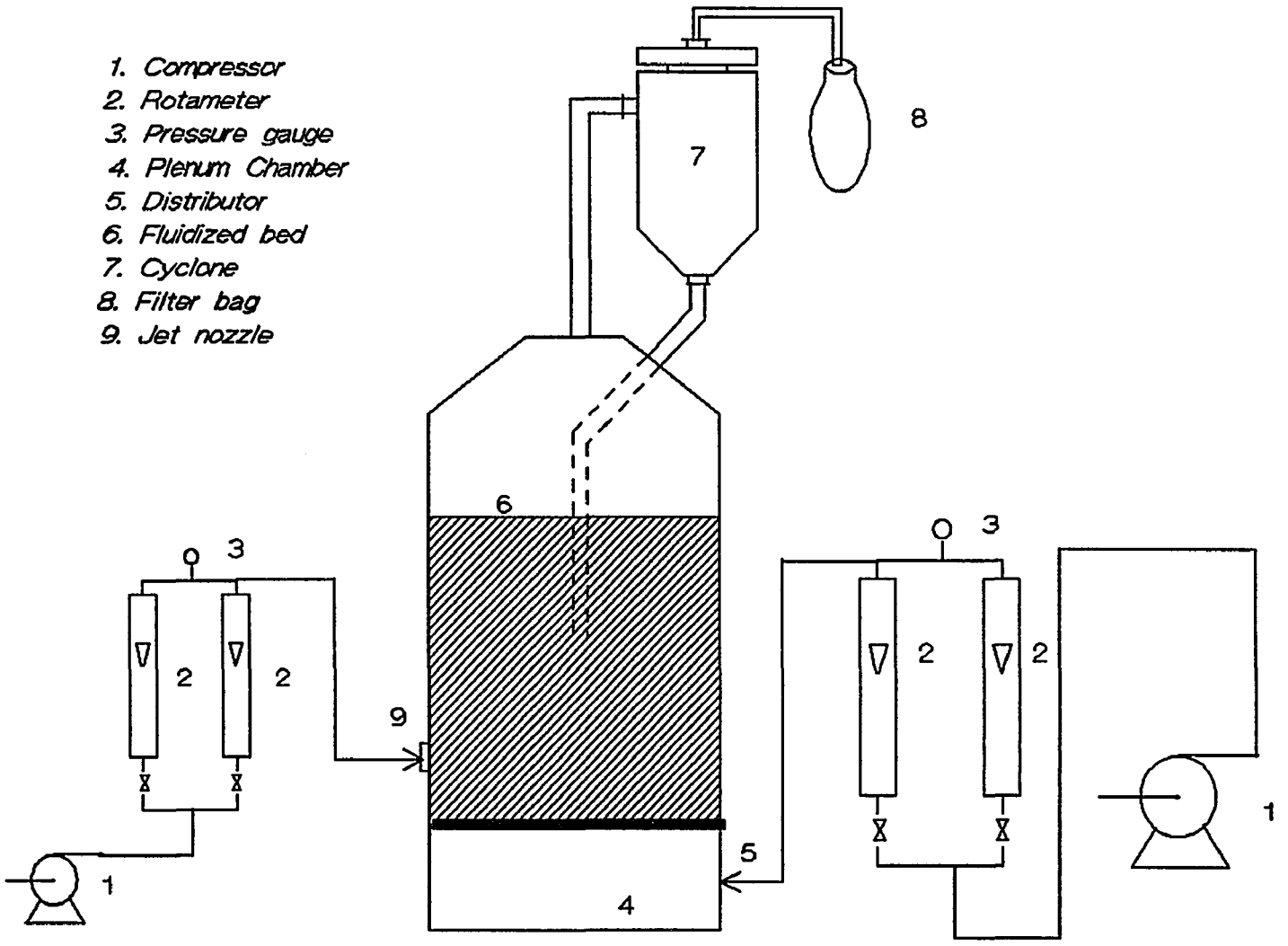

Fig.II1. Schematic diagram of experimental apparatus

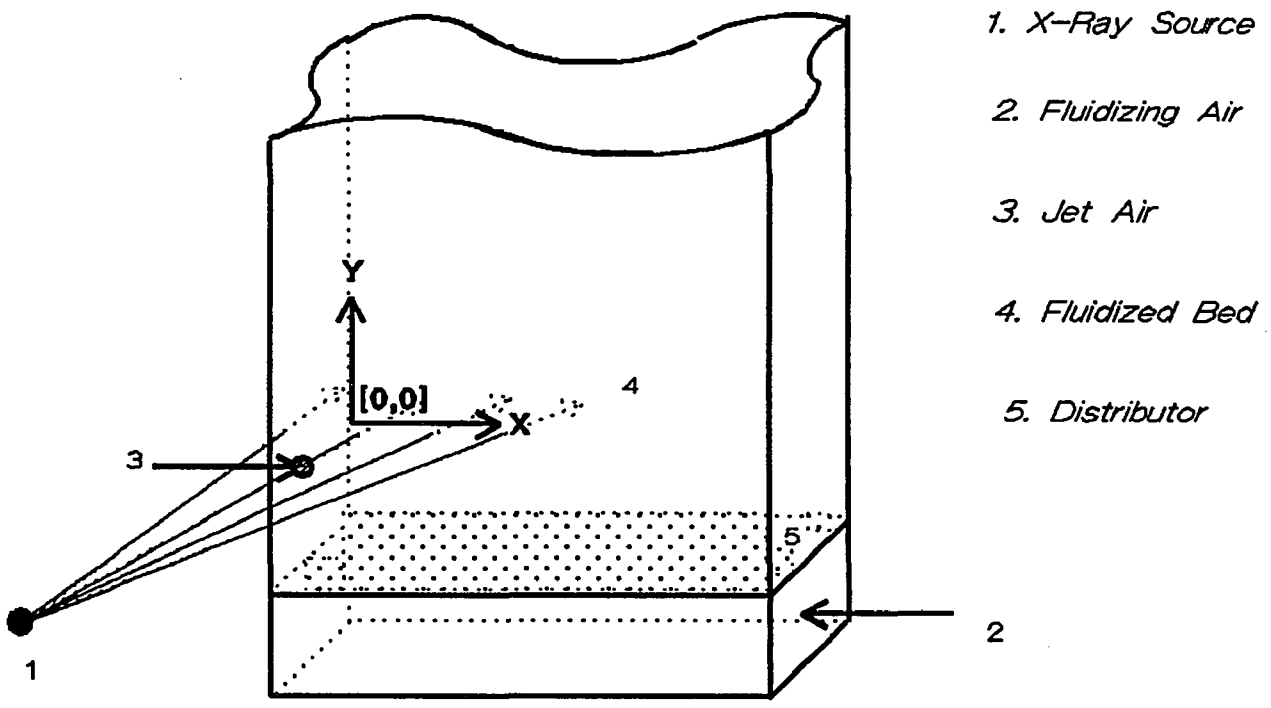

Fig.II2 Schematic of X - ray Absorption system

Fig.II3A Solid Fraction Decrement as a Function of Horizontal Position with Vertical Position as Parameter

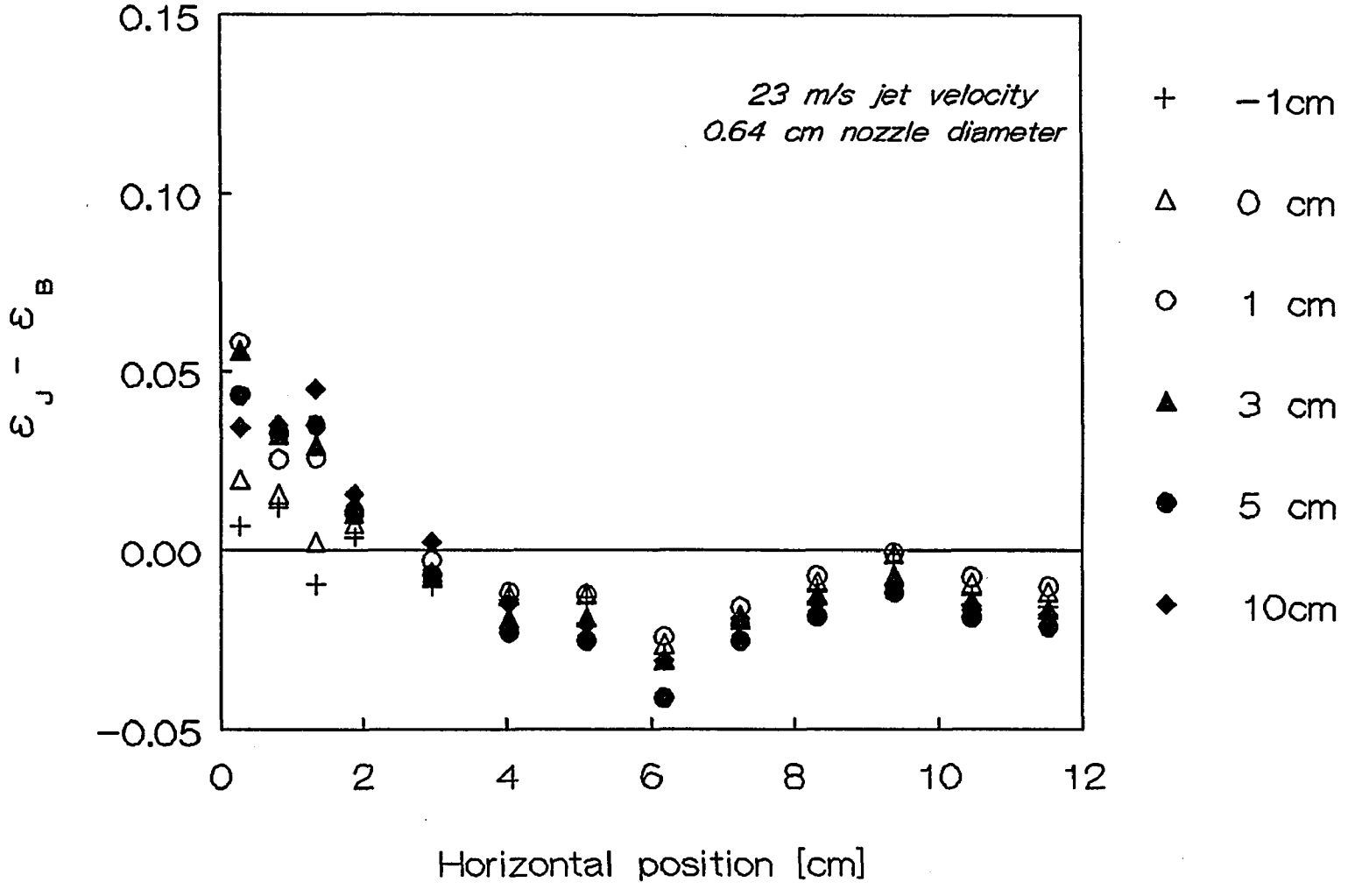

Fig.II3B Solid Fraction Decrement as a Function of Horizontal Position with Vertical Position as Parameter

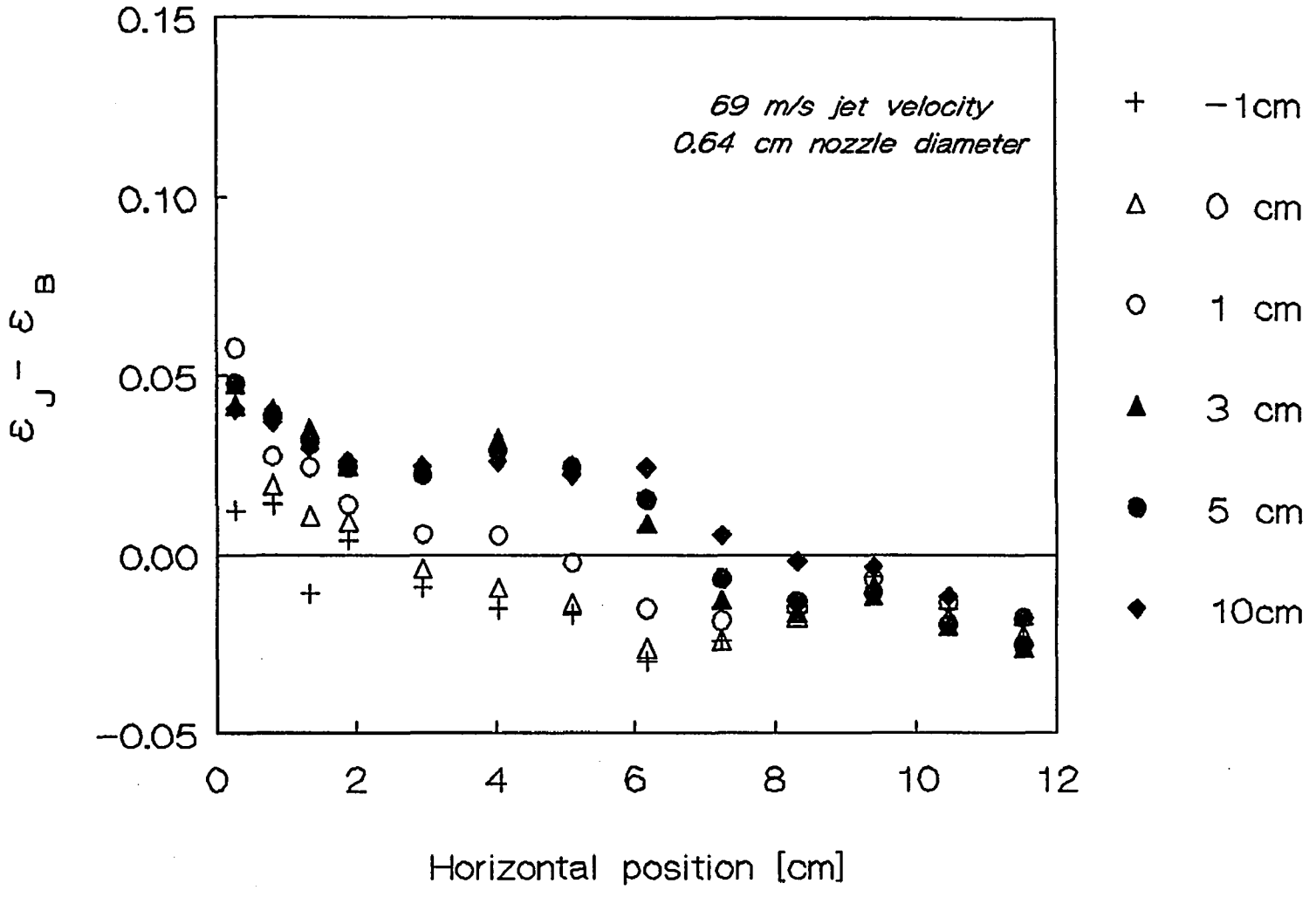

Fig.II3C Solid Fraction Decrement as a Function of Horizontal Position with Vertical Position as Parameter

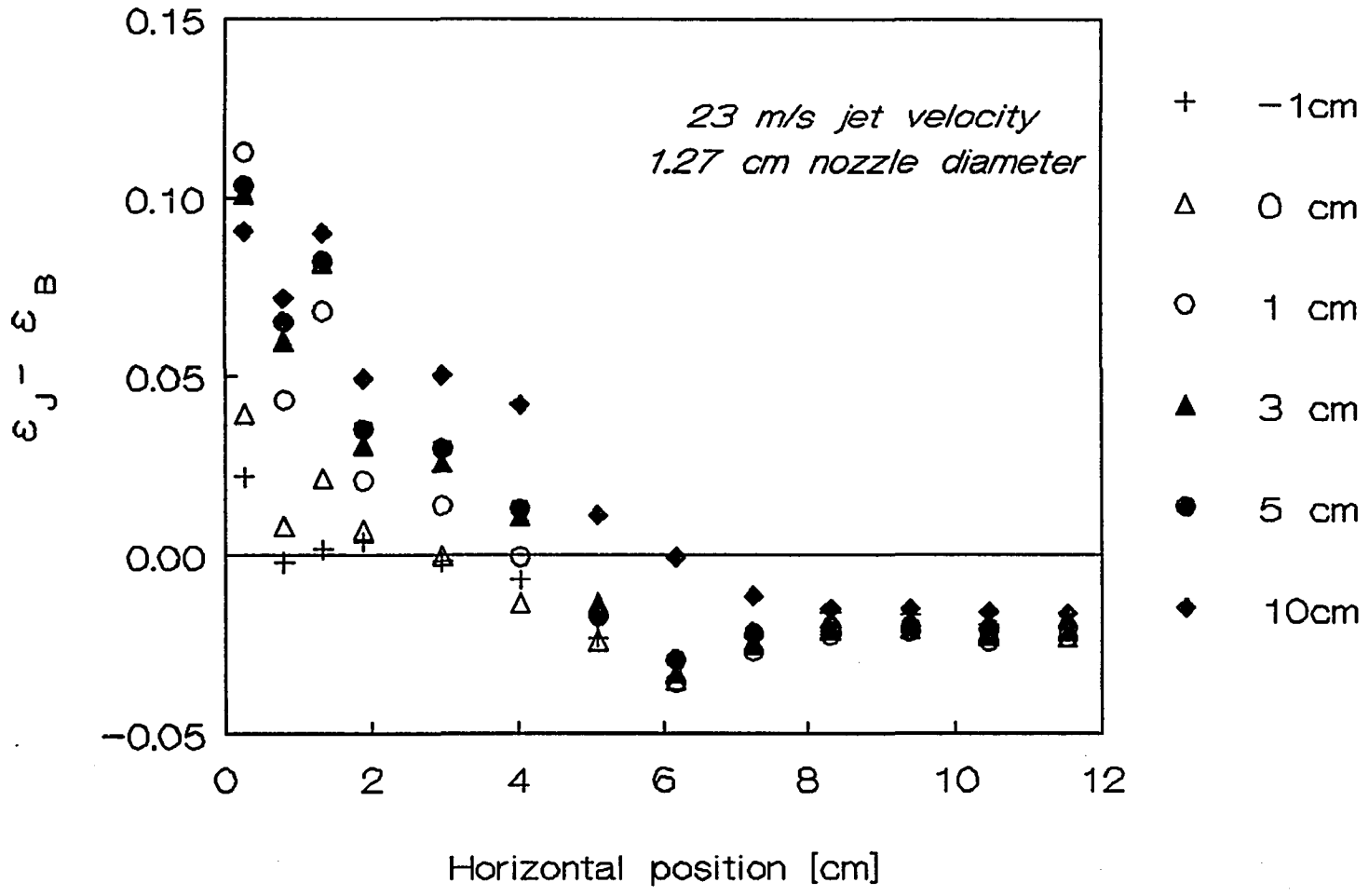

Fig.II3D Solid Fraction Decrement as a Function of Horizontal Position with Vertical Position as Parameter

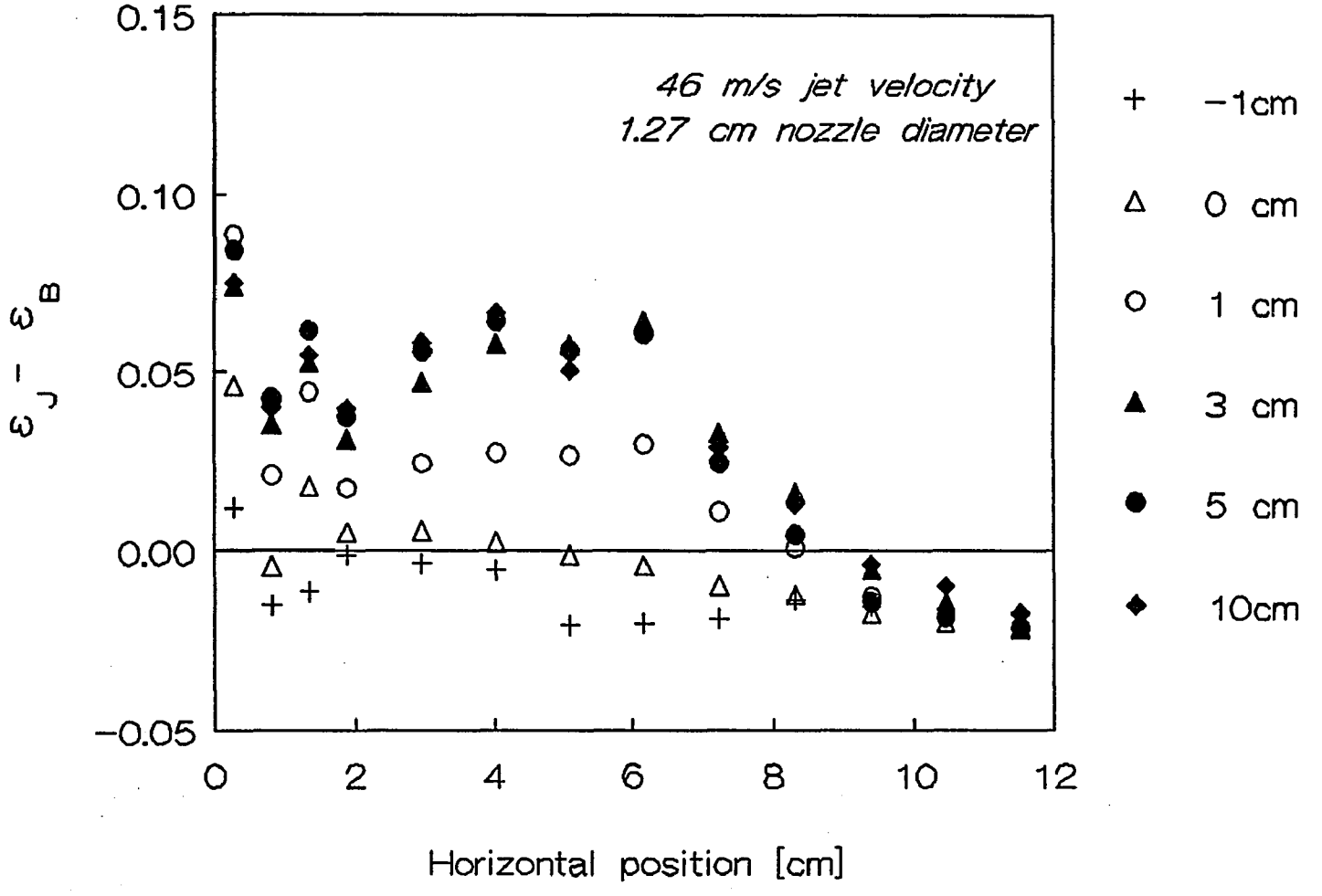

Fig.II4A Void, Bubble Track and Compaction Regions

23 m/s jet velocity 0.64 cm nozzle diameter

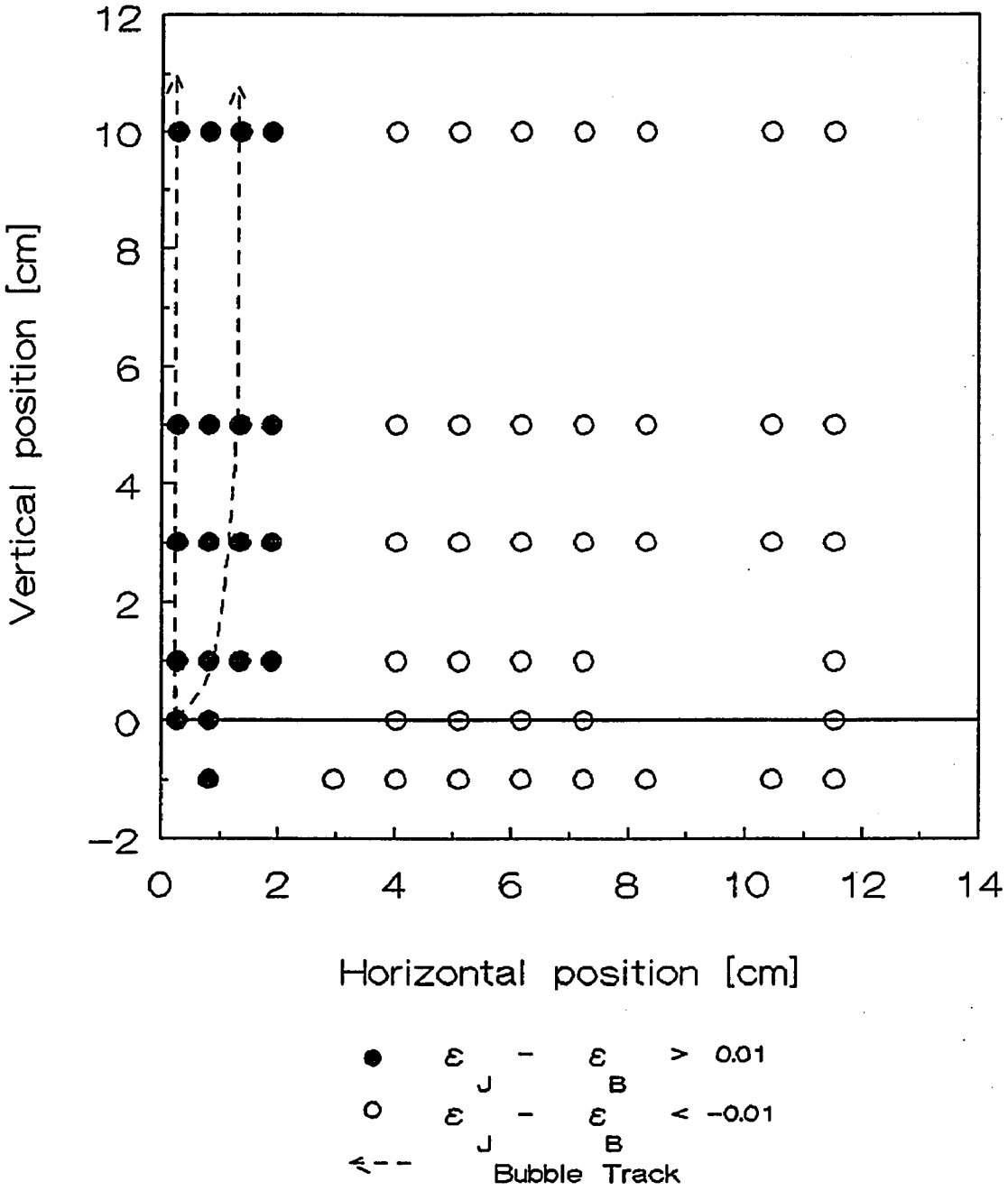

Fig.II4B Void, Bubble Track and Compaction Regions

69 m/s jet velocity 0.64 cm nozzle diameter

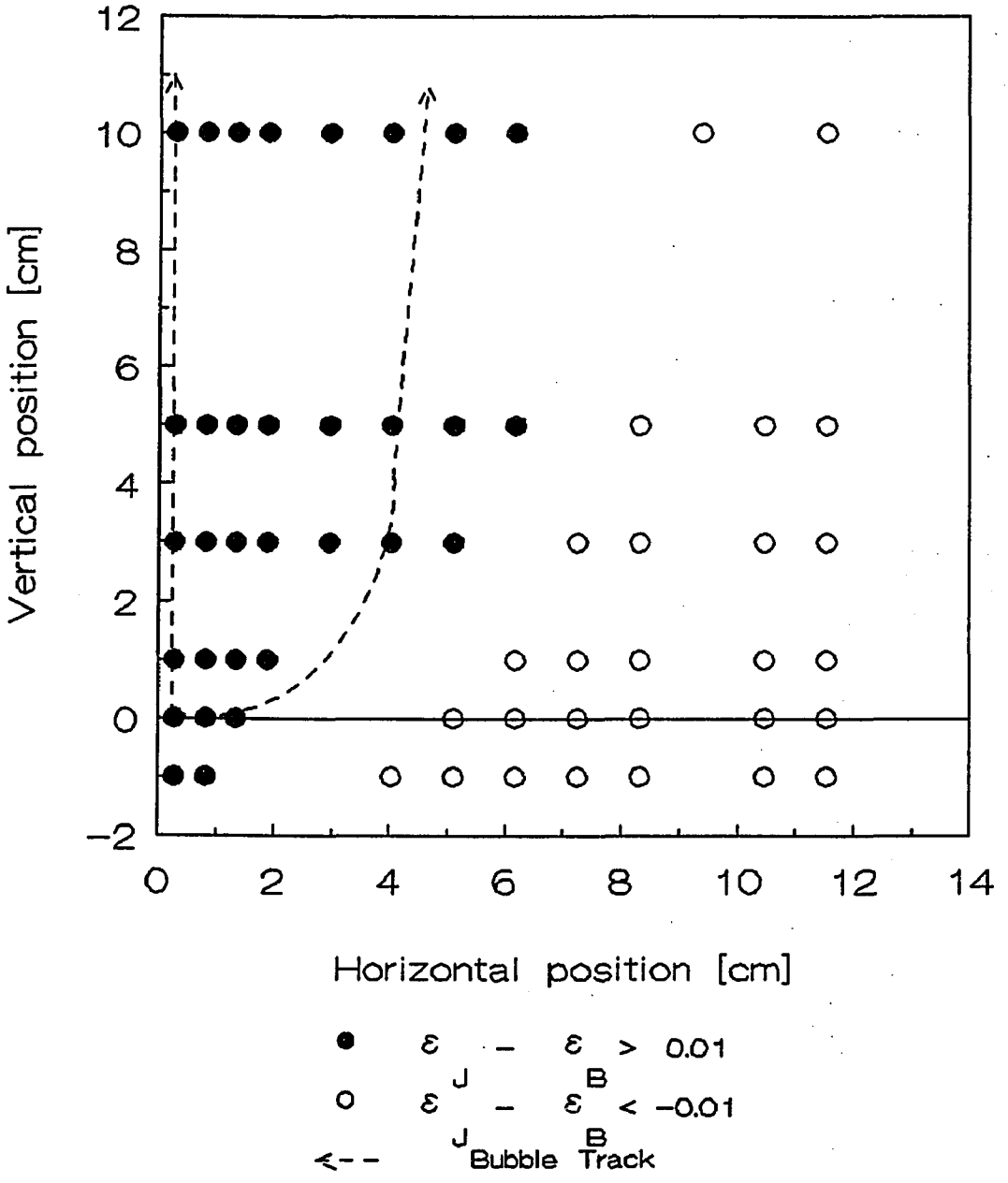

Fig.II4C Void, Bubble Track and Compaction Region

23 m/s jet velocity 1.27 cm nozzle diameter

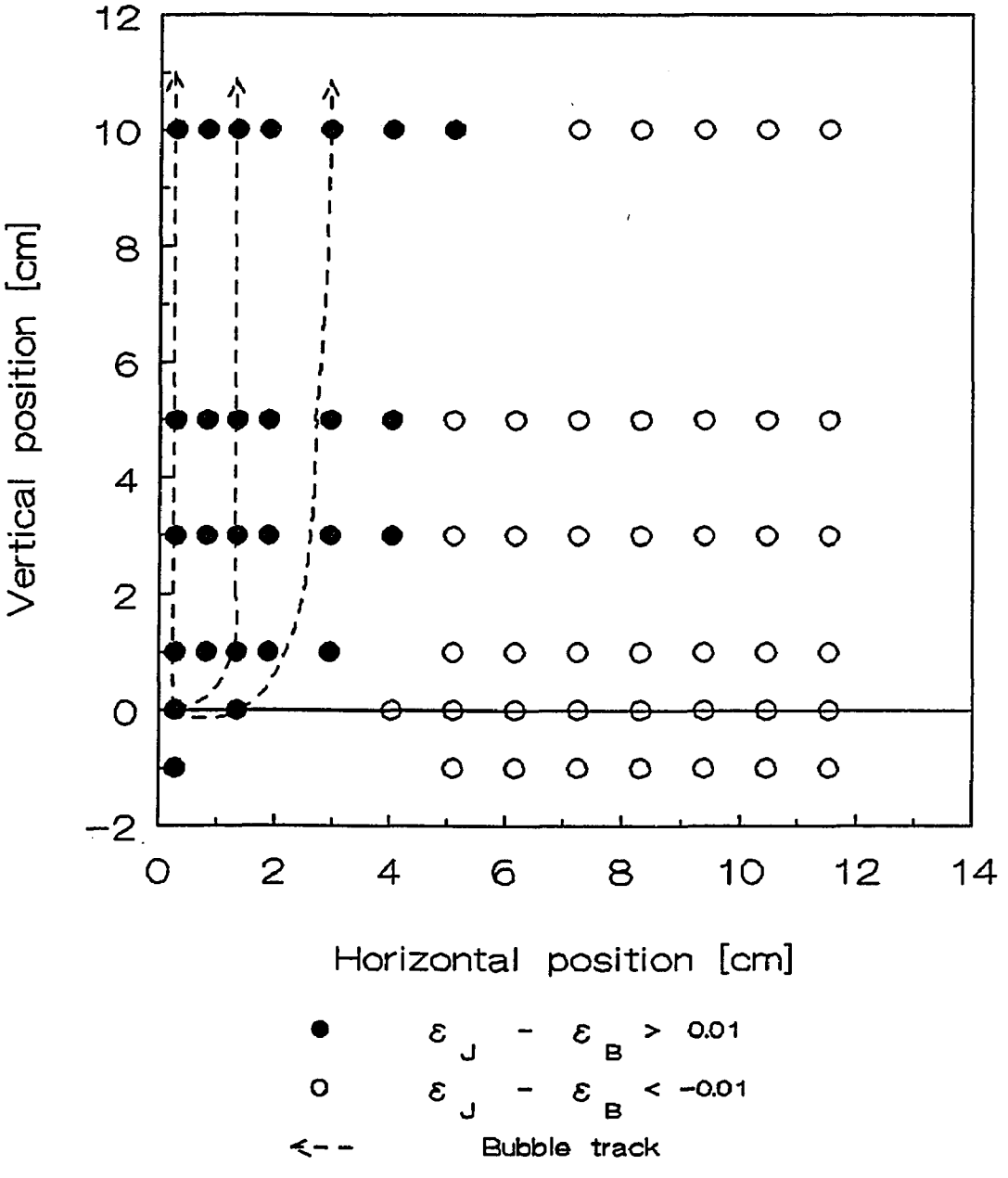

Fig.II4D Void, Bubble Track and Compaction Regions

46 m/s jet velocity 1.27 cm nozzle diameter

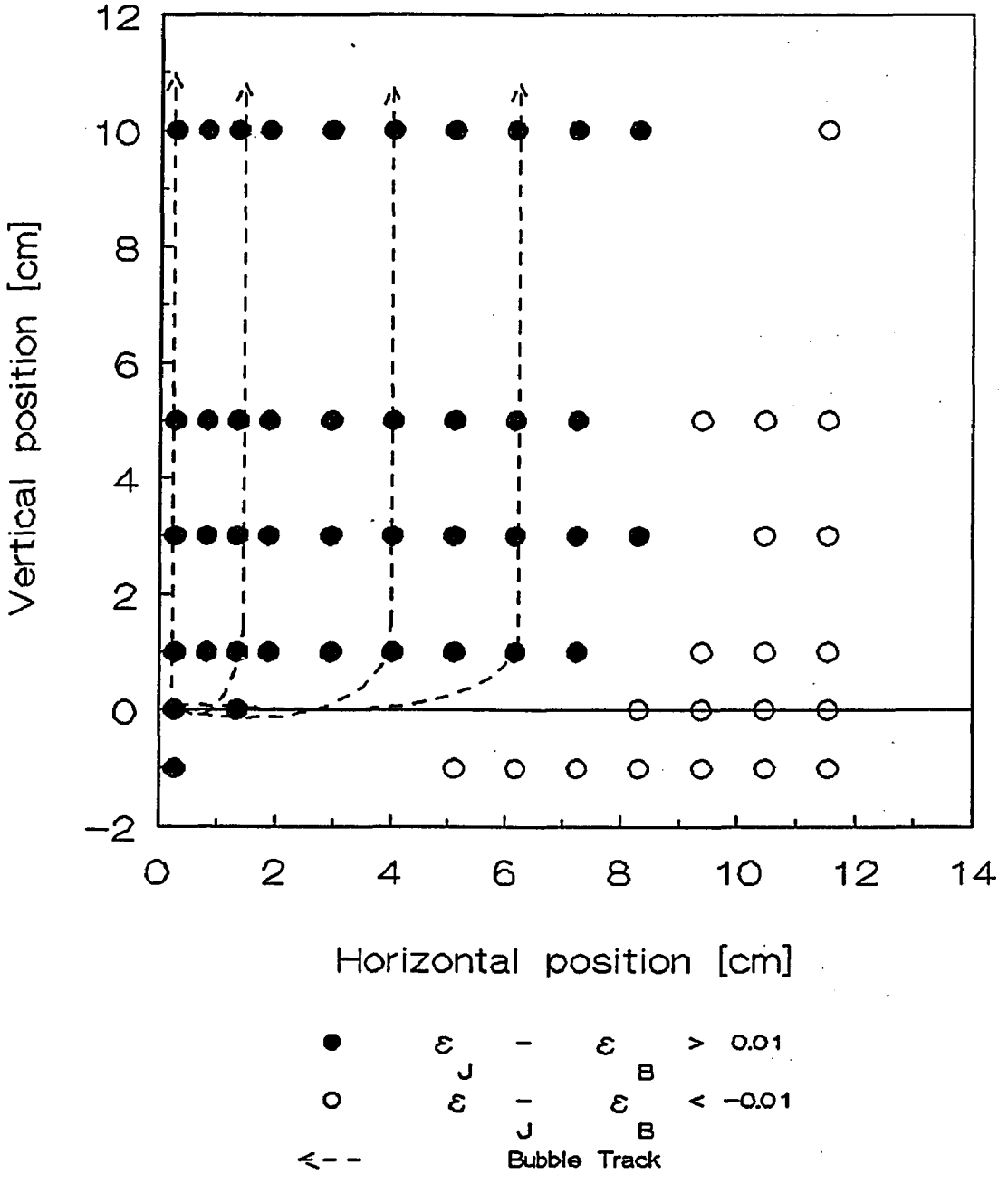

Fig.II5A Normalized Standard Deviation of Solid Fraction Fluctuations with Horizontal Position as Parameter

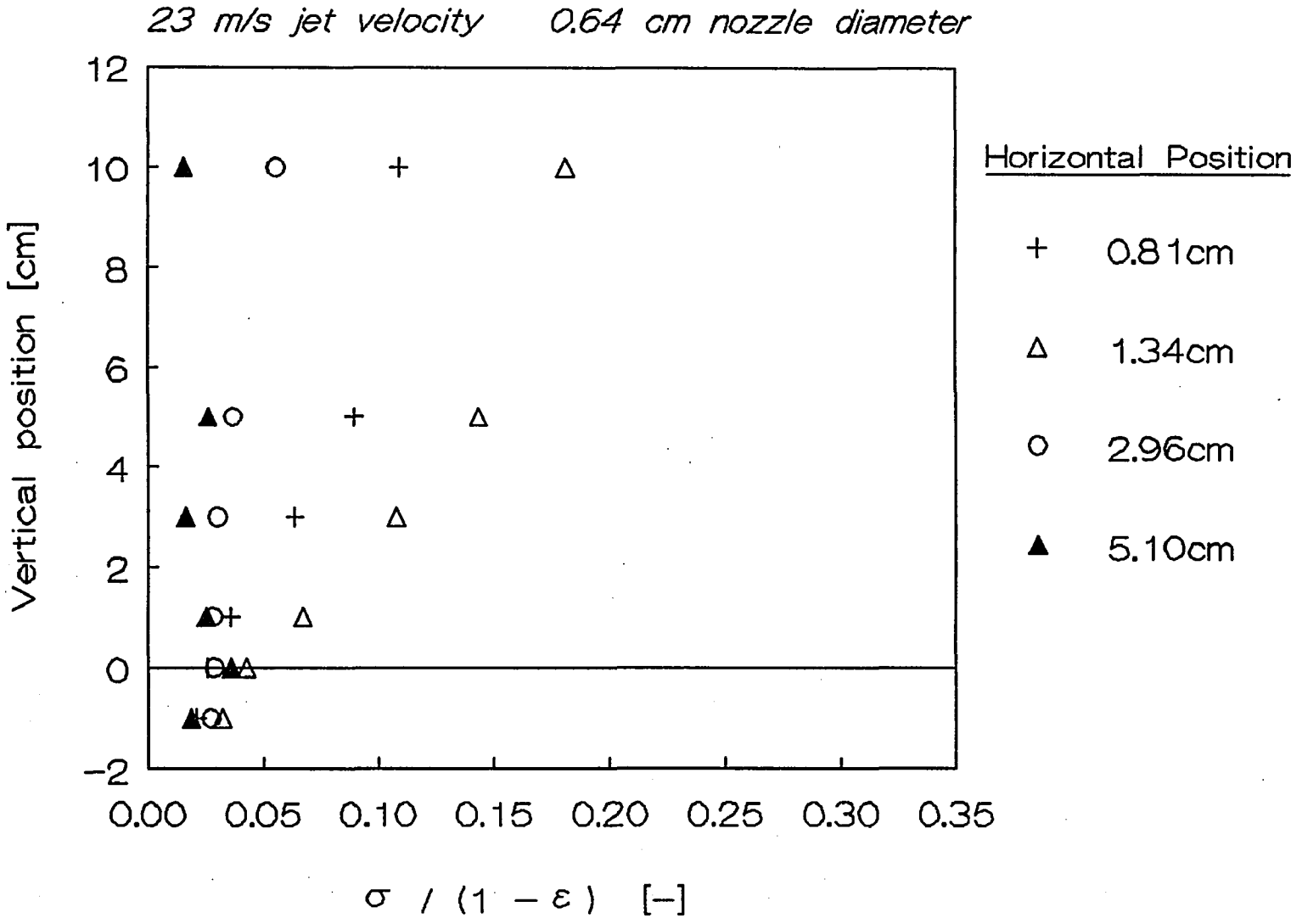

Fig.II5B Normalized Standard Deviation of Solid Fraction Fluctuation with Horizontal Function as Parameter

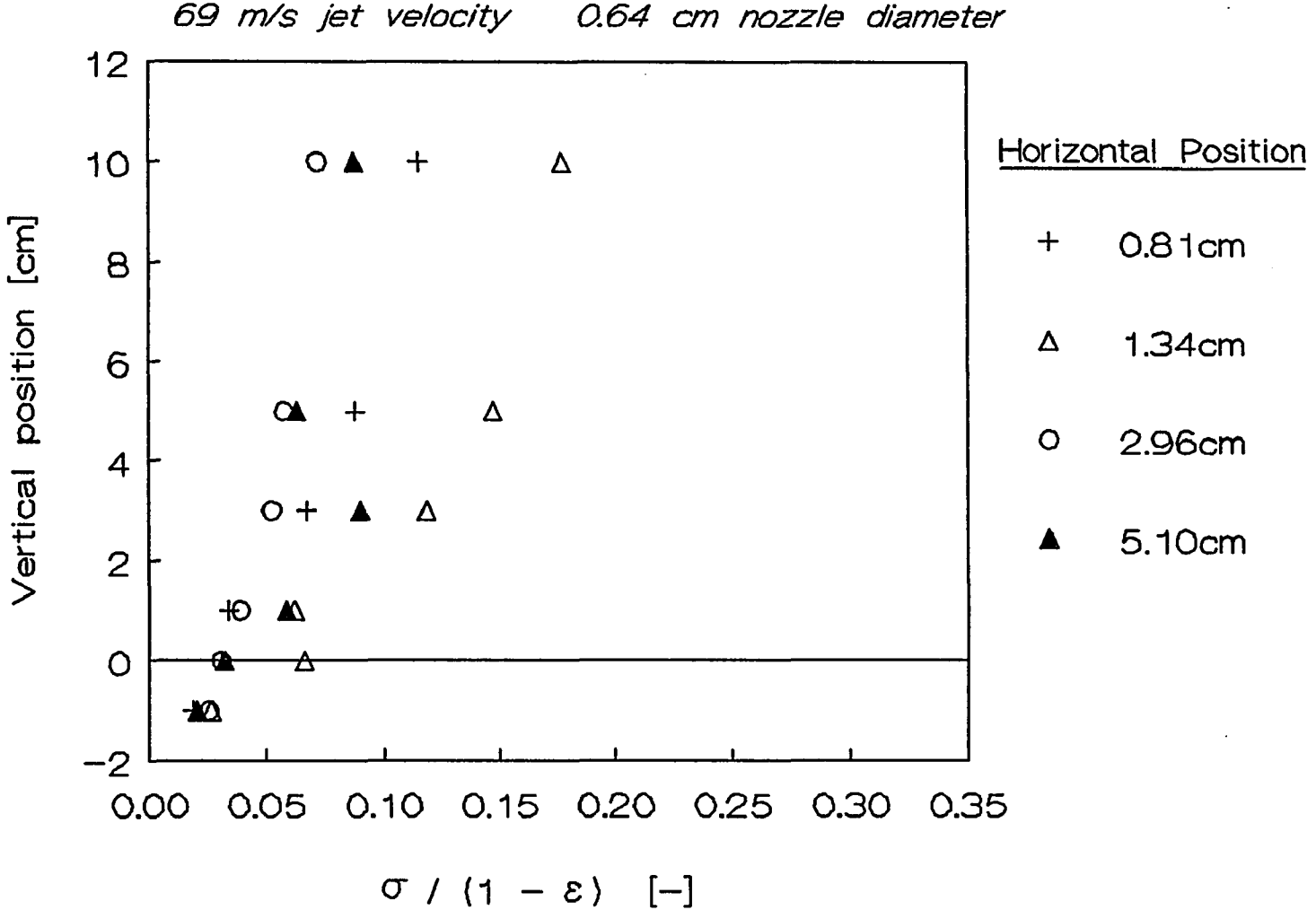

Fig.II5C Normalized Standard Deviation of Solid Fraction Fluctuation with Horizontal Function as Parameter

23 m/s jet velocity 1.27 cm nozzle diameter

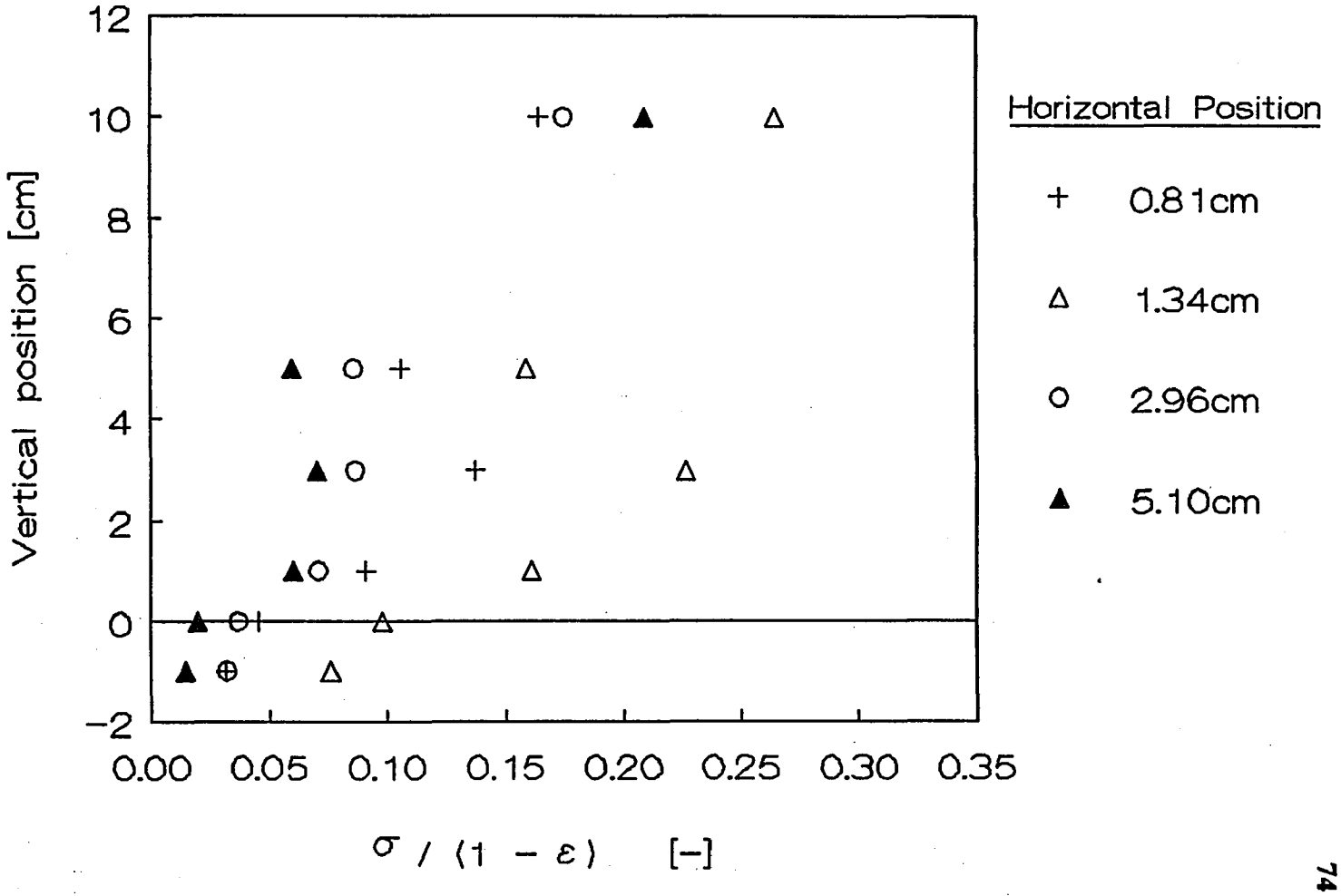

Fig.II5D Normalized Standard Deviation of Solid Fraction Fluctuation with Horizontal Position as Parameter

46 m/s jet velocity 1.27 cm nozzle diameter

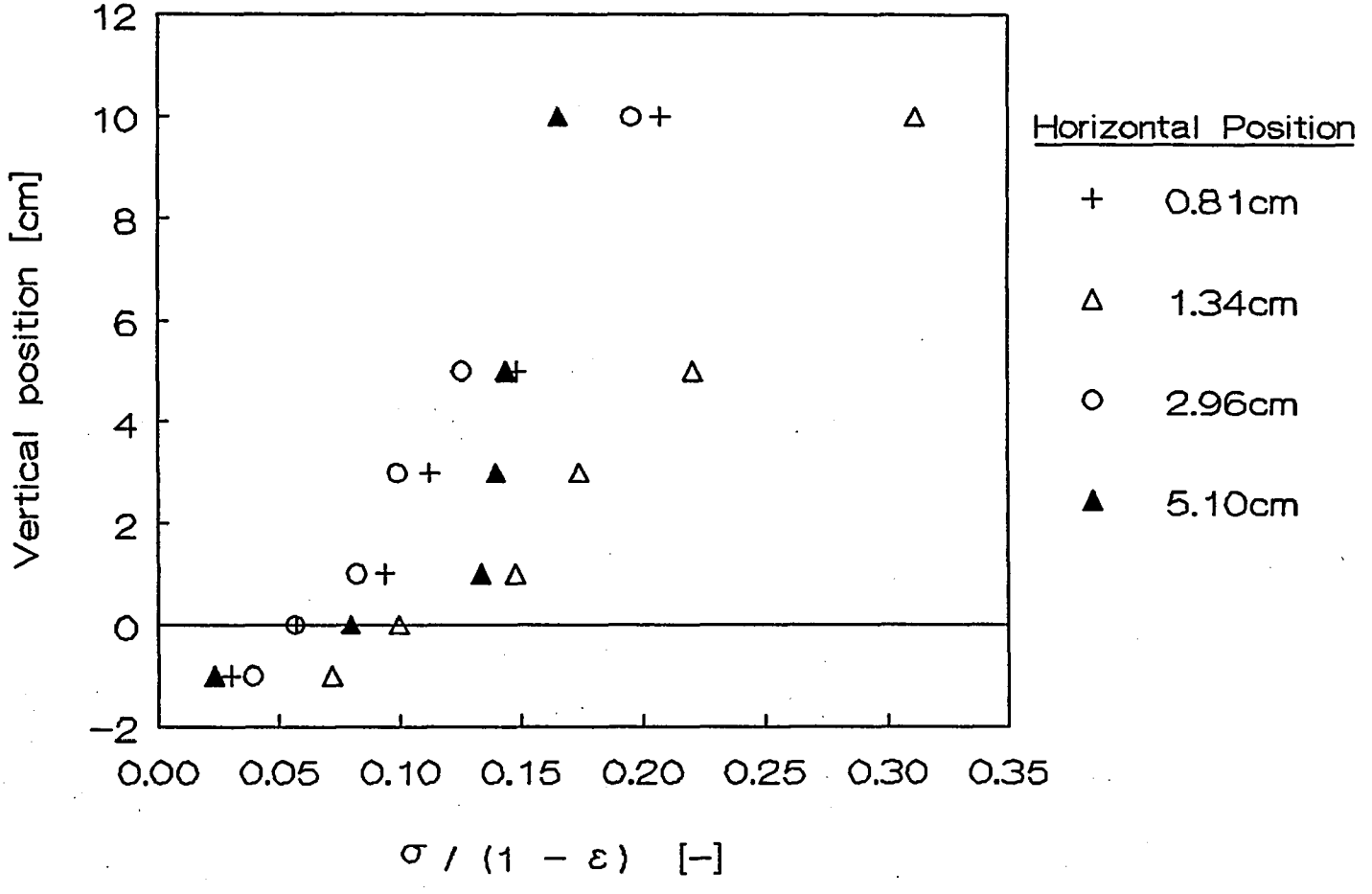

Fig.II6 Comparison of Experimental data for Jet Penetration Length with Predicted Values

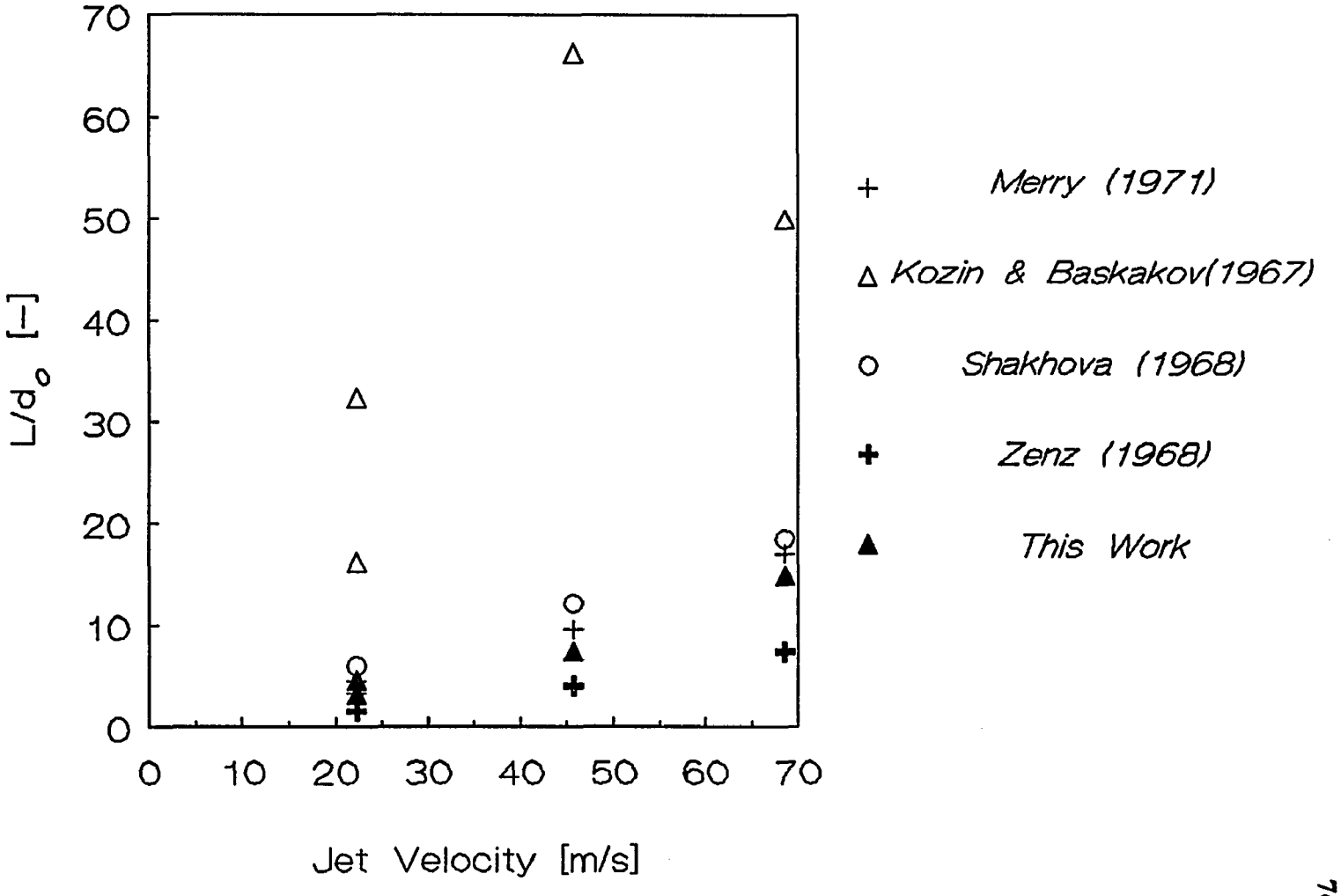

Fig.II7 Comparision of Autocorrelation Functions at a Fixed Position (Y=1cm, X=1.34cm)

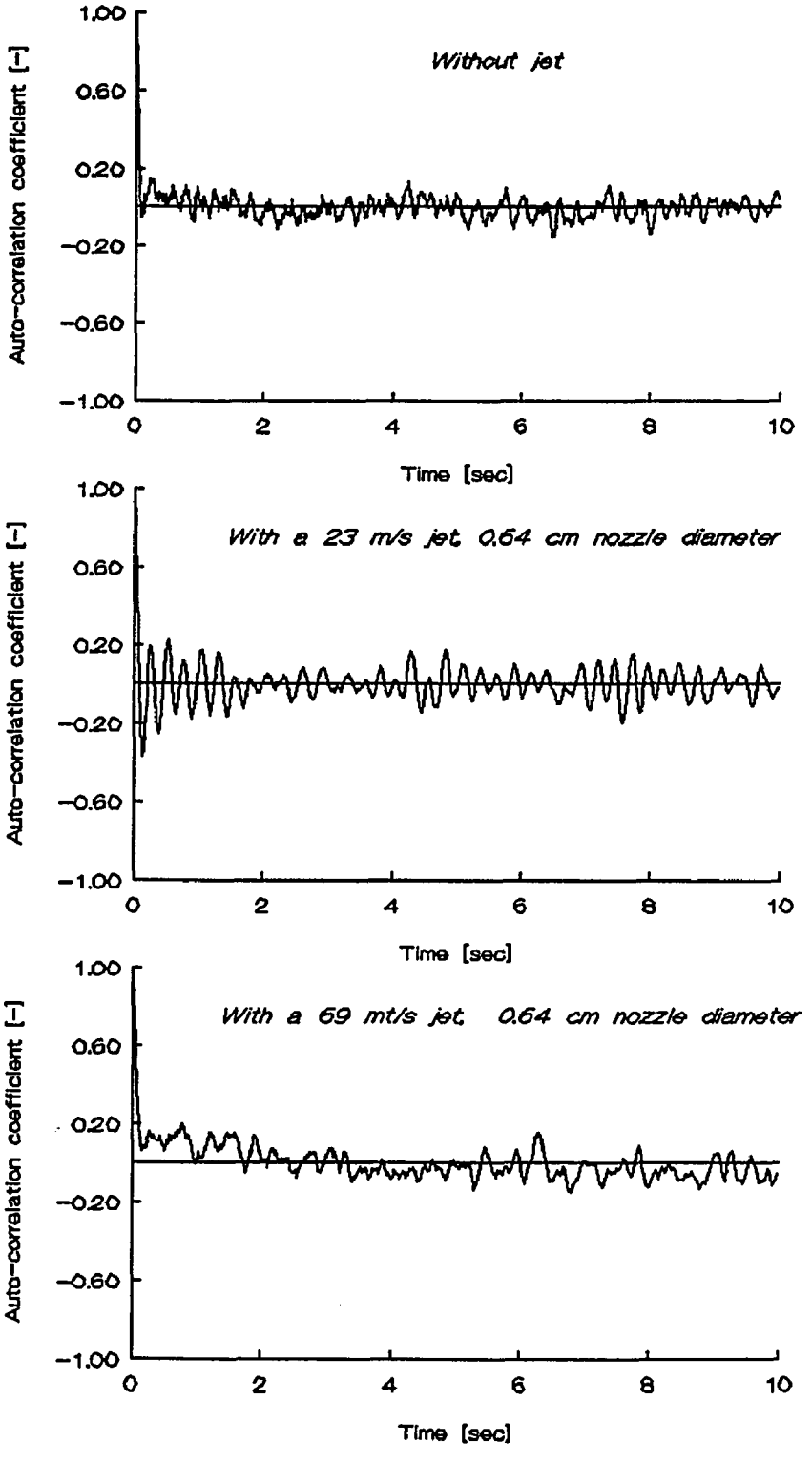

Fig.II8 Comparision of Autocorrelation Functions at a Fixed Position (Y=3cm, X=5.1cm)

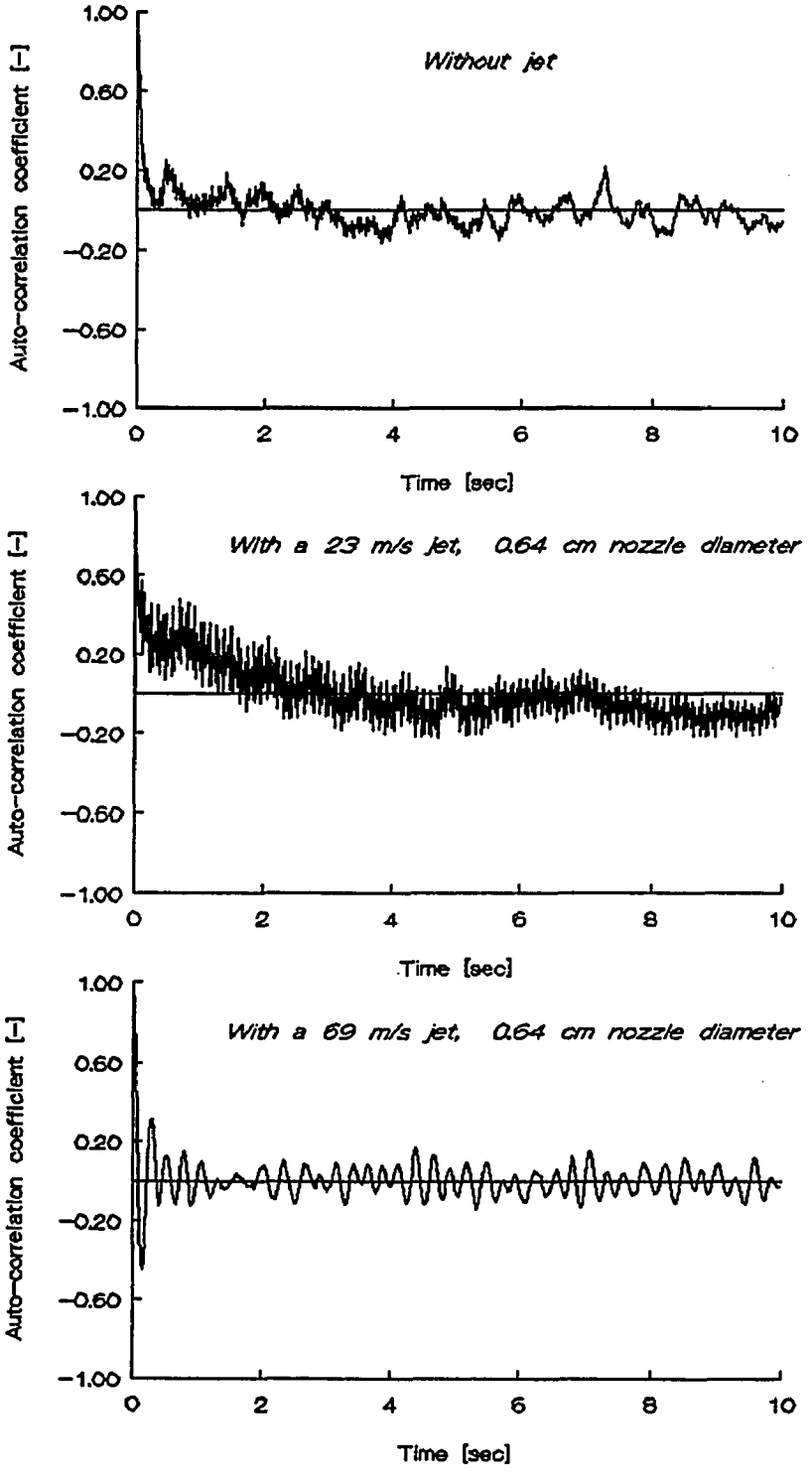

Fig.II9 Comparision of Power Density Functions of Solid Fraction Fluctuation Signals at a Fixed Position (Y=3cm, X=5.1cm)

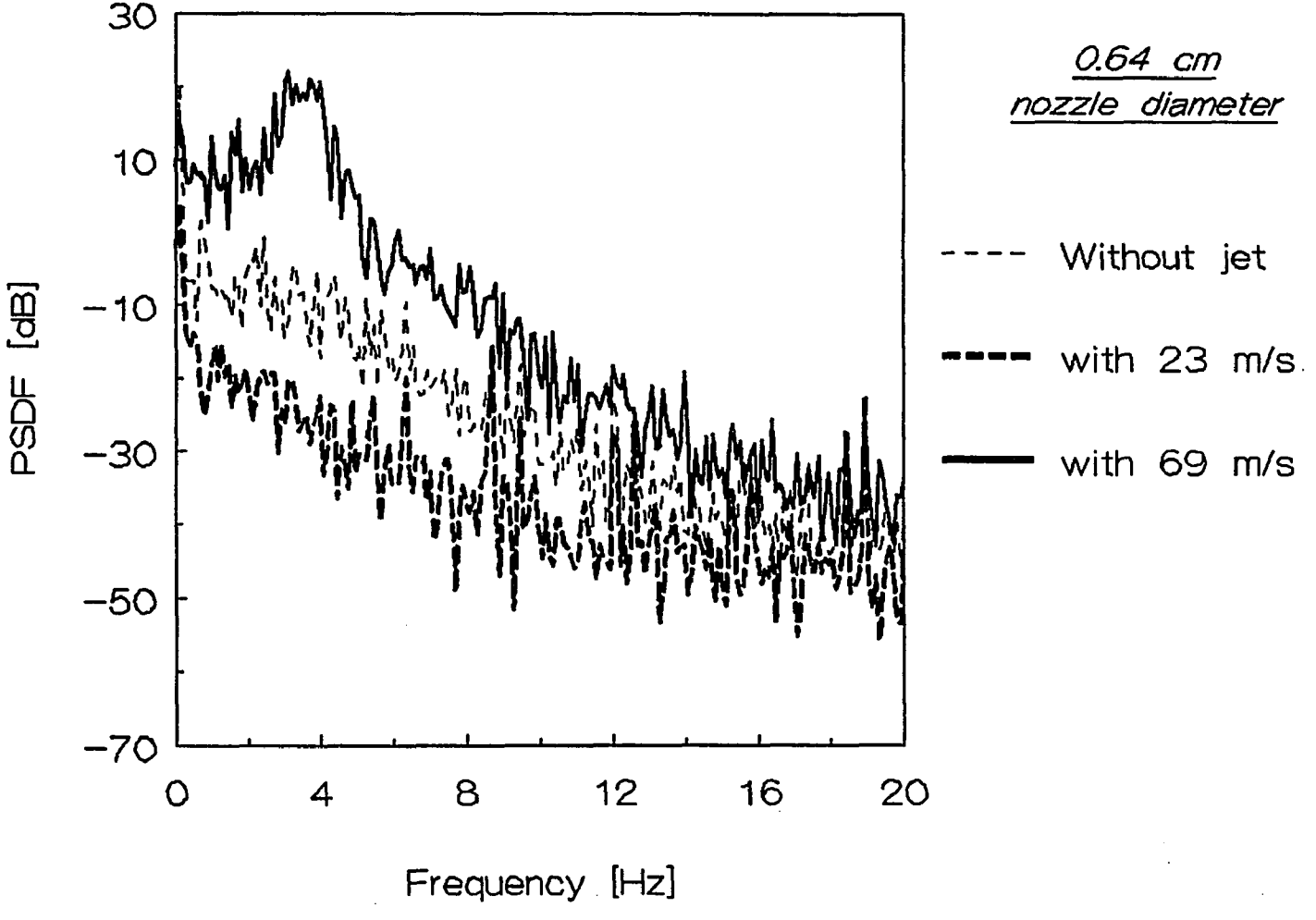

Fig.II10 Map of Flow Regions

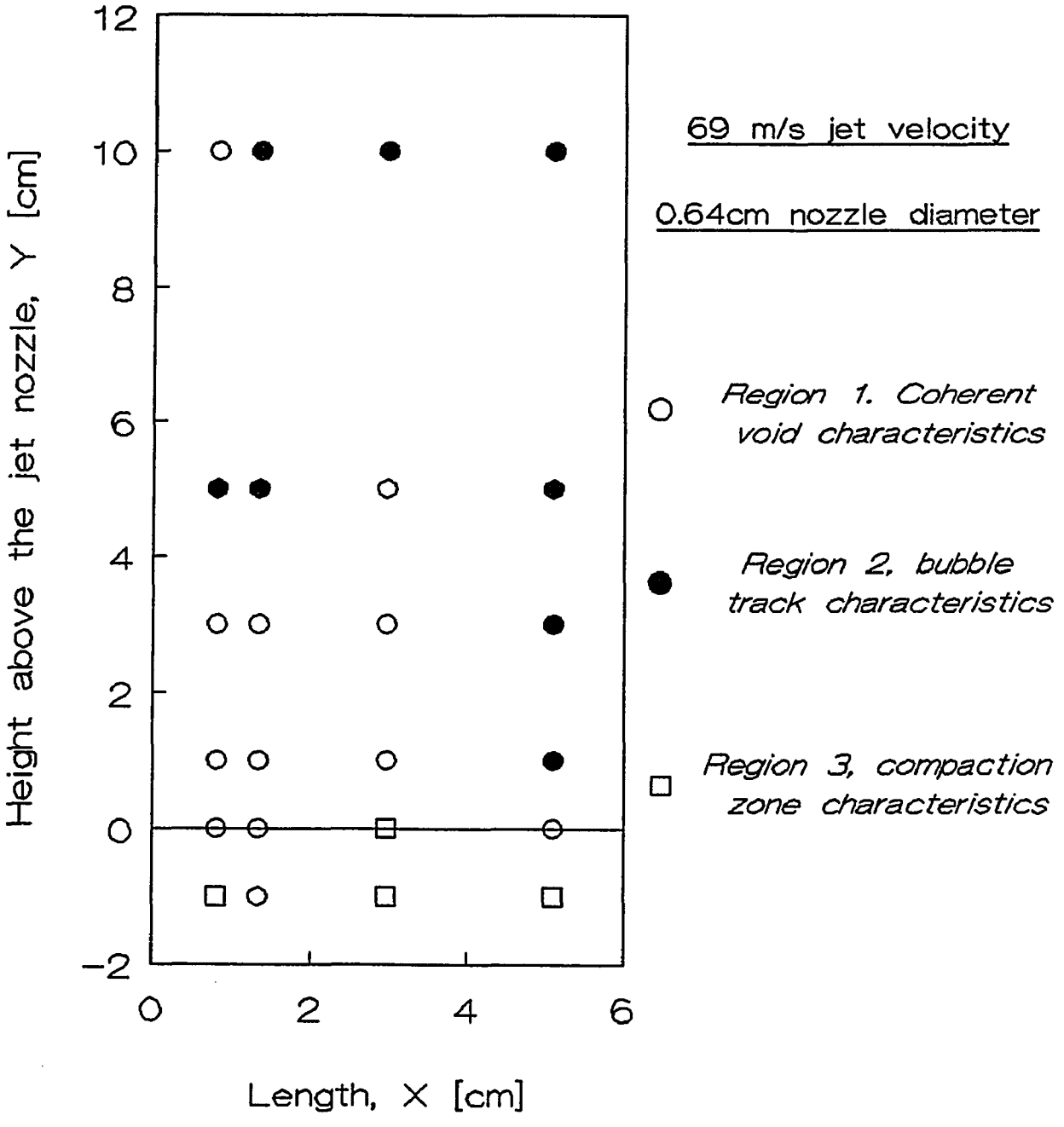

Part III. Axial and Radial Pressure Measurements in a Transported Fluidized Bed

INTRODUCTION

Commercially important applications of high velocity fluidized beds, e.g. catalytic cracking, are carried out in large diameter flow chambers that are rarely longer than about thirty diameters. The two-phase flow in these chambers is characterized by very large gas-phase Reynolds' numbers and strong stochastic and/or quasiperiodic fluctuations. These flows are, in fact, turbulent entrance region flows and must be treated as such.

The evaluation of the most basic fluidization property, i.e. solid fraction or holdup, which is made most often with a differential pressure measurement at the bed wall must be made carefully to avoid introducing error due to the fluctuations in flow variables. Previous work[1] has shown that in high velocity fluidized beds a turbulent "structure" appears to exist which is at least as long as one bed diameter. This study was first undertaken to determine if the mean differential pressure reading, and hence the solid fraction prediction, is affected by the tap spacing with respect to the bed diameter. Furthermore, since the magnitude of the

standard deviation of the pressure fluctuations about the mean has been used to identify regime transition[2], the effect of tap spacing on the standard deviation was also investigated.

The existence of a radial gradient of particle concentration in the vertical transport of a solid powder by a gas has been known for over thirty years. Experiments using gamma ray [i.e.3,4] and X-ray absorption [i.e.5] have shown the existence of the phenomenon and quantified it to some extent. The prediction of the radial variation using the equations of motion of gas and solid has also been accomplished with the incorporation of constitutive equations designed to produce the gradient.[i.e.6,7,8] The physics underlying these constitutive equations have, however, been tenuous.

A second experimental study was carried out to determine whether or not a measurable mean radial pressure gradient coexists with the particle concentration gradient. Recent work by Jackson and coworkers[9] have predicted analytically that such a gradient exists. The existence of such a pressure gradient could help explain the mechanisms which maintain the strong radial particle concentration gradient and which aid in the construction of physically acceptable constitutive relations for modeling with the equations of motion. The magnitude and direction of the radial pressure gradient were also to be measured, if the gradient existed,

along with statistical properties of any fluctuations in the gradient.

EXPERIMENTAL

The City College circulating fluidized bed apparatus[10] used for these experiments consists of a riser section, 0.15 m D by 8.5 m high. A standpipe holds solids received from the riser in a fluidized state with down flow. The 6 m high standpipe terminates in a U-tube 2 m off the floor. The solids flow control valve sits in this U-tube. The section of the U-tube which connects directly to the riser contains three nozzles which supply the air to the riser.

The gas used for all the experiments was air at ambient conditions. The solid powder used was HFZ-33 FCC cracking catalyst supplied by the Englehard Corp. The powder properties are: particle density 1.45 g/cm^3, particle mean diameter 60μm, particle sphericity 1.

To demonstrate the effect of tap spacing on the measurement of axial pressure gradient in high velocity fluidized beds, the circulating system has a nest of pressure taps, as shown in Figure 1, which are flush with the inside column wall.

The distances between any two pressure taps connected across a transducer in the nest varied from 0.06 m to 0.80 m. To prevent significant damping of the pressure signals (amplitude reduction) due to the dead volume in tap stem, pressure transducers were located as close as possible to the wall of the riser and on each side of the transducer the tapping was equal. Purge air was used to prevent tap blockage, whose flowrate was controlled using needle valves.

To investigate the radial pressure gradient, a schematic diagram is shown in Figure 2. A pair of small diameter (~3 mm) pressure taps, both traversable along a bed diameter, were mounted at the same elevation on the City College riser.[10] The taps were purged continuously with an air flow. The purge gas velocity through the probe tip was varied from ~ 0.3 m/s to ~ 1.5 m/s. No detectable effect of purge gas velocity on the pressure measurement was found as long as the velocity in each probe was approximately the same. The velocity in both probes was then held at ~ 0.3 m/s for all the measurements. A set of experiments was performed in which one tap was set at a fixed radial position and the other tap was traversed across the bed.

All pressure taps were connected across sensitive pressure transducers. The transducers were the piezo-resistive type and were hard wired to a real time computer system through an A/D board capable of reading signals with a frequency

of 10 KHz. The pressure was sampled at 100 Hz for each run. About 20,480 readings were taken at 100 Hz for each data point in ten sets of 2048 readings, This was sufficient to give an accurate mean value. The 2048 data points sets were used for online analysis including Fast Fourier Transform (FFT) analysis.

Measurements of both axial and radial pressure gradients were performed at gas velocities which spanned the bubbling, slugging, turbulent, and dense and dilute conveying regimes. This range of data provides some information on the flow structural changes with regime transitions as well as a validation of the data in the bubbling bed regime.

RESULTS AND DISCUSSION

The effect of tap spacing on the measurement of axial pressure difference in a high velocity fluidized bed

Riser flows exhibit strong stochastic and quasiperiodic components and the overall appearance of the flow with X-ray visualization is highly turbulent. In order to determine the effect of tap spacings on the measurement of axial pressure

difference, the pressure difference signals were converted to mean and fluctuation components of pressure difference,

$$\Delta P=\overline{\Delta P}+\Delta P'$$

Where,

$$\overline{\Delta P}=\frac{1}{T}\int_0^T \Delta P dt$$

measurements of time-averaged axial pressure profiles are conveniently used to infer the apparent solid fraction in the section of the riser. Hence, the differential pressure is equal to the bulk weight per unit area in the riser section:

$$\frac{\overline{\Delta P}}{\overline{\Delta X}}=[\rho_s\overline{\epsilon_s}+\rho_g(1-\overline{\epsilon_s})]g$$

The value of ε_s calculated with this equation is essentially correct if the flow is fully developed.

It is clearly shown in Figure 3 that the measured pressure gradient (pressure difference/tap spacing) reported as the apparent solid fraction, is a function of tap spacing for tap spacings significantly smaller than the bed diameter. This is

particularly true in the turbulent and dense phase flow regimes where the solid fraction is in the range of 0.15~0.30.

The standard deviation (rms) of the apparent solid fraction fluctuation, normalized by the mean value of the solid fraction (NSD), is plotted in Figure 4 as a function of pressure tap spacing. Both dense and dilute riser flow cases are shown. It is seen that for spacing less than one L/D, The NSD is very large. However, above 2 L/D the two values are about the same. This is a strong indication that the length scale for the flow structure is about two L/D for both dense and dilute riser flow.

This result is in agreement with Figure 3, where the "turbulent" flow structure is at least one bed diameter in length and pressure gradient must be averaged over at least one flow structure length to give an accurate reading of the average solid fraction. However, the agreement does not constitute a proof of this conclusion.

The normalized standard deviation (NSD) of the pressure difference is plotted in Figures 5 and 6 as a function of gas superficial velocity with tap spacing as a parameter. Figure 5 is for the dense phase transport and Figure 6 for the dilute phase transport. The NSD increases with decreasing tap spacing over the whole regime spectrum. Also, the NSD's for spacings less than one diameter are

considerably larger than those for larger spacings. This observation also supports the flow structure hypothesis described above. It is also interesting that these figures demonstrate the characteristic shape for transitions from the bubbling to the slugging to the turbulent regimes for all tap spacing dimensions. However, the discrete differences between the data for tap spacings less than one diameter and greater than one diameter are not evident until the transition to turbulent flow .

The effect of the differential pressure tap spacing on the magnitude of the differential pressure fluctuation can be seen from the time series of the differential pressure fluctuation as a fraction of the mean differential pressure fluctuation. Typical instantaneous values of pressure difference, normalized by the mean pressure difference, are summarized in Figure 7, operating at the same superficial gas velocity of 4.5 m/s for dense flow. These time series, with a length of 10 seconds, indicate the high velocity gas-particle flows in risers are inherently unsteady with large fluctuations. Furthermore, it is clearly shown that the amplitude of the differential pressure fluctuation, as a fraction of the mean differential pressure, increases with decreasing tap spacings.

The power spectrum and the auto-correlation function for ΔP measurements with various tap spacings are compared in Figure 8 and Figure 9. As can be seen from the power spectra, the major pressure fluctuations in the riser (Fig.8) have

a frequency of about 1 Hz. This has already been observed with X-ray technique in previous work[10]. The cause of this superimposed low frequency may be explained by accelerations and decelerations of solid particles in the oscillating wall region. It is worth noting that the riser seldom exhibits pressure fluctuations of frequencies greater than 20 Hz and almost all the pressure fluctuation energy is contained in the frequency range 0 - 20 Hz. The effect of tap spacing on the power spectrum can be seen in the higher frequency range, 20 - 40 Hz, in Figure 8. The power spectrum of a large tap spacing case decreases rapidly with an increase in this frequency range compared to that of smaller tap spacing case. This suggests that there is considerably more power in small scale fluctuations that have higher frequencies which are averaged out with large tap spacing. The tap spacing does not affect the frequency range but does have an effect on cumulative energy.

Figure 9 illustrates a typical set of auto-correlation coefficients corresponding to different tap spacings. It appears that each signal recorded with different spacing contains a wave-like component and a stochastic component. Their relative magnitude seems to depend on the tap spacing. These figures show that pressure fluctuations processed in the larger spacing are dominantly represented by a deterministic component, while those in the smaller spacings strongly reflect a random component. The effect of the periodicity of pressure fluctuations increases, or the random component decreases, with increasing the tap spacing.

In conclusion, the effect of tap spacing on the measurement of axial differential pressure has been shown to exist in vertical gas-solid particulate transport. Measurements of mean axial pressure difference made with tap spacing less than one column diameter, will be underpredict the true axial pressure gradient. The quasiperiodic components of the fluctuations in pressure have an elongated flow structure with a length of 1 ~ 2 diameters. The amplitude of the differential pressure fluctuation, as a fraction of the mean differential pressure, increases with decreasing tap spacing. The small spacing reveals there is considerably more power in higher frequencies than are apparent with larger tap spacing. Further, the normalized standard deviation of the pressure fluctuations increases with decreasing tap spacing over the whole regime spectrum. However, the characteristic shape of the NSD curve over the velocity range was independent of tap spacing.

The Radial pressure gradient in a high velocity fluidized bed

The traversable pressure tap probes used in this experiment were straight horizontal tubes open at the end to the flowing gas-powder mixture. Taps of this type could be used because of the relatively high solid fraction of the mixture, i.e. greater than 0.01. Consider a case where, at the centerline, the solid fraction is only 0.01 and the gas and solid velocities are 5 m/s and 4 m/s, respectively. The

gas dynamic head is ~25 kg/ms^2 and mixture dynamic head is ~260 kg/ms^2, ~ ten times as large. A poorly designed probe could cause local acceleration of the turbulent continuous gas phase, increasing its dynamic head by as much as a factor of two[11]. Therefore, the local gas velocity would increase from 5 m/s to ~7 m/s. Since the tap is only 3 X 10^{-3} m in diameter, gas takes only about 0.5 X 10^{-3} seconds to pass the tap. Now, a single particle in equilibrium with Stokes flow around it which is instantaneously accelerate a velocity 2 m/s greater than that at the equilibrium condition, there results an unbalanced force per unit mass on the particle of ~175 m/s^2. Setting 175 m/s^2 equal to the delta particle velocity/delta time, gives a change in particle velocity of ~0.09 m/s due to the change in gas velocity. Thus, while the gas dynamic head doubles from 25 kg/ms^2 to 50 kg/ms^2, the mixture dynamic head increases only by ~35 kg/ms^2, less than 15%. Since the pressure difference from centerline to wall is typically at least equal to a mixture dynamic head, the error introduced by the crude probe design is small.

Results were obtained by stationing one probe essentially at the wall and traversing the second probe along a diameter. The data were confirmed by repeating selected cases with the traversing probe fixed at the wall and traversing the other probchange occurring in the region where the core meets the denser annulus. The offset at the wall for the dense transport was always present and is, as yet, unexplained. This offset of ~ 0.8 mbar can be taken as the magnitude of

the error in the measurements. As supported by these interpretations, Figure 12 shows data for the dense transport case with one probe fixed at the centerline and the second probe traversed back to the wall. At the centerline, no pressure difference exists between the probes and the pressure difference between the centerline and the wall is essentially the same as shown in Figure 11, about 1.25 mbar. As further confirmation, the measurements of radial pressure gradient in both bubbling and slugging beds are shown in Figure 13. It demonstrates that there is no significant radial pressure gradient in the either bubbling or slugging bed.

The measured radial pressure difference, wall pressure less centerline pressure, is plotted as a function of cross-sectional average (CSA) solid fraction in Figure 14. The dashed line is the pressure difference across a 7.5 cm vertical column riser as a function of the solid fraction. Since the radius of the City College riser is 7.5 cm, data points above the line have an average radial pressure gradient greater than the local axial pressure gradient. All of the data points lie very close to or above this line, indicating that the radial gradient plays a significant role in the dynamics that support the radial solid particle concentration gradient.

The radial pressure difference divided by the column radius and the axial pressure gradient is shown as a function of gas superficial velocity in Figure 15.

Both dense phase and dilute phase cases are plotted. It is seen that below 1 m/s, the bubbling and slugging cases, the radial pressure gradient is negligibly small. (The small value occurs because of wall effects due to bubble diameter being a significant fraction of column diameter.) With transport of solids, $u_g \geq 2$ m/s, the radial gradient becomes larger than the axial gradient and the ratio appears to increase with increasing gas velocity.

The radial pressure difference is characterized by the size of the fluctuations about the mean value, Figure 16. The standard deviation of the fluctuations is typically greater than the mean value as can be seen by comparing Figure 16 with Figure 12. The power spectra of the normalized fluctuations in both the radial and axial directions are compared in Figure 17 for both dense and dilute cases. It is seen that the frequency distributions are the same in both directions but the amplitudes in the radial direction are much larger.

In summary, a strong radial pressure gradient exists in vertical gas-solid particulate transport. Its value is the same order of magnitude as that of the local axial pressure gradient. If we Interpret the gradient in terms of the accepted core-annulus structure of this flow, the dilute core flow region is at a lower pressure than the dense annulus. Further, the standard deviation of the pressure fluctuations is considerably larger than the mean value.

CONCLUSIONS

Measurements of radial pressure gradient in the transported fluidized bed show a strong radial pressure gradient does exist in such fluidized beds. The results so obtained could be used to support Jackson's model[9] for riser flow and could help elucidate the mechanism which maintains the turbulent-like structure in the riser flow.

The study of axial pressure gradient in transported fluidized beds shows that measurements of the axial pressure gradient with tap spacings less than one bed diameter give erroneously low readings. Regime transitions, as followed by the rms of the pressure fluctuations, are less clearly seen with small tap spacings than they are with large tap spacings.

NOTATION

g	acceleration of gravity, m/s^2
D	diameter of riser
L	tap spacing, m
NSD	normalized standard deviation
PSDF	power spectrum density function
u_g	superficial gas fluidizing velocity, m/s

GREEK LETTERS

ε_s	solid fraction
ΔP	pressure drop
ρ_s	density of solid particle, kg/m^3

ACKNOWLEDGEMENT

EXXON Research Engineering Company provided partial support of this work. Dr. William B. Heard of EXXON suggested the method for the simple proof of the validity of the probe pressure measurement.

REFERENCES

1. H.Weinstein, H.J.Feindt, L.Chen and R.A.Graff, "The Measurement of Turbulence Quantities in High Velocity Fluidized Beds", In Fluidization VII O.E. Potter and D.V.Nicklin, Eds., Engineering Foundation, New York, 1992

2. Yerushalmi, J. and N. T. Cankurt "Further Studies of The Regimes of Fluidization", Powder Tech., 24, 1979

3. Bartholomew, R. & R. Casagrande, R. "Measuring solid concentration in fluidized systems by gamma-ray absorption," Ind. Eng. Chem., 49, 428 (1957).

4. Saxton, A. & A. Worley, "Modern catalytic cracking design,"Oil and Gas J., 68, 82 (1970)

5. Weinstein H., M. Shao, & L. Wasserzug, "Radial solid density variation in a fast fluidized bed," A. I. ChE. Symp. Ser., 74,1 (1978)

6. Berker, A.& T. Tulig, T. "Hydrodynamics of gas-solids flow in a catalytic cracker riser: implications for reactor sensitivity performance," Chem. Eng. Sci., 41, 821 (1986).

7. Sinclair, J. L., and R. Jackson, "The effect of particle-particle interactions on the flow of gas and particles in a vertical pipe," A. I. ChE., 35, 1473 (1989).

8. Tsuo, Y. P., and D. Gidaspow, "Computation of flow patterns in circulating fluidized beds", A. I. ChE., 36, 885 (1990).

9. Dasgupta S., R. Jackson and S. Sundaresan, "Turbulent gas-particle flow in vertical

risers", A. I. ChE., in press

10. Feindt, H. J. "Radial and axial density fluctuations in a high velocity fluidized bed", Ph.D. Thesis, The City Univ. of New York (1990)

Fig.III1 Illustration of Pressure Tap Positions

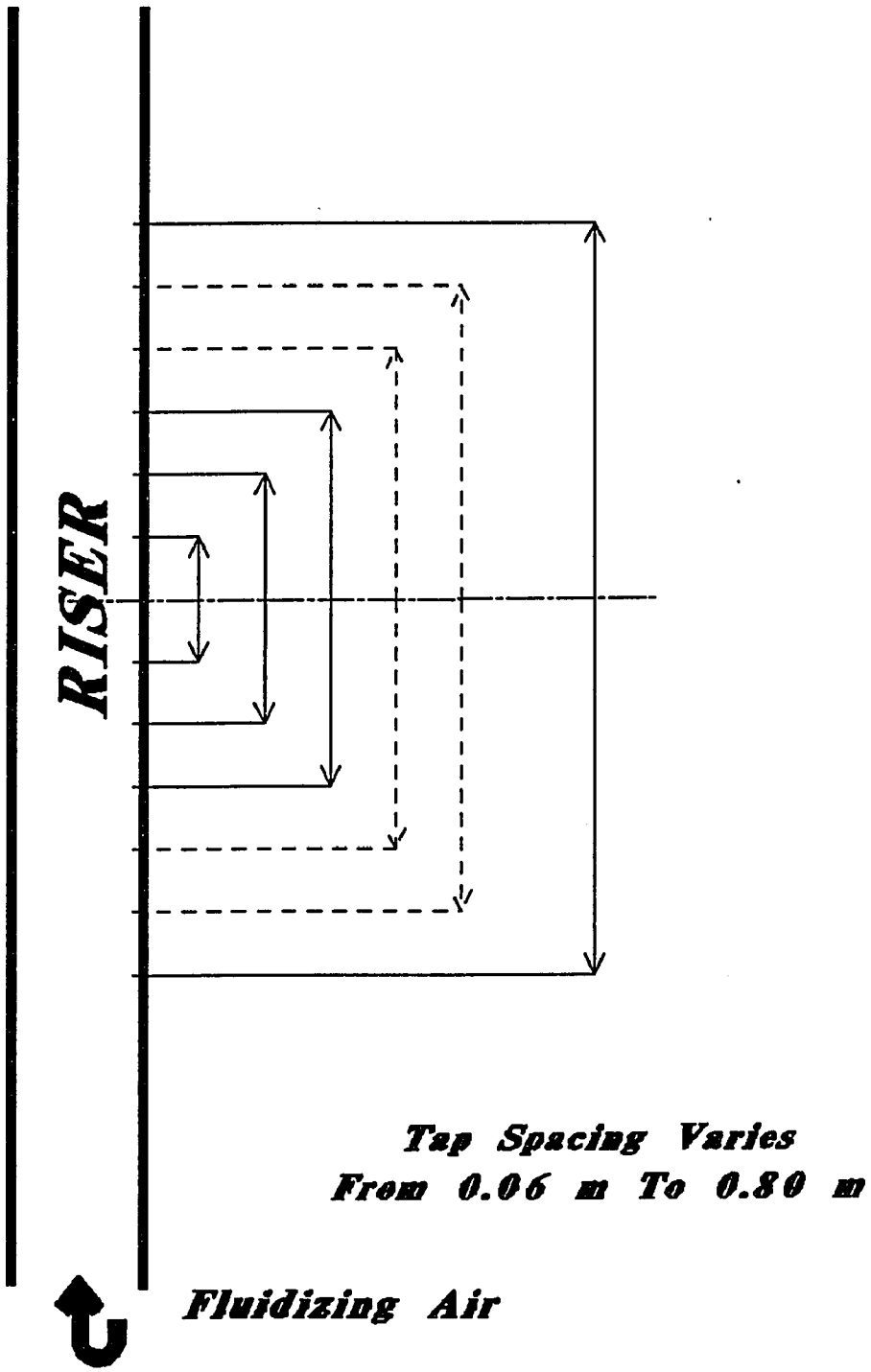

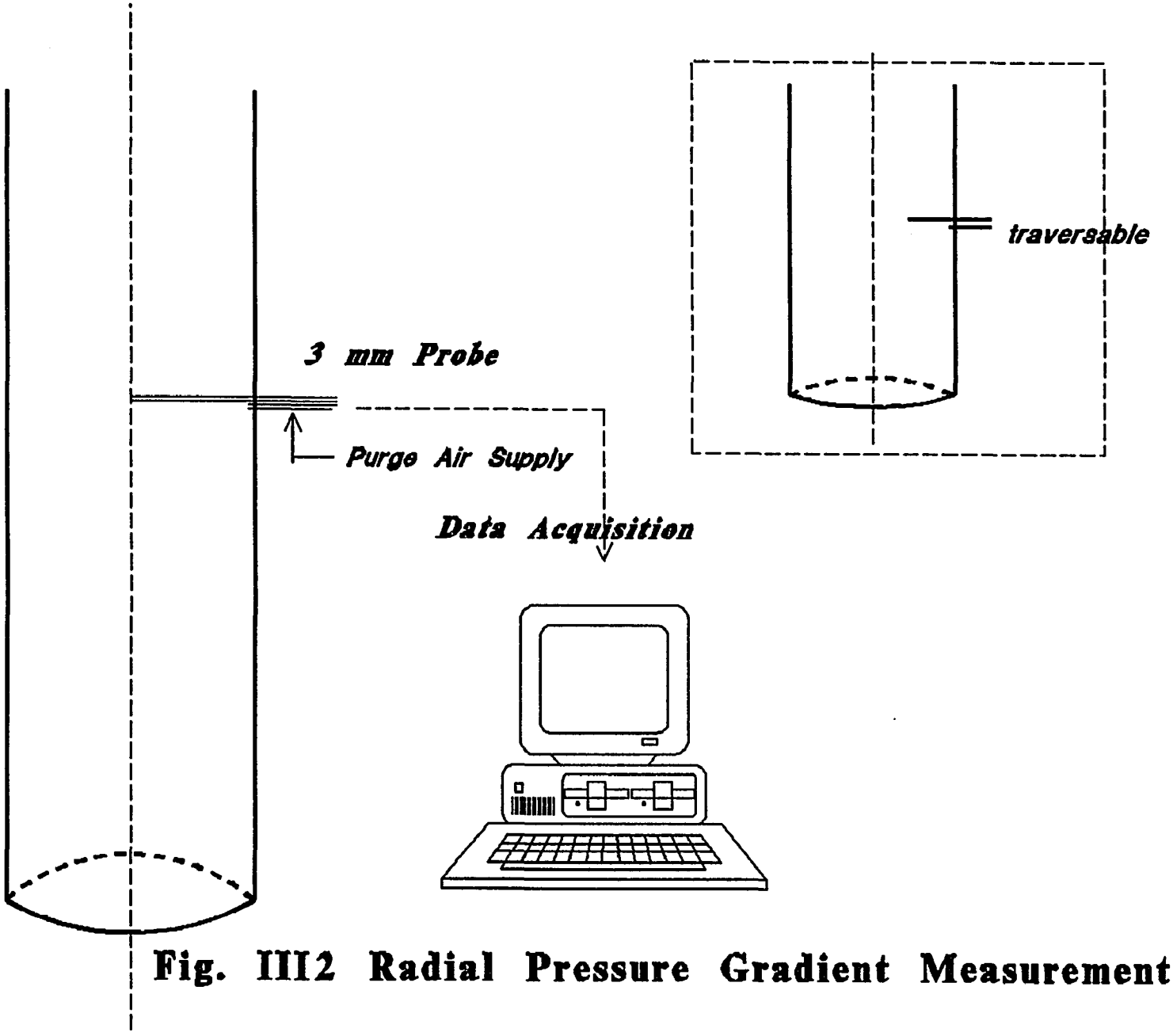

Fig. III2 Radial Pressure Gradient Measurement

Fig.III3 Comparison between the Apparent Solid Fraction Obtained with Various Tap Spacings and by Averaging Large Tap Spacing Data

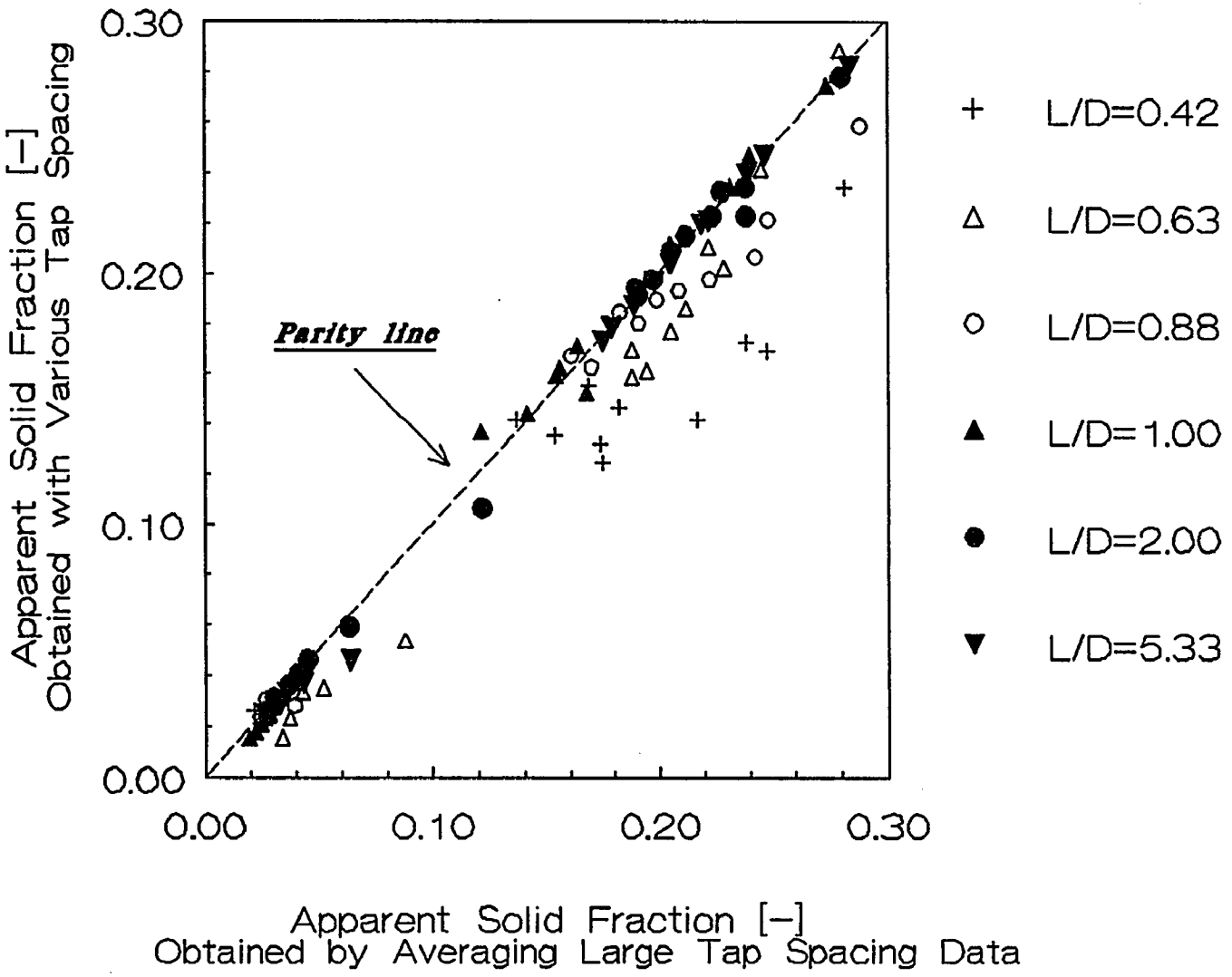

Fig. III4 Normalized Standard Deviation of the Fluctuations as a Function of Tap Spacings

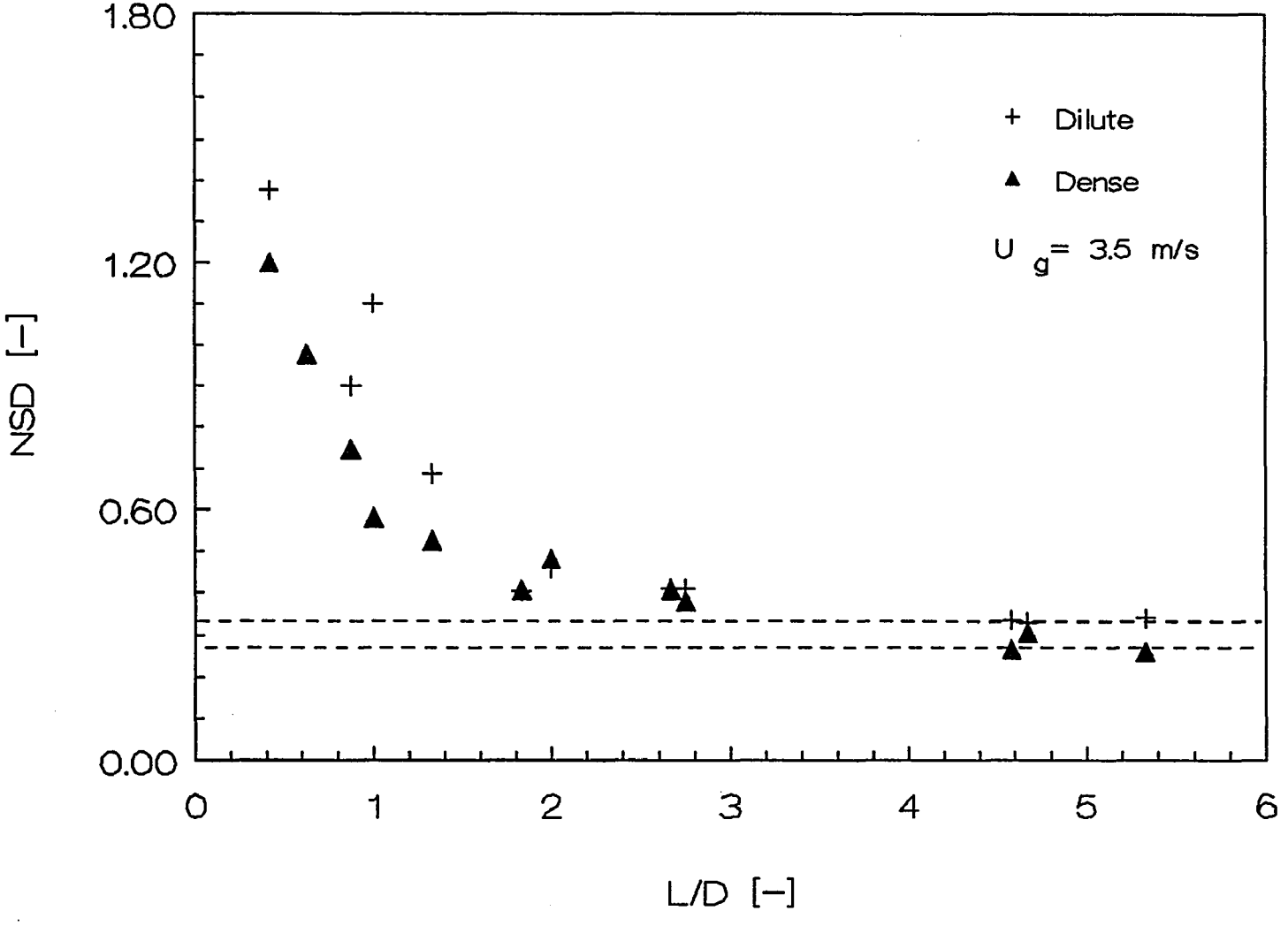

Fig.III5 Normalized Standard Deviation of the Fluctuation as a Function of Gas Velocity over the regime Spectrum

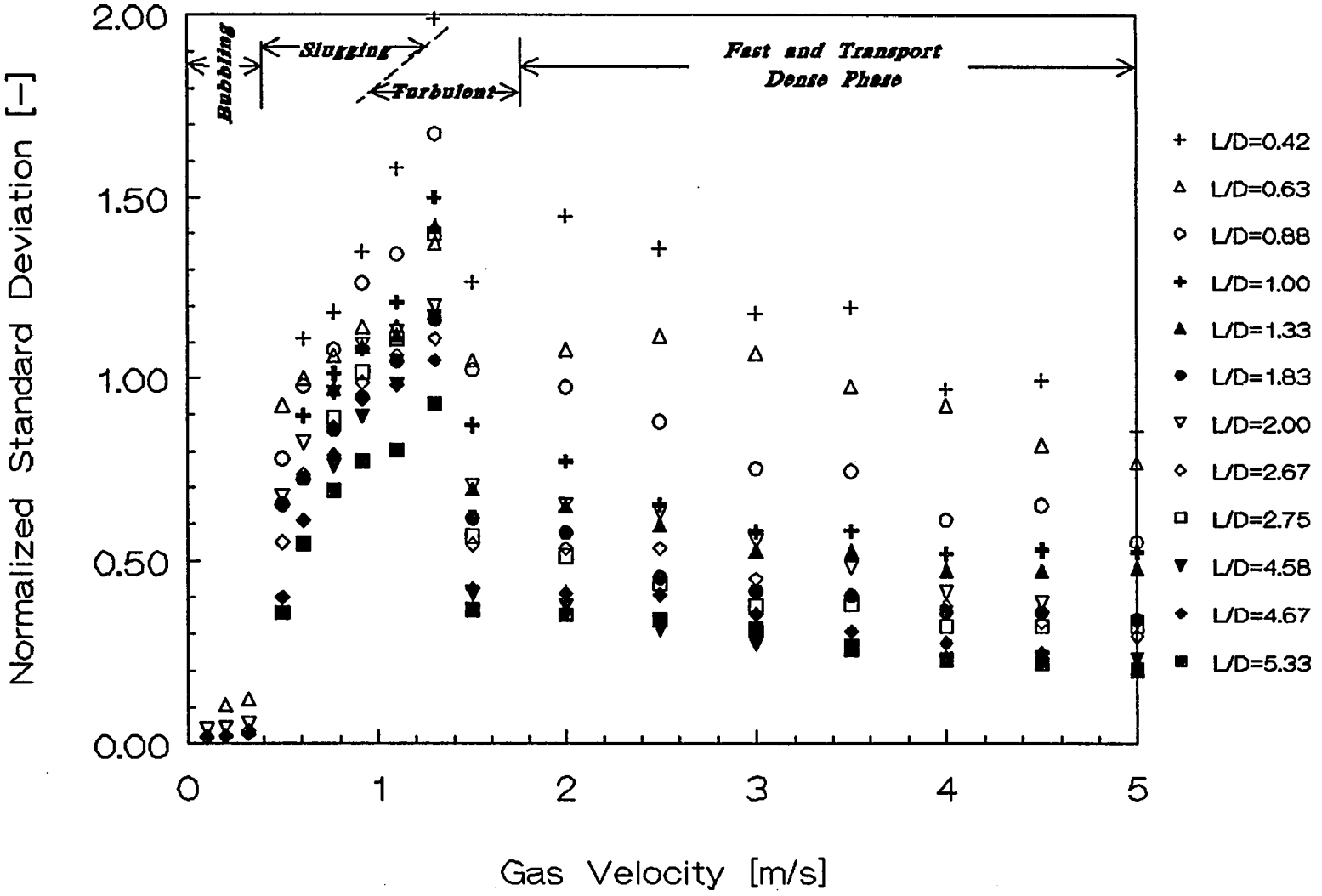

Fig.III6 Normalized Standard Deviation of the Fluctuation as a Function of Gas Velocity over the regime Spectrum

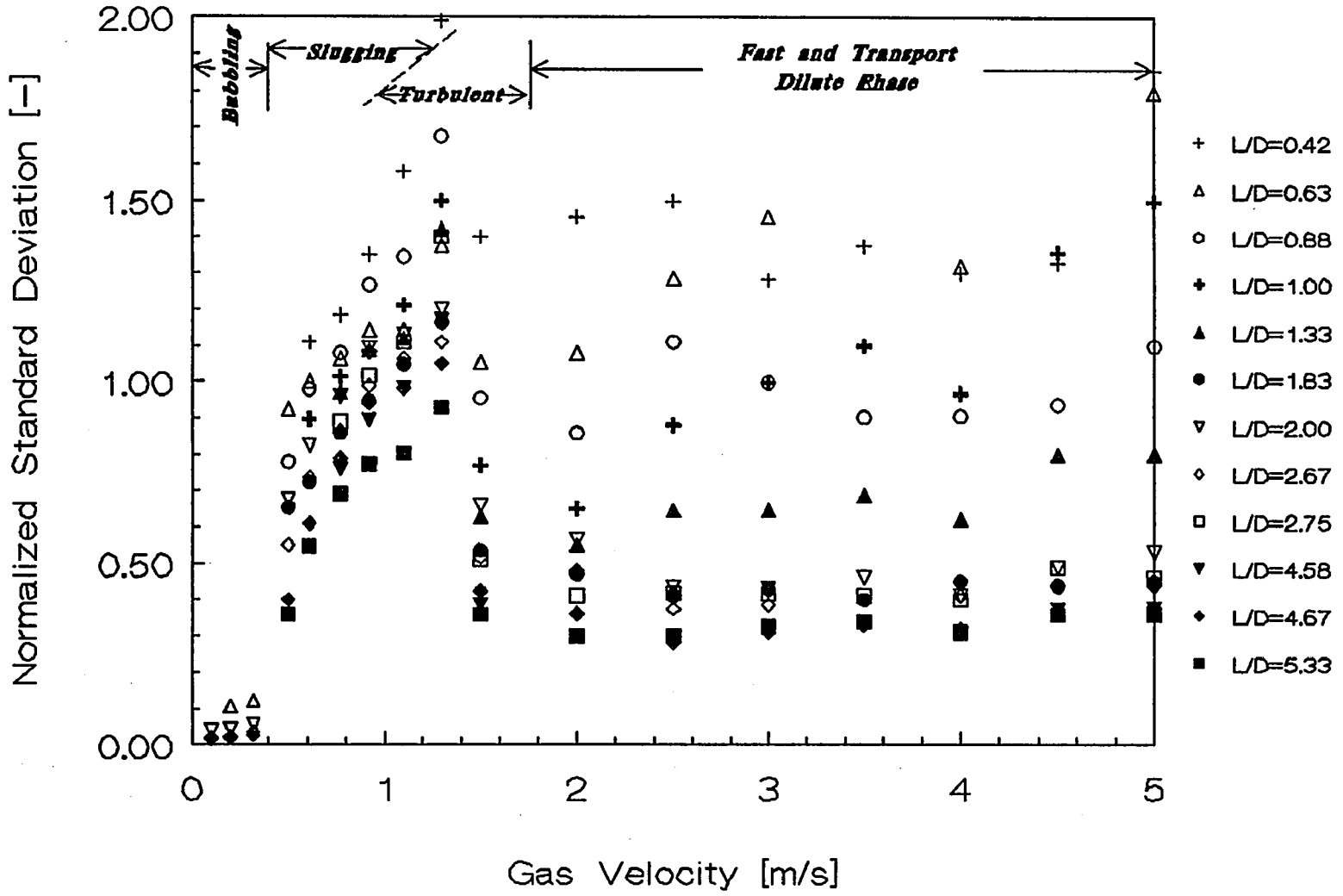

Fig. III7 Time Series of the Fluctuation of Pressure Difference Normalized by the Mean Pressure Difference with Various Tap Spacings

4.5 m/s Dense Flow

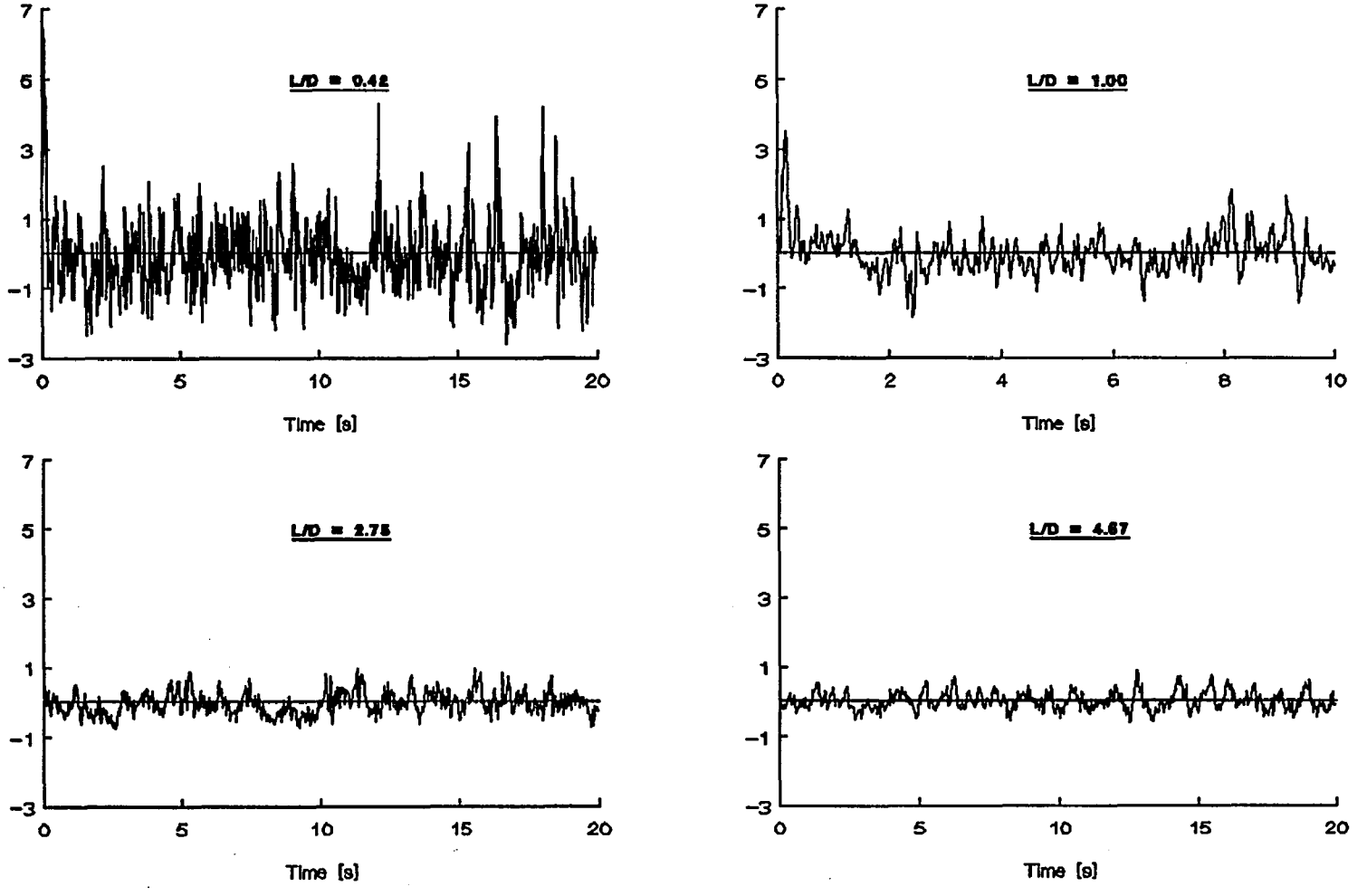

Fig.III8 Power Spectra of the Fluctuation in Pressure Difference Normalized by Mean Pressure Difference with Various Tap Spacings

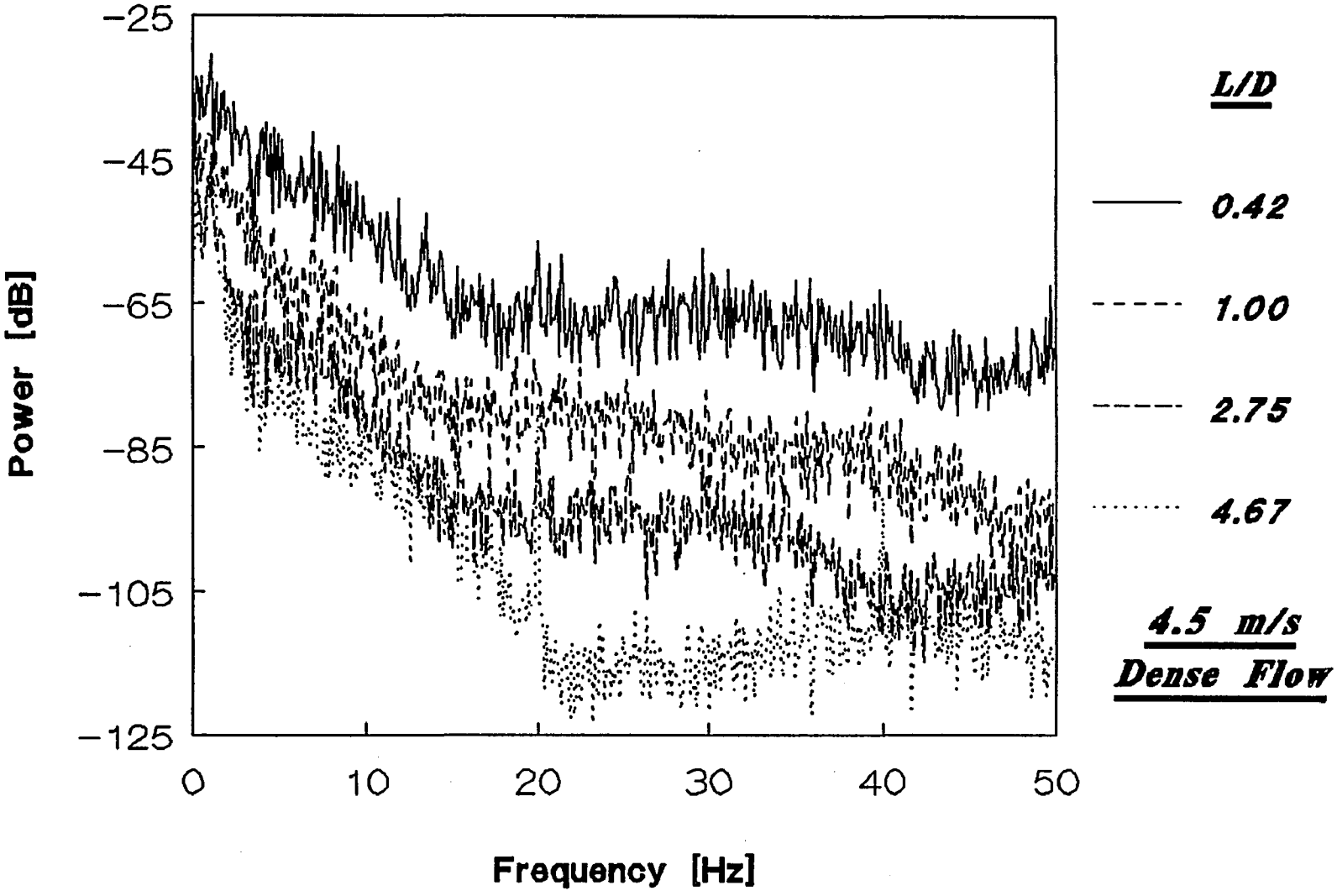

Fig.III9 Autocorrelation Function of the Fluctuation in Pressure Difference Normalized by Mean Pressure Difference with Various Tap Spacings

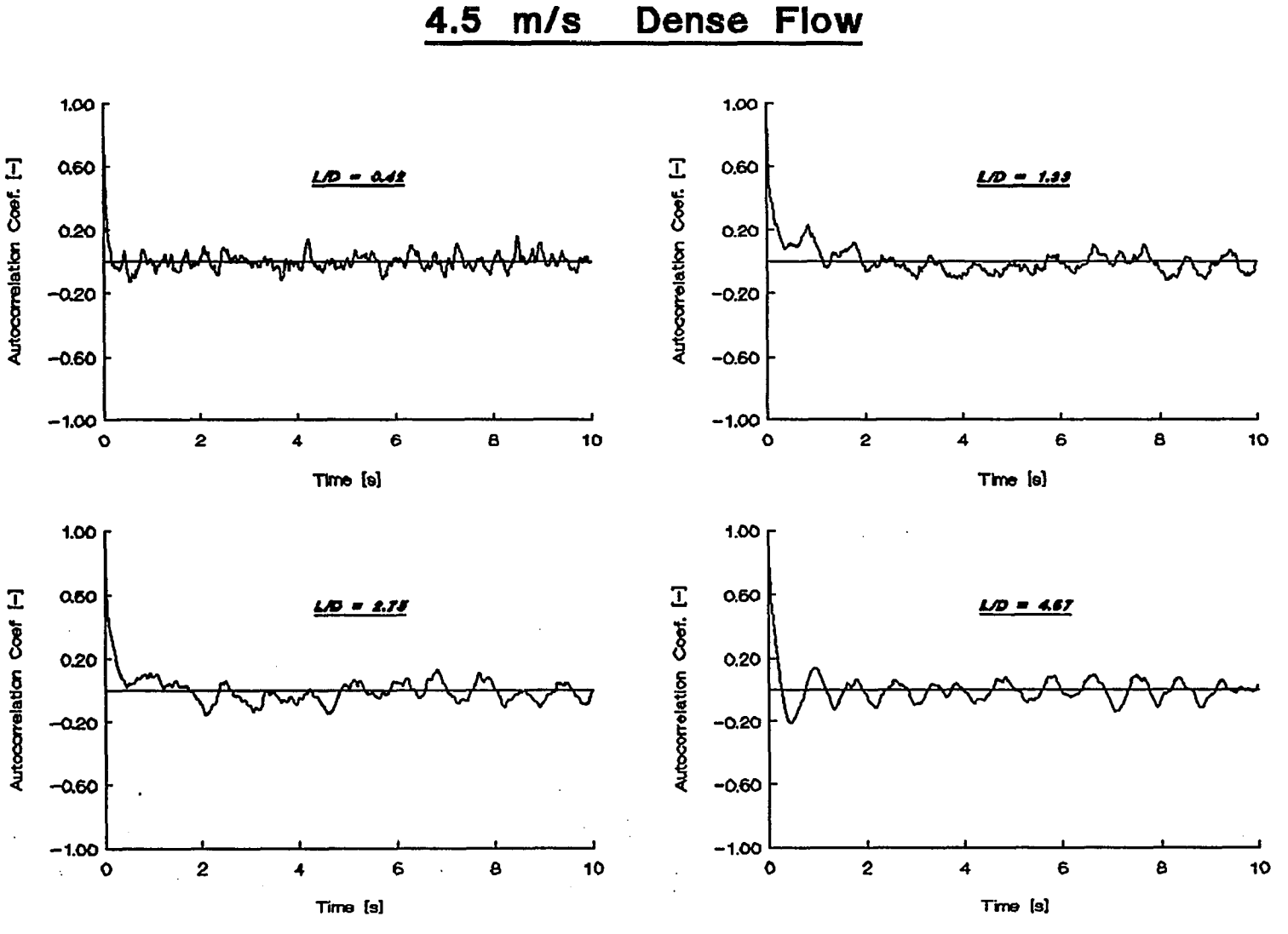

Fig. III10 Axial Symmetry for Radial Pressure Profile

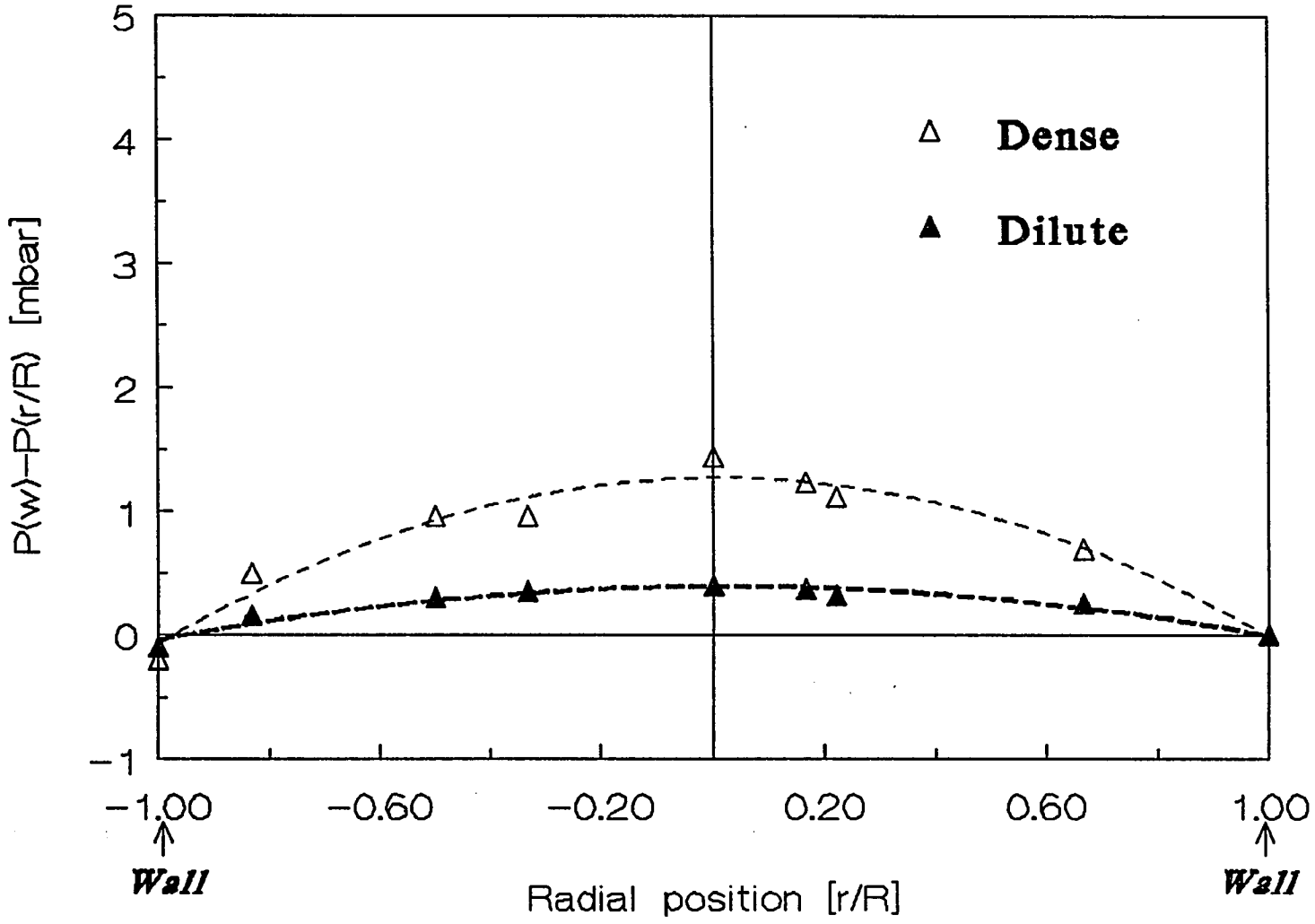

Fig. III11. Pressure Difference From Column Wall as a Function of Position

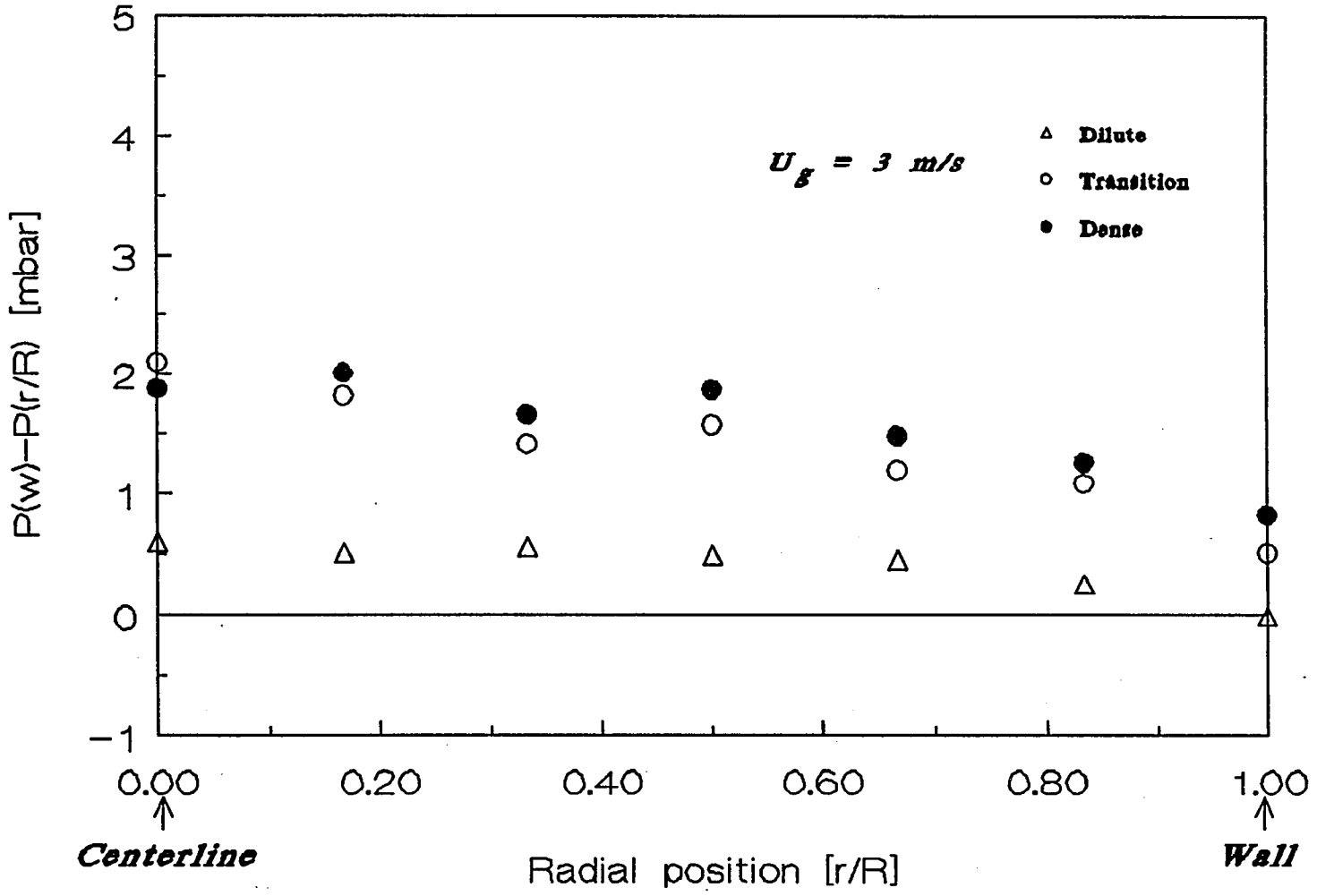

Fig. III12. Pressure Difference From Centerline as a Function of Position

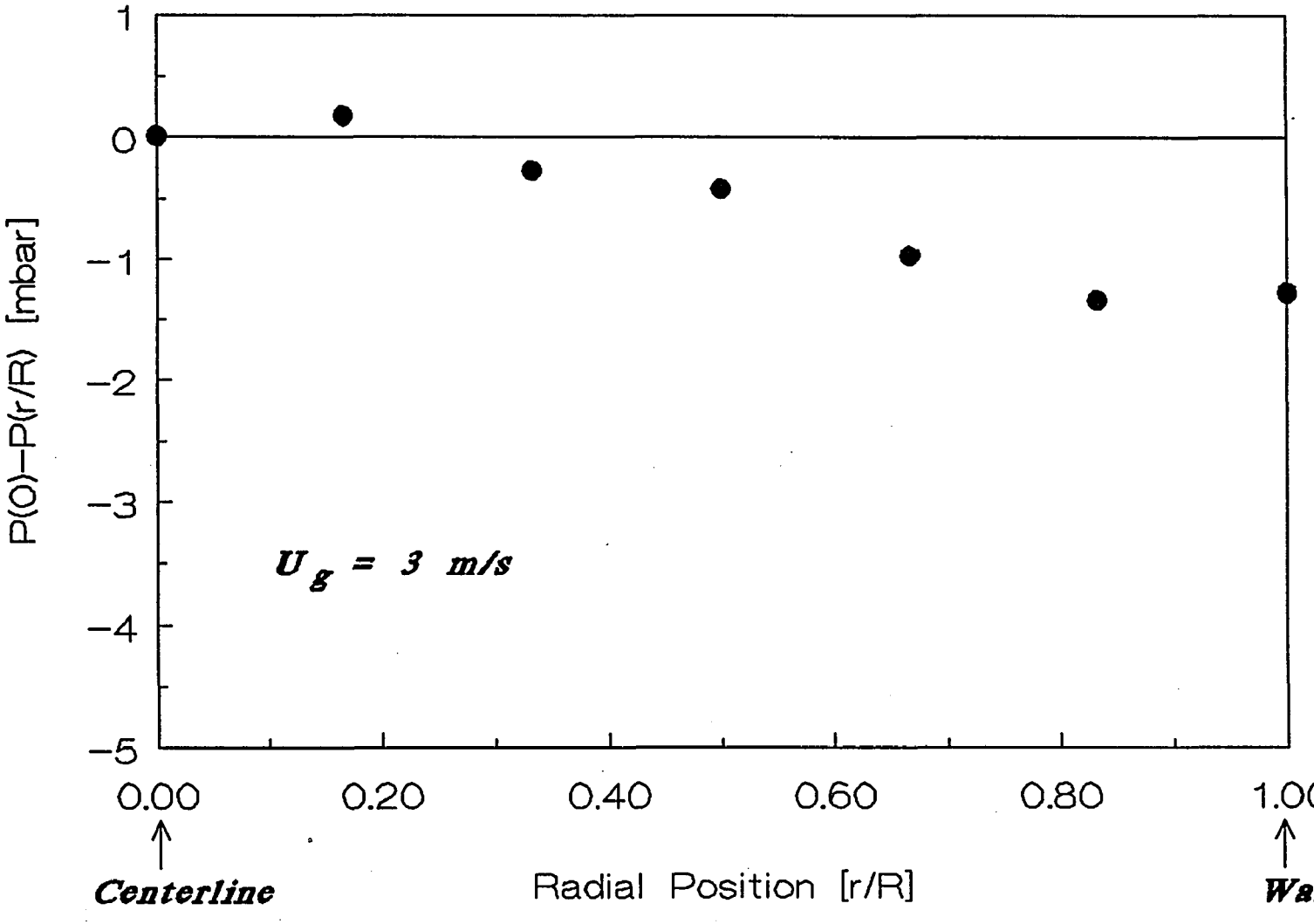

Fig. III13 Pressure Difference From Column Wall as a Function of Position

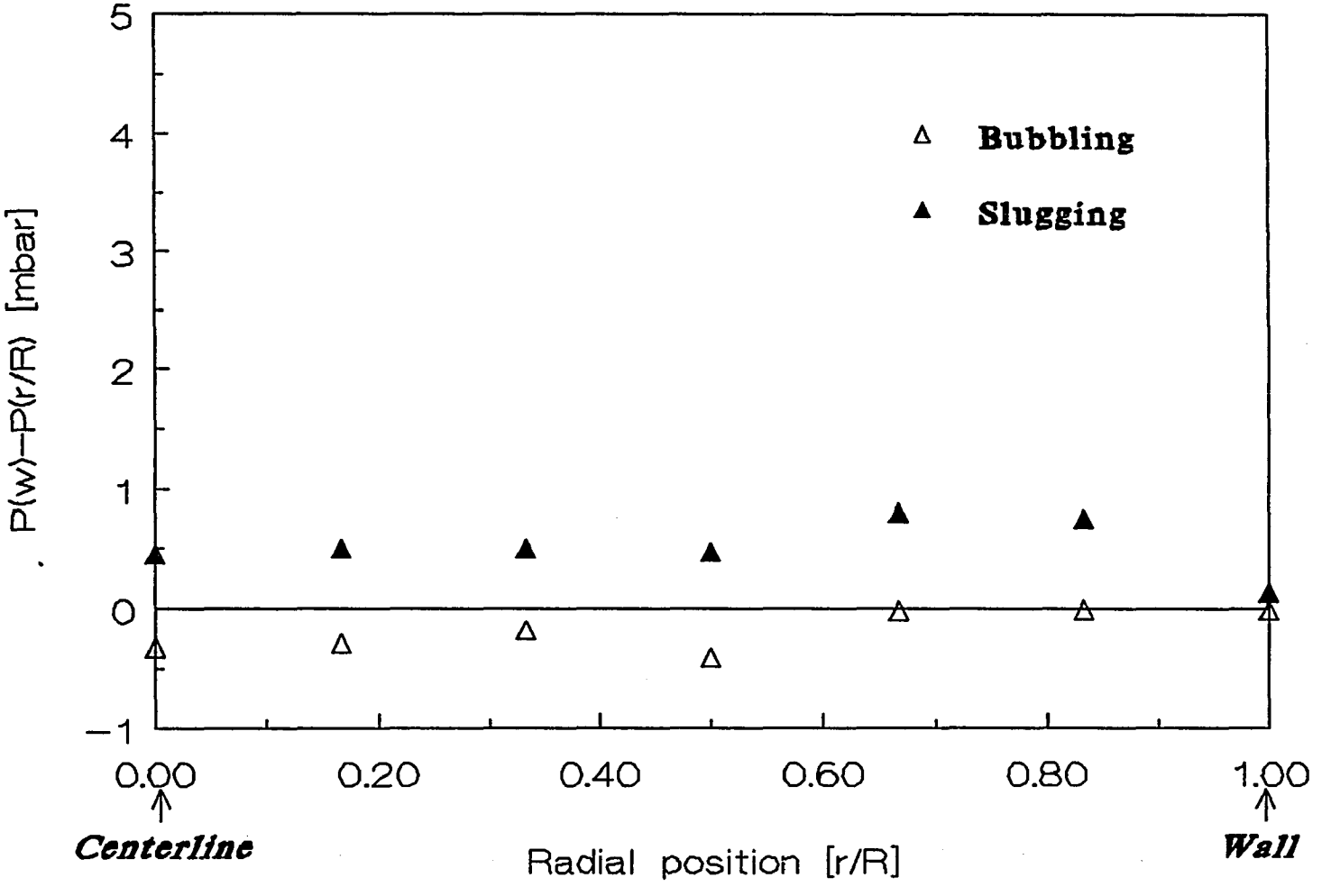

Fi. III14. Radial Pressure Difference as a Function of Cross-Sectional Average Solid fraction in a High Velocity Fluidized Bed

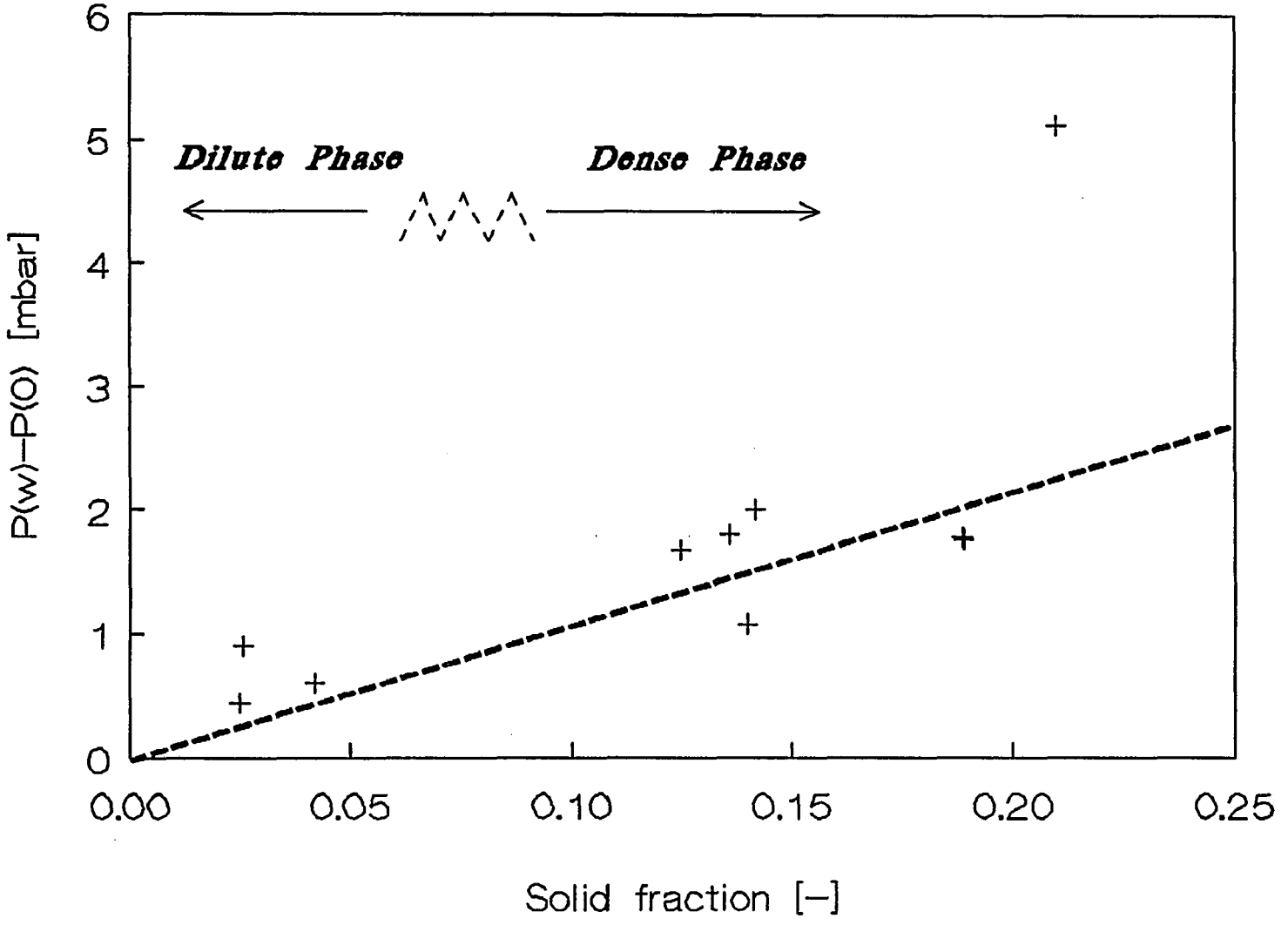

Fig. III15 Average Radial Pressure Gradient Normalized with The Axial Pressure Gradient as a Function of Superficial Gas Velocity

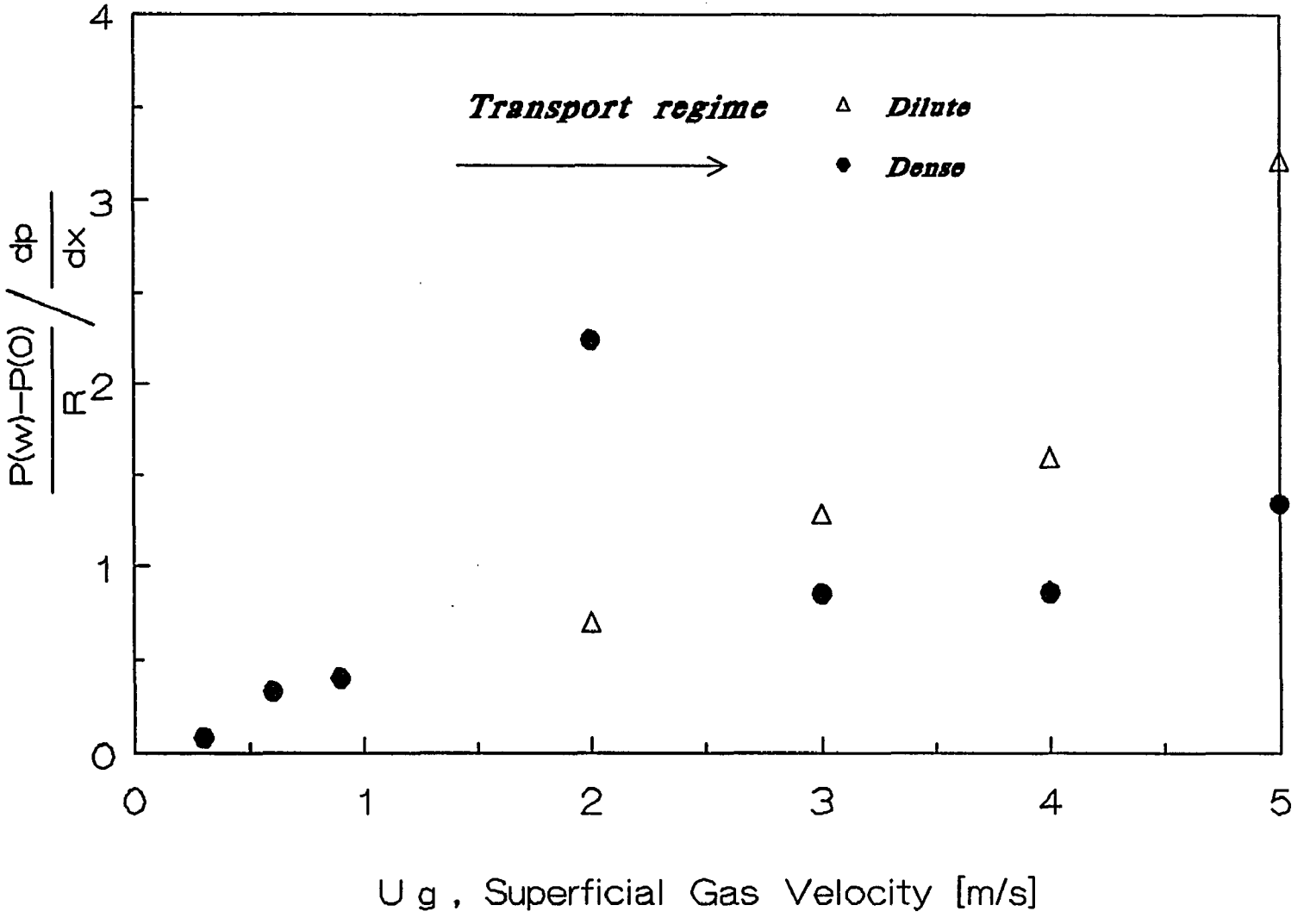

Fig.III16 Standard Deviation of The Radial Pressure Difference Fluctuations as a Function of Superficial Gas Velocity

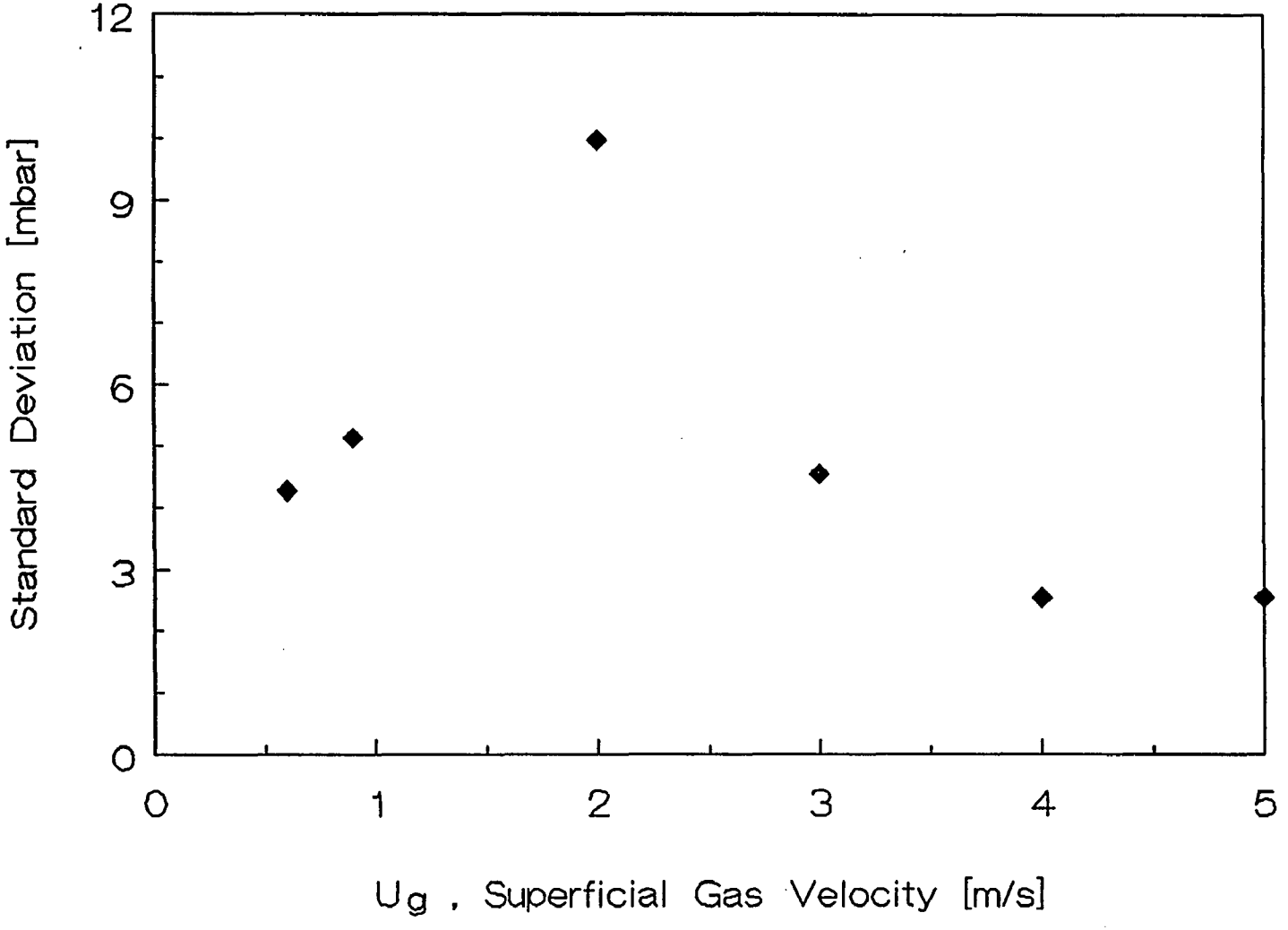

Fig. III17 Comparision of Power Spectrum of Radial Pressure Gradient and Axial Pressure Gradient

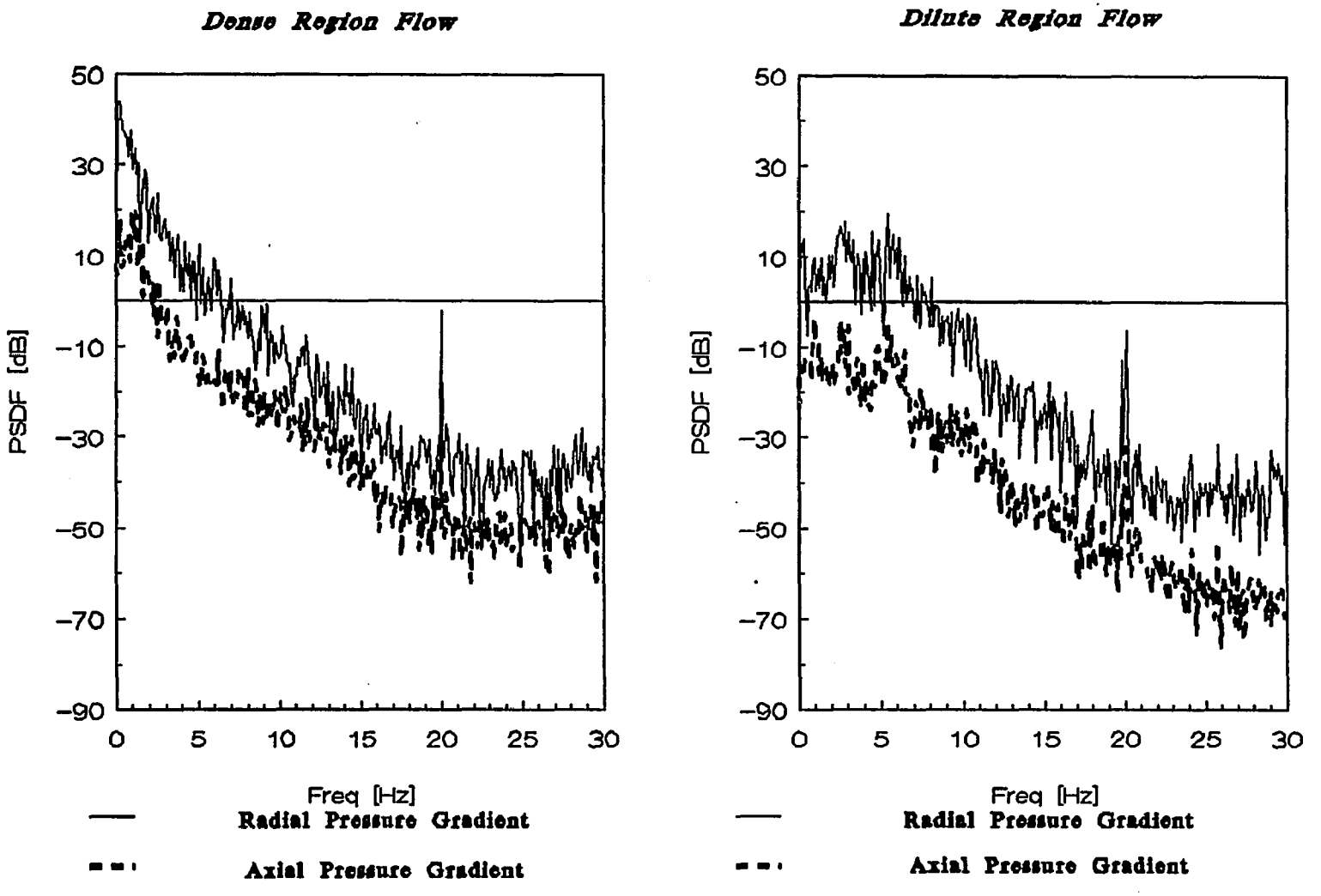

BIBLIOGRAPHY

PART I

Abrahamsen, A. R. and Geldart, D., 1980, Behaviour of gas-fluidized beds of fine powders. Part I. Homogeneous expansion. Powder Technol. **26**, 35-46.

Aldis, D. F. and Gidaspow, D., 1989, Combustion of a polydispersed solid using a particle population balance. Powder Tech. **57**, 281-294.

Bouillard, J. X., Lyczkowski, R. W., Folga, S., Gidaspow, D., and Berry, G. F., 1977, Hydrodynamics of erosion of heat exchanger tubes in fluidized bed combustor. Can. J. Chem. Engng. **67**, 218-229

Ettehadieh, B., Gidaspow, D., and Lyczkowski, R. W., 1984, Hydrodynamics of fluidization in a semicircular bed with a jet. A.I.Ch.E. J. **30**, 529-536

Feindt, H. J., 1990, Radial and axial density fluctuations in a high velocity fluidized bed. Ph.D Thesis, The City University of New York, New York

Gidaspow, D., and Ettehdieh, B., 1983, Fluidization in two-dimensional beds with a jet: 2. Hydrodynamic modeling. I & EC Fundam. **22**, 193-201

Gidaspow, D., Shih, Y. T., Bouillard, J. X., and Wasan, D., 1989, Hydrodynamics of a lamella electrosettler. A.I.Ch.E. J. **35** 714-724

Jean R.-H., Rhonda J.Eubanks, Jiang Peijun and Liang-Shih, 1992, Fluidization behavior of polymeric particles in gas-solid fluidized beds. Chem. Engng. Sci. **47**, 325-335

Massoudi M., Rajagopal, K. R., Ekmann, J. M., and Mathur, M. P., 1977, Remarks on the modeling of fluidized systems. A.I.Ch.E. J. **38**, 471-472

Mutsers S. M. P. and Rietema, K., 1977, The effect of interparticle forces on the expansion of homogeneous gas fluidized beds. Powder Technol. **18**, 239

Richardson, J. F. and Zaki, W. N., 1954, Sedimentation and fluidization. Trans. Instn. Chem.Engr. **32**, 35-53

Shih, Y. T., Gidaspow, D., and Wasan, D. T., 1986, Sedimentation of fine particles in nonaqueous media. Colloids and Surf. **21**, 393-429

Shih, Y. T., Gidaspow, D., and Wasan, D. T., 1987, Hydrodynamics of sedimentation of multisized particles. Powder Tech. **50**, 201-215

Tsinontides, S.C.and Jackson, Roy , 1991, Yield stresses in uniformly fluidized suspensions. DOE/NSF workshop on flow of particles and fluids.

PART II

Feindt, H.J. "Radial and Axial Density Fluctuations in A High Velocity Fluidized Bed" Ph.D. Thesis, The City Univ.of New York (1990)

Kozin, B.E. and Baskakov, A.P. Khim. Tekhnol.Topl.Masel 3, 4(1967)

Lummi, A.P. and Baskakov, A.P., Khim. Prom., 43,7,522 (1967)

Merry, J.M.D "Penetration of A Horizontal Gas Jet into A Fluidized Bed" Trans. Instn. Chem. Engrs.49, 189(1971)

Shakhova, N.A. Inzh. Fiz. Zh. 14, No. 1, 61,(1968)

Shakhova N.A. and G.A. Minayev "Aerodynamics of Jets Discharged into Fluidized Beds" Heat Transfer-Soviet Research, 4(1) 133 (1972)

Xuereb, C., C.Laguerie and et T.Baron "Etude du comportement de jets continus horizontaux ou inclines introduits dans un lit fluidise pan un gaz, deuxieme partie: profils de vitesse du vitesse du gaz dans les jets horizontaux" Powder Technol.,64, 271 (1991)

Xuereb, C., C.Laguerie and et T.Baron "Etude du comportement de jets continus horizontaux ou inclines introduits dans un lit fluidise pan un gaz, I:Morphologie des jets" Powder Technol.,67, 43 (1991)

Zenz, F.A. Inst. Chem. Eng. Symp. ser. 30, 136 (1968)

PART III

1. H.Weinstein, H.J.Feindt, L.Chen and R.A.Graff, "The Measurement of Turbulence Quantities in High Velocity Fluidized Beds", In Fluidization VII O.E. Potter and D.V.Nicklin, Eds., Engineering Foundation, New York, 1992

2. Yerushalmi, J. and N. T. Cankurt "Further Studies of The Regimes of Fluidization", Powder Tech., 24, 1979

3. Bartholomew, R. & R. Casagrande, R. "Measuring solid concentration in fluidized systems by gamma-ray absorption," Ind. Eng. Chem., 49, 428 (1957).

4. Saxton, A. & A. Worley, "Modern catalytic cracking design,"Oil and Gas J., 68, 82 (1970)

5. Weinstein H., M. Shao, & L. Wasserzug, "Radial solid density variation in a fast fluidized bed," A. I. ChE. Symp. Ser., 74,1 (1978)

6. Berker, A.& T. Tulig, T. "Hydrodynamics of gas-solids flow in a catalytic cracker riser: implications for reactor sensitivity performance," Chem. Eng. Sci., 41, 821 (1986).

7. Sinclair, J. L., and R. Jackson, "The effect of particle-particle interactions on the flow of gas and particles in a vertical pipe," A. I. ChE., 35, 1473 (1989).

8. Tsuo, Y. P., and D. Gidaspow, "Computation of flow patterns in circulating fluidized beds", A. I. ChE., 36, 885 (1990).

9. Dasgupta S., R. Jackson and S. Sundaresan, "Turbulent gas-particle flow in vertical risers", A. I. ChE., in press

10. Feindt, H. J. "Radial and axial density fluctuations in a high velocity fluidized bed", Ph.D. Thesis, The City Univ. of New York (1990)